Remote Assessment of High Voltage Porcelain Insulators Using Radiated Electromagnetic Field Signature

by

Ehsan Azordegan

A Thesis Submitted to the Faculty of Graduate Studies of
The University of Manitoba
in Partial Fulfilment of the Requirements for the Degree of
Doctor of Philosophy

Department of Electrical and Computer Engineering
University of Manitoba
Winnipeg, Manitoba, Canada

Abstract

A novel approach for inspecting the condition of porcelain insulators based on statistical analysis of electromagnetic radiations of live insulators is demonstrated in this thesis. Physical defects such as puncture and contamination can degrade the insulators performance and result in power outages, potentiating costs to utilities. Therefore, condition assessment of line insulators has always been one of the most important aspects of maintenance programs in power networks. Realistic replicas of punctured and contaminated insulators were created in the High Voltage Lab at University of Manitoba, following the IEC standards. These defective insulators were tested under high voltage stress while the electromagnetic radiations originated from the partial discharge activities on the insulators were captured using electromagnetic sensors. During the experimental part of this thesis, a multitude of tests were conducted and resulted in measuring and recording a total of 410,000 cycles of discharge activities. The feature extraction algorithm, developed as part of this thesis, calculates the statistical features of the phase resolved interpretation of partial discharge (PD) pulses. The results of analyzing the extracted features from the radiated signature of defective insulators indicate that the scale and shape parameters of a two sided Weibull distribution function fit to

the recorded measurement entail distinct information about the source of discharges that can be used to identify the source of defects. Based on the library of features extracted from the recorded electromagnetic radiations, a support vector machine (SVM) classifier, developed as part of this thesis, can successfully classify the radiation signature of punctured and contaminated insulators. Therefore, the main outcome of this research was introducing a novel porcelain insulator inspection technique that can remotely differentiate the defective punctured and contaminated insulators using their electromagnetic radiation signature in a laboratory environment. By utilizing the signature of common discharge activities present in the recorded signature of all tested insulators, a gating algorithm was developed which improved the successful classification rate from the 51 % to 75%. The inspection technique proposed in this research can eliminate the safety hazards involved in the live maintenance of line insulators, lower the maintenance costs, and improve the inspection efficiency considering the conventional labour intensive live maintenance assessments.

Acknowledgements

I would like to extend my utmost gratitude to the many people who have helped along the way to make this research project possible and to bring it to its completion. First, I would like to express my sincerest appreciation to Dr. Behzad Kordi for providing me the opportunity to take part in his research work. I am so deeply grateful for his help, invaluable guidance, and support throughout this project and my entire program of study.

I would like to thank the committee members Dr. Douglas Thomson, Dr. Greg Bridges, and Dr. Yunhua Luo for their advice, guidance, and support through the completion of the project. Without their participation and input, the project could not have reached the level of fruition it has achieved. I would also like to thank Dr. Chi Yung Chung, my external PhD examiner, for his time to review my thesis and make valuable suggestions and comments.

I would also like to acknowledge Dr. David Swatek, from Manitoba Hydro, who provided technical guidance and support throughout this research as well as accommodating the temporary test setup of the project at Manitoba Hydro High Voltage Test Facility (HVTF). I also want to thank Bill McDermid for his technical support, assistance,

and discussions that allowed me to better understand some of the fundamental concepts of this work.

Furthermore, many thanks to Nathan Jacob who assisted with the lab experiments at Manitoba Hydro High Voltage Test Facility and accompanied me when running tests and conducting measurements as well as numerous conversations we had discussing results that aided me in solution development.

Also I would like to thank Daryl Hamelin and Cory Smit at the University of Manitoba for their help with the experimental setup of this project.

I would like to acknowledge financial support from Manitoba Hydro, Mitacs Accelerate, Natural Science and Engineering Research Council of Canada (NSERC), and the faculty of Graduate Studies, University of Manitoba.

I must also express my very profound gratitude to my parents; my dear mother Parvin, who always brightens my day with her positive energy, and for my reassuring father Firouz, for making me find the strength to continue my research, and to the rest of my family for the many thoughts and words of encouragement that helped me get through challenging times.

Lastly, I want to thank my friends for their unfailing encouragement and support throughout my years of study, researching, and writing this thesis. Thank you all for all the wise words, your efforts and everything you did for me, I could not have done it without you.

Table of Contents

List of Tables

List of Figures

1

Synopsis

1.1 Introduction

With the emergence of new technologies and higher demand for the reliable transmission of electric power, utilities are facing economical and technical challenges to reduce the duration of line outages and keeping their lines energized that make live line maintenance services a more desirable option. In any power network, the condition assessment of line insulators is one of the most important maintenance services. Physical defects, such as punctures and contamination, can degrade the insulators performance. Line insulators should be checked regularly to ensure maximum service reliability. However, due to the large number of insulators on the transmission and distribution network, this is a daunting task. For example, in North America there are more than 150 million porcelain insulators in service where some are 50 years old [1].

A number of inspection methods ranging from close contact tools to acoustic, ultraviolet, and infrared methods have been proposed by industrial companies and

scientists for insulators condition assessment. There has always been a trade-off between the reliability of these inspection tools and how convenient they are for linemen to use. A comparison of the successful rate of detection of faulty insulators for different tools shows that the inspection methods which require close contact to the insulators are far more accurate compared to remote inspection methods. However, remote inspection methods can assess the insulators condition from a distance and without the need to climb towers. Considering the importance of avoiding an outage and the convenience and safety of using remote assessment tools, the remote inspection tools are a better and more desirable solution to the maintenance of line insulators. Moreover, the recent progress made in digital signal processing has significantly increased the reliability and successful detection rate of the remote inspection methods. Remote detection methods need to capture a symptom of faulty insulators without making physical contact. These methods will monitor the variations of certain parameters depending on the nature of their detection algorithm. For example, acoustic methods monitor the sound wave parameters originating from faults on the insulators or infrared detection tools focus on the thermal distribution along a string of insulators. Each inspection method has its own advantages and drawbacks which are discussed in Chapter 3.

1.2 Problem Statement

The motivation for this PhD thesis is the need of utility companies and the power system industry to employ innovative methods for the remote detection of defective porcelain insulators. The objective of the research was not only to detect the abnormal signature of a defective insulator, but also to distinguish and classify

the source of the behaviour, a novel approach for condition assessment of outdoor porcelain insulators. Therefore, the main focus of my research was to remotely inspect and classify defective porcelain line insulators in a lab environment, taking into consideration the two most common types of defects on porcelain insulators; puncture and contamination [2, 3, 4].

1.3 Objectives

The main objective of this PhD thesis is to study and characterize the electromagnetic radiation signature of partial discharges from defective insulators. Defective insulators had to be made in the lab according to the available standards. Due to the randomness of partial discharge behaviour, a time domain statistical analysis platform was developed to separate the radiation signature of different defects. The research was conducted inside a laboratory using a clean fog chamber that was built to duplicate a realistic environment for testing the insulators. At the High Voltage Laboratory of the University of Manitoba, punctured and contaminated insulators were made and tested. Obtaining accurate and reliable measurements was one of the most important aspects of this research. To analyse the raw measurement data obtained in the lab, a MATLAB graphical user interface (GUI) was developed to calculate statistical features of captured partial discharge activities. A classifier was also developed to differentiate and classify the radiation signature of contaminated and punctured insulators.

1.4 Research Outcomes and Contributions

The published literature related to the topic of this research have reported similar efforts on classification of partial discharges captured from contaminated insulators [5, 6, 7, 8]. However, most of the methods for capturing the partial discharges are based on leakage current waveform taken from the ground lead. Also, the signal processing and classification algorithm reported in each research is different, but it mainly involves time-frequency algorithms. One of novel ideas presented in this research is the use of electric field sensors to remotely capture the electromagnetic radiations, a technique never used for PD detection of line insulators. Also, although performing statistical analysis on PD pulses have been reported in the literature, the mixture Weibull distribution developed as part of signal processing of this research has not been used before. Moreover, research on PD signature of realistic samples of punctured insulators (created in the High Voltage lab) have never been reported in this extent before. Another advantage of this research compared to the published literature is the partial discharge database developed throughout the lab measurements. During this project, a multitude of tests were conducted and resulted in an excessive amount of measured data for a meaningful statistical analysis. A total of 410,000 cycles of radiated partial discharge activities from normal (clean and healthy), punctured, and contaminated insulators were captured and recorded. Further, methodologies and procedures were developed to perform remote measurements of insulators electromagnetic radiation.

A MATLAB based GUI has been developed that performs statistical analysis on recorded measurements and classifies recorded signatures. The classifier uses unique statistical features (output of the GUI) to separate the signatures of punctured

and contaminated insulators, considering the baseline signatures of healthy and clean insulators. Based on a number of classifications performed in various feature domains, the shape and scale parameter of a fitted Weibull distribution in the negative half cycle of the voltage is proved to have distinct information to differentiate partial discharge activities on contaminated and punctured insulators.

This novel remote assessment tool utilizes unique statistical features of partial discharge activities to differentiate the type of defects on porcelain insulators. The results obtained from the measurements and analysis of samples tested in a high voltage laboratory, indicate the successful use of feature domains to classify radiation signatures. This innovative remote assessment tool, using statistical processing kernels, can help utilities rank the condition of porcelain insulators in service and determine the proper maintenance program, based on the remote assessment results.

The outcomes of this research have been published in a conference paper and one journal paper [9, 10]. A second journal paper is in preparation that will be submitted soon.

2

Outdoor Insulators

2.1 Introduction

Overhead transmission lines are responsible for delivering electric power from generators to industrial and residential customers. The energized conductors on the overhead transmission lines have to be attached to the tower while they are electrically insulated from the grounded towers. The device that can hold the weight of the conductors while it provides electrical insulation between the line and the tower is called an insulator. Insulators are able to handle electrical and mechanical stresses when the line is energized. Most of the insulators have outdoor applications where they are subjected to environmental conditions such as moisture, high temperature, contamination, and icing. To choose the right type of insulator before the installation, the environmental conditions of the site has to be studied.

2.2 Insulator Types

Insulators are mainly composed of a dielectric material, electrodes, and end fittings. Outdoor insulators can be classified either by the dielectric material that is used in them or by their application. By application, they can be divided into four groups; suspension, post, interphase, and bushing [11, 12]. In this research, we mainly focus on suspension outdoor insulators. Insulators can also be classified by the type of dielectric material that has been used in them. The three main dielectric materials that are mostly used in outdoor insulators are polymer, glass, and porcelain. In some documents, these insulators might be called by other names; for example, porcelain insulators are also known as ceramic insulators or polymer insulators are also known as non-ceramic or composite insulators. Polymer insulators have recently become very popular in high voltage transmission line applications because of their lower weight, easier installation, higher resistance to vandalism and their excellent performance in polluted environments. Surveys also show that the maintenance costs for non-ceramic insulators are lower [13]. The manufacturing technique for these insulators has a minimum amount of waste and sheds can be produced using a single mold. However, polymer insulators have not been in the service for a long time and therefore, it is not clear how they would perform after being used for more than 50 years, whereas toughened glass insulators have been in service since 1947. Around 10 million of them have been reported in service in North America. Inspection of these insulators is quite easy. Any defect on the insulator string will cause the glass shell to shatter and only the stub remains on the string. Although simple detection of faulty glass insulators makes them a good option for 500 kV transmission line, they are quite heavy and also a very good target to vandal.

Porcelain insulators have been in the market since 1910. More than 150 million of these insulators are now in service in North America. They are by far the most commonly used outdoor insulator in service. Apart from the problems due to vandalism or poor quality control from some manufacturers, they have served very well in high voltage transmission systems for the past 50-60 years. For maintenance purposes, these insulators have to be checked from a close range which involves either taking them down from the line (random sampling) or climbing the tower to attach the measurement probes to the cap ends. The weight of porcelain insulators used to be a problem, but the newer generations do not suffer from the weight issue anymore [14].

The main focus of this research is on porcelain suspension insulators since Manitoba Hydro, the industrial sponsor of this research, has a large number of these insulators currently in service.

2.3 Design and Manufacturing

Pin type insulators and cap-and-pin type insulators are the two most commonly used suspension porcelain insulators in service. The main challenge in manufacturing these insulators is the cement connection between the metal pin and porcelain. Most of the failures of porcelain insulators are due to cracks and punctures caused by expansion of the cement joint [15]. Depending on the line voltage, the porcelain composition could be different. In North America, a combination of Quartz, ball clays, and silica is used in lower voltages such as distribution networks. Alumina on the other hand, which is high-strength porcelain, is used in manufacturing of porcelain insulators in transmission line networks. Glazing is the last step in

manufacturing porcelain insulators which adds more features such as high strength and self-cleaning ability to the insulators. The type of cement used in gluing the metal pin to porcelain is an important parameter in manufacturing porcelain insulators. Portland cement is the most common type of cement that is used in manufacturing suspension porcelain insulators. The cement should be designed to handle the mechanical stress as well as the electrical stress. Figure 2.1 shows the cross section of a typical porcelain suspension insulator [12].

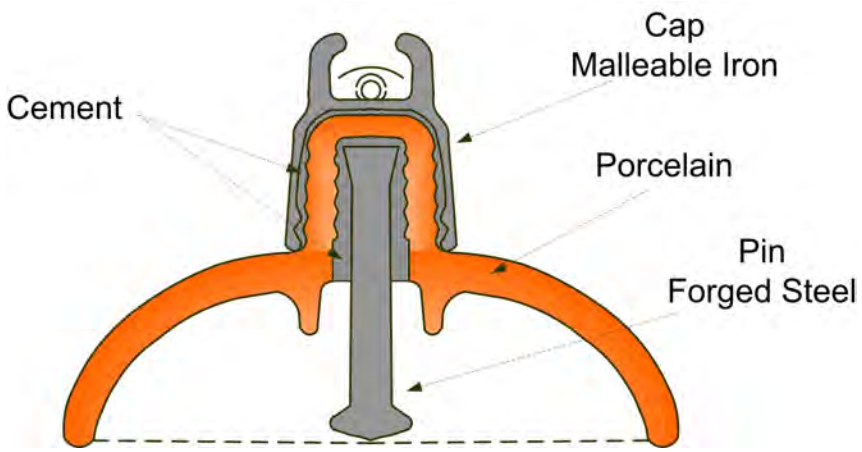

Figure 2.1: Cross section of a porcelain insulator.

2.4 Electrical and Mechanical Performance

Electrical properties of insulators come from the dielectric that they are made of. In order to study the electrical properties of porcelain insulators, dielectric properties of porcelain should be studied. It should be noted that there are two dielectric property measures; volume dielectric property and surface dielectric property. When there is a puncture or void inside the porcelain, the dielectric strength of the insulator drops. The electric field in that area will be magnified and partial discharge will take place

in that region which may eventually cause a failure within the insulator (Appendix A provides more details on this topic) [16]. Surface dielectric property relates to the conductivity of the surface of the shells. Under humid and contaminated conditions, the surface conductivity rises which may cause a discharge arc on the surface of the shell. These failures are called surface flashovers which are the results of the air breakdown around the shells [17, 18].

The mechanical performance of insulators on the overhead transmission lines is as important as the electrical performance. The conductors will fall if the insulators fail mechanically resulting in disastrous consequences. The mechanical properties of insulators, such as internal attachment of the metal pins to the dielectric, are mainly concerned during the manufacturing process. The electrical properties of porcelain insulators will be the main focus of our work.

2.5 Standard Quality Tests

Before installing porcelain insulators, they have to pass standard tests to ensure their good performance in service. In order to perform these tests in lab environment, the conditions inside the lab should be similar to the actual outdoor environment. Electrical (and even mechanical) sources and monitoring instruments are also needed to perform the tests. In order to get consistent test results for a certain insulator in different labs, standard tests have been developed. Standard tests can be divided into two main categories; sample tests and type tests. For sample tests, random samples of insulators are selected and tested to verify the quality of the material and manufacturing process consistency. Type tests are usually performed on new products, either changing the design or the materials. These tests are aimed to

identify the main characteristics of the insulators for each unique design. For most of the sample and type tests, it is more desirable to have both the mechanical and electrical stress on the insulator to duplicate the real operating conditions.

Routine tests, which are one of the most important transmission line maintenance tests, guarantee the performance of insulators during the service. Some of these tests are performed at a higher voltage (ie. puncture tests are performed at 500 % of the rated voltage)than transmission line's rated voltage to guarantee the performance of insulators under short overvoltage periods such as lightening, surges, or icing [19]. Contamination tests will determine the performance of the insulators in heavy contaminated environments. Contamination tests conducted inside a fog chamber will produce more realistic results as they can resemble the environmental conditions in real environment[20].

2.6 Failures of Porcelain Insulators

Porcelain insulators can fail due to a variety of reasons. Prior to the installation, some insulators might get physically damaged during shipping and transportation. Vandalism is another reason of porcelain insulators failure. However, glass insulators are by far a better target when it comes to vandal. Gun shots break the surface of porcelain shells which increases the chance of flashovers under wet conditions. Poor manufacturing and low quality control are two other reasons of porcelain insulators failures.

The expansion of Portland cement used in cap-and-pin insulators causes radial cracks on insulator's shell. The expansion mostly happens under wet condition when the cement absorbs the moisture. Cement expansion decreases the strength

of porcelain and increases the chance of surface cracks [21].

Punctures can develop inside the porcelain insulators when there is an overvoltage due to lightning on the transmission line. Puncture paths mostly develop inside the cap and in the area between the cement connections of cap and pin to the porcelain. Cracks develop over time inside porcelain shells when the quality of manufacturing is poor. During the manufacturing, there is a layer called 'Bitumen layer' which is laid on top of the cement joints. When the quality of this layer is poor, it will dry out over time and causes internal cracks inside the porcelain [21, 22].

Continuous corona is another reason of porcelain failure. Corona usually happens between the cap and porcelain or pin and cement. In both cases, over time, the strength of dielectric drops and it eventually breaks [23]. Contamination is another reason of porcelain failures. Heavy contamination under moist conditions will increases the leakage current which will ultimately result in hardware erosion. High leakage current can also cause flashovers [5, 8, 24]. More details on contaminated insulators will be presented in the following section.

2.7 Contamination of Insulators

Contaminated insulators under humid and moist conditions can cause contamination flashover and eventually system outages. Some of the contaminants that can be found on the polluted insulators are salt from the sea, dust and rubber particles from the nearby highways, bird secretions, desert sand, and industrial pollution from the factories. Type of contaminants near the sea is different from contaminants in desert or near industrial sites. Contaminants are mostly salt (NaCl), Gypsum ($CaSO_4$) and some type of sand (SiO_2). The speed of accumulation of these contaminants

on the surface of insulators depends on speed of the wind, direction of the wind, type of insulators, and transmission lines orientation. Over time, the contaminants will accumulate on the surface of the insulators, however, they also get washed off by rain and heavy winds. The top surface of insulators is usually cleaner than the bottom ribs. The bottom ribs on the vertical oriented insulators (known as I formation) accumulate more contaminant compared to the horizontal and V oriented insulators. The contaminants on the insulators will become conductive when they are exposed to moisture. When the contamination layer becomes conductive, the magnitude of the leakage current through the string increases [25]. Contamination level is one of the key parameters in insulator design. Insulators should be tested for performance under contamination prior to installation.

The main problem under heavy contamination conditions is the contamination flashover [26]. Dry band arcs form over the wetted and contaminated surfaces, increasing the total surface conductivity and eventually the chance of contamination flashover. Details on formation of dry bands will be presented in next section. To standardize the contamination level, the ESSD (equivalent salt deposit density) parameter is defined. According to [20] , "ESDD is the amount of sodium chloride that, when dissolved, gives the same conductance as that of the natural deposit removed from a given surface of the insulator divided by the area of this surface; generally expressed in mg/cm^2." Therefore, ESDD can be used to classify the contamination level of insulators. Although soluble contaminants have a higher effect on the performance of insulators, in order to precisely classify the contamination level, non-soluble contaminants should also be taken into account. Non-Soluble Deposit Density (NSSD) is a measure for evaluating the level of non-soluble contaminants like sand and dirt. To precisely study the contamination profile

of installation sites, ESDD and NSDD paramters should be taken into account [27]. However, the impact of NSSD is very small compared to ESDD.

According to IEC standards, contamination tests inside the lab can be conducted in three ways; salt-fog tests, wet-contaminant tests, or clean fog test. For the salt fog tests, the voltage is kept constant during the whole test and the string of insulators is exposed to a salty fog condition where its salinity can be anywhere between 2.5 kg/m^3 and 224 kg/m^3 depending on the desired contamination severity. During the wet-contaminant test, the insulators are sprayed with the polluted suspension and the voltage is applied to the string shortly after the contamination process is over, while the insulators are still wet. The voltage is then raised until the flashover occurs. In case of a clean fog test, the insulators will first go under the contamination process and will be put aside to dry. The string will be hung inside a clean fog chamber and the voltage will be applied on the wetted contamination layer. This technique resembles the actual environmental conditions much better than the other test methods [27].

2.8 Formation of Dry-Band Arcs

One of the most important stages of contamination flashover is the formation of dry-band arcs. There have been several studies to investigate the formation and behavior of dry bands [28]. The leakage current starts flowing through the string of insulators when the polluted surface gets exposed to moisture. The behavior of this current depends on the how this conductive electrolyte behaves under high voltage stress. The electrical properties of a common electrolyte solution, such as NaCl solution, depend on the concentration of ions, ion charges, and the mobility of

the ions. The viscosity of water drops quickly when the temperature goes up which speeds up the movement of water ions [14]. High electric field will also make the ions move faster. Therefore, the conductivity of NaCl solution on the surface of insulators under the high voltage tends to increase. The increase in the leakage current under the high electric field stresses will increase the temperature and eventually will cause the water on the surface of insulators to evaporate, forming high surface resistivity areas known as Dry Bands. Dry bands will then experience recurring discharge activities where the surface electrical properties of both the dried and wet parts determine the magnitude of the leakage current [14, 29]. It should be noted that the sinusoidal part of the leakage current has more contribution to the water evaporation compared to the arcs and small bursts [14]. In order to investigate this behavior in one of the published studies [29], pollution layers were deposited on strips of glass while the high voltage was applied across the strip. The pollution layer was wetted inside a clean fog chamber and the voltage was measured using coupling capacitors attached to the structure. Figure 2.2 shows the steps of this observation. After wetting the strip, the dry bands appear on the surface until one dry band dominates (Figure 2.2.c). The arcs appear on this dry band and extend throughout the strip until they completely bridge the strip (Figure 2.2.f). Not all the arcs can extend to the whole strip and completely bridge the strip. Survival of the arcs from extinguishing to propagate along the strip, requires a minimum electric field which is calculated and formulated in [14].

The leakage current can be calculated knowing the voltage drop across the dry bands and the resistance of the wet polluted layer in series with it. Not all of the initial dry bands will survive to spark over. If the resistance of the band is too high, the arcs will extinguish. Further wetting will drop the resistance of dry bands and

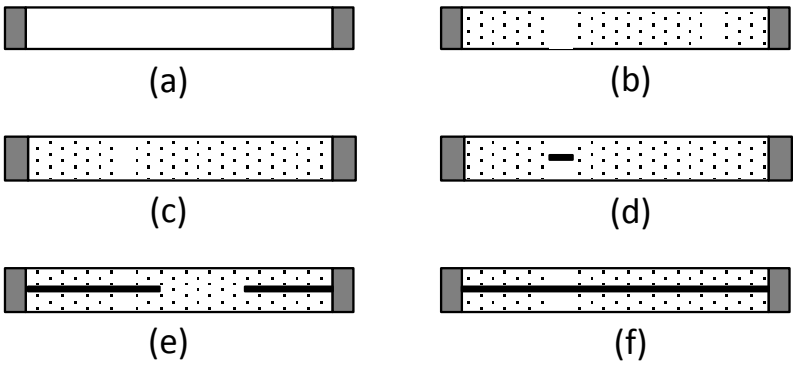

Figure 2.2: (a) Wetting the pollution layer
(b) Formation of dry bands
(c) Dominance of one dry band
(d) Sparks on the dry band
(e) Extension of arc on the surface
(f) Complete propagation of the arc along the strip (flashover)

eventually can increase the length of dry bands. When the surface contamination is high, the resistance drops significantly after wetting and therefore the arcs start to grow and bridge the insulation. In case of low surface contamination, the resistance of dry bands is quite high and local arcs continue to happen but they will extinguish eventually. The results of the study presented in [28] proves that dry contamination is harmless to the insulators. However, light contamination under wet conditions can cause continuous arcing and eventually insulation degradation and aging.

2.9 Summary

In this chapter, a brief description of transmission line insulators with their application in power networks was presented. Various types of insulators as well as advantages and drawbacks in using each type of insulator was explained. Because of a large number of porcelain insulators that are currently in service in Manitoba and

North America, this thesis focuses on condition assessment of porcelain insulators only. A short background on failure mechanism of porcelain insulators was also presented. Also the flashover mechanism due to surface contamination on the porcelain insulators was briefly discussed.

3

Condition Assessment of Porcelain Insulators–A Literature Review

3.1 Introduction

Enhancing reliability of power networks has recently become a very serious challenge for power companies. Considering the continuous electricity demand mainly due to manufacturing industries, network failures and power outages due to equipment failure can be very costly for power utilities [30, 31]. On the other hand, all the equipment installed in power networks have a limited life span and they need to be replaced before they fail in service. That is why condition assessment of all high voltage equipment, including high voltage insulators, is a very important regular maintenance in power networks. In case of transmission line insulators, defective units have to be identified and replaced before they fail. Among different types of insulators, detecting defective toughened glass insulators is very easy as the glass shell shatters when it becomes defective. In case of porcelain insulators however, the

defects cannot be identified simply by performing visual inspections. These defects can be developed either before or after the installation. The defects developed prior to installation are mostly caused during shipping, handling, and transportation. Cracks, voids, and flaws inside porcelain shells are defects that are invisible to visual monitoring and can cause failures after the insulators are installed [12]. Many inspection methods to identify faulty porcelain insulators have been reported in the literature. These methods can be classified based on their application. One way to categorize these methods is based on the symptom they detect from a faulty unit For example, thermal inspection methods identify the defective insulators by analyzing the heat distribution along a string of insulators. In case of acoustic detection methods, faulty units are detected based on the sound propagation and reflections from the insulators. Cracks inside the shells change the reflection and propagation of the incident sound wave.

Considering the electrical properties of defective porcelain insulators, they have lower resistance, can undertake lower voltage, will let a higher current to pass through them, and have a distorted electric field distribution along the string. Detection methods which use these symptoms to identify a faulty unit are categorized as electrical detection methods. The Buzz method, using DC resistance or electric field meters, and leakage current measurement techniques are examples of this method. These detection methods either need a close physical contact to the insulators or they can remotely inspect them. Methods which need a physical contact of the measuring instrument to the insulators are quite dangerous especially when a live maintenance is needed. Although remote detection methods are very convenient and safe for linemen to use, the remote detection methods that have been proposed so far are not reliable enough to substitute the widely used close contact

techniques such as DC impedance meters [4, 32].

3.2 Detection of Defective Insulators

There are different detections methods to identify defective insulators. Each method has advantages and drawbacks. Depending on the application, one might do better than the other. In this section, a brief summary of the most commonly used inspection tools for condition assessment of porcelain line insulators will be presented.

3.2.1 Close Contact Methods

One of the most commonly used techniques by linemen to identify faulty insulators is inspecting each insulator shell by connecting a resistance measuring instrument across the shell. The two popular instruments that are developed based on this concept are the Buzz meter and the DC resistance meter. This method of inspection is considered to be a quite low-tech detection tool for linemen to use. As shown in Figure 3.1, in the Buzz method, two sharp pins on the inspection rod will be connected across each shell. If the shell is not defective, a breakdown will occur between the pins because of the high voltage across the pins and a Buzz noise can be heard. But if the shell is damaged, there would be no significant voltage drop across the pins and the breakdown will not happen. This method can only be used for porcelain insulators as they have the metallic cap and pin that the rod can connect to [12].

The resistance of the shells should ideally be very high if they are not damaged [33]. When they become defective, the resistance drops and the current

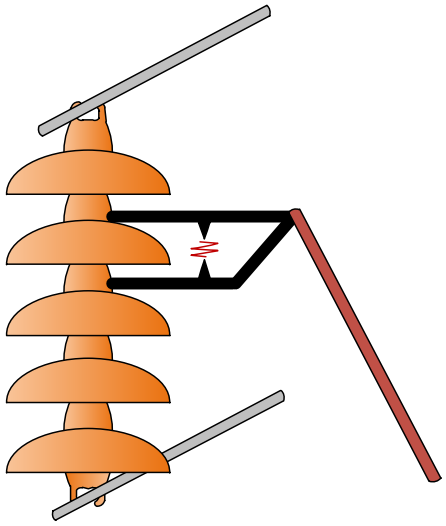

Figure 3.1: Detection of defective insulators using the Buzz method.

starts flowing through them. Another simple method to inspect porcelain insulators is to connect a DC resistance meter to the string and measure the resistance of each shell. Defective shells show a lower resistance on the meter compared to the healthy shells. This method is also very effective in detecting internal conductive paths inside the insulating material. However, using this inspection tool on live lines is not as convenient as the remote detection methods. Moreover, the low resistance can also be a result of high contamination on the surface of insulators and the DC resistance meter is not able to determine the possible reasons of the low resistance readings [34].

3.2.2 Acoustic Detection Methods

Detecting acoustic emissions from a faulty insulator is one of the inspection methods than can be used to identify the defective insulators. Partial discharge activities on

defective insulators make an audible noise as well as electromagnetic radiations in the ultrasound band. These radiations can be captured by ultrasonic microphones. When there are surface discharges on the insulators, electrons start to move more rapidly which will ultimately create an acoustic wave. This acoustic wave travels in the ultrasound band and its frequency is centred at 40 Khz [35]. Although this method has been used in detection of faulty outdoor insulators, it has more applications in detecting and locating the PD inside the transformers [36]. The main difficulty with the acoustic PD detection on outdoor insulators is the relatively high background noise levels near the live insulators in service.

3.2.3 Ultraviolet and Infrared Detection Methods

Partial discharges also emit light that can be captured and analyzed to assess insulators conditions. There are commercially available UV cameras that can be used for imaging and monitoring outdoor insulators. However, sun light and other ultraviolet waves that exist during the day time will affect the performance of these cameras. Because of these interferences during the day, inspection of insulators using these cameras are mostly carried out during the night. Light emissions due to partial discharge activities inside voids were the topic of one of the recent studies [37]. It was shown that there is a good correlation between the light emissions and the magnitude of partial discharge pulses. For the measurement setup, a 7 kV square pulses was used as a source of electric stress and a wideband Photomultiplier tube was used to capture the light emissions. The captured signals were fed to a 5 GS/sec and 500 MHz oscilloscope and then transferred to the computer for further analysis. Voids with different geometries were tested and the relation between the dimension

of the voids and the corresponding light emissions was studied. In another study on non-ceramic insulators [38], UV cameras were utilized to identify and locate different types of corona. Corona can be present at the live end fittings especially when the corona ring is not used. Newer UV cameras can detect the light emissions even during the day. These cameras can detect certain frequency components that are still below the frequency of natural daylight. They are capable of filtering daylight emissions and also enhancing the image resolution.

Infrared cameras are capable of detecting the temperature distribution on the insulators. Insulators temperature can rise due to corona, leakage current on the surface, arcs on the dry-bands, and even punctures inside the insulation. In one of the latest studies on detection of faulty insulators on live lines, Infrared cameras were used to double check the results obtained from acoustic receivers [39]. The pictures taken by the camera still need to be interpreted by trained personnel in order to evaluate the condition of insulators. The camera is also very sensitive to the environmental condition such as local weather, season, and illumination. In order to have an accurate reading from the camera, the maximum and minimum temperature should be entered manually into the camera considering the ambient temperature. The pictures can also be transferred to a computer to detect high temperature spots and further analysis.

In summary, Although the pictures taken by these cameras contain valuable information about insulators condition, a successful assessment of their condition requires additional testing and investigation.

3.2.4 Leakage Current Analysis

Monitoring the leakage current waveform can reveal useful information about insulators condition, especially in evaluating the contamination level of insulators. One way to classify the contamination severity of porcelain insulators is using the ESDD method which will be discussed in more detail in Section 4.2.6.1. However in order to determine the contamination level of an insulator using ESDD method, the unit has to be taken down to the lab for the measurements. In other words, this method cannot be used for live line maintenance purposes. The alternative method for measuring the contamination severity of insulators is monitoring the leakage current. There are quite a few parameters in the leakage current pulse that can be monitored in order to prevent a contamination flashover. Maximum value of the leakage current, number of pulses and location of the highest peak of the pulses are examples of these parameters [40, 41]. To properly study the leakage current pulses, time domain and frequency domain characteristics of the waveform should be taken into account. The leakage current can go through three stages before the actual flashover takes place. These three stages are security, forecast, and danger stages. The leakage current is much larger during the forecast and danger stages compared to the security stage. However, the duration of the pulses are shorter in those stages. If the possibility of a contamination flashover is detected in early stages, there would be enough time to avoid it. Most of the research on leakage current monitoring is focused on time domain analysis of the pulses. Some recent studies have been focused on the frequency domain parameters and how monitoring other harmonics can lead to an early diagnosis of a contamination flashover [42]. The effect of RTV (room temperature vulcanization) silicone coating on the long term withstand performance

of porcelain insulator been investigated in another study by monitoring the leakage current [6]. The relation between the ESDD level of contaminated insulators and the flashover voltage has also been studied while monitoring the leakage current [5].

Contamination along with the operating voltage and environmental conditions are the three important factors in developing a flashover. Environmental factors are mostly the temperature and relative humidity. However, the impact of humidity is much higher than the temperature on the development of a flashover.

3.2.4.1 The Effect of Humidity

High ambient humidity and heavy surface contamination are the two most common reasons for high leakage current. Properly distinguishing the source of this increase in leakage current can be quite challenging. High leakage current due to high ambient humidity is a false positive output when using this method. In [24], to properly distinguish the source of high leakage current, two tests were conducted. During the first test, already contaminated insulators were kept inside a fog chamber and the humidity inside the chamber was varied in order to study the effect of humidity. During the second experiment, the contamination level of insulators was changed throughout the tests where the humidity of the chamber was kept constant. The results of these measurements were used to distinguish the effect of humidity and contamination level on the leakage current waveform, reducing the number of false alarms in detecting contaminated insulators.

3.2.4.2 Leakage Current Monitoring

To duplicate the realistic environmental conditions during contamination tests, a fog chamber is required. The leakage current waveform can be monitored through the

ground wire that connects the insulators to the ground. To take samples from the ground wire, two methods can be used. The current signal can be either measured from the voltage drop across a resistor in series with the ground wire or can be measured using current sensors such as Rogowski coils. The contamination distribution on the surface of insulators in the service is a function of different parameters such as wind direction, elevation, and etc. For the lab tests, however, a uniform distribution of the contamination layer on the surface of insulators is assumed. To make artificially contaminated insulators, a salty suspension will be sprayed on the insulators. Details of this procedure will be discussed in Section 4.2.6.1.

3.2.4.3 Frequency Domain Analysis of Leakage Current

Frequency domain analysis of leakage current is basically monitoring the power of different harmonics. It has been shown that by increasing the relative humidity and contamination severity, the amplitude of the 60 Hz component of the leakage current has the most significant increase. Also the amplitude of the third and fifth harmonics change significantly when the contamination is high [43]. In another study [7], the leakage current waveform is classified into six stages before the occurrence of flashover. The classification is based on the frequency spectrum of the leakage current waveform. The experiments showed that the insulators with heavy contamination will ultimately have a flashover. On a heavy contaminated insulator, the leakage current waveform was captured and monitored [7]. In time, the leakage current waveform shows some distortions compared to the smooth sinusoidal waveform that was captured at the beginning. After 12 minutes of testing the heavy contaminated insulator, the leakage current waveform started experiencing

all the six stages starting from a smooth and low amplitude sinusoidal waveform to a distorted waveform with relatively high power harmonics [24]. It was reported that in all cases that contamination flashover ultimately happened, the third harmonic amplitude of the leakage current spectrum exceeded - 40 dBA. They also reported that the information in the fifth and seventh harmonics cannot predict whether the flashover is happening or not. This conclusion came from the observation of leakage current power spectrum during the test where those two components remained almost unchanged from the beginning of the test until the flashover occurred.

3.2.4.4 Phase Angle Analysis

Studying the time domain parameters of the leakage current waveform can reveal important information about the contamination severity of the insulators. There are numerous studies on the rise time, duration, amplitude, and other time-domain parameters of the leakage current waveform [44, 45]. The phase angle between the voltage and the current is one of the important time domain characteristic of the leakage current waveform. During clean and dry conditions, applied voltage and leakage current resemble an RC circuit where the current leads by almost 70 degrees. This relation stays the same for the case of dry polluted insulators. But in case of wet contaminated insulators, the phase difference is significantly lower (almost 30 degrees) and also the amplitude of the leakage current is higher [8]. The pollution layer becomes conductive when it is exposed to the moisture and therefore the phase angle decreases. Under heavy contamination the phase difference could be as low as 5 degrees. This means that under wet contamination, the overall system acts more like a resistive circuit. By just inspecting the phase difference, the clean dry insulator can be distinguished from a wet contaminated insulator. But as soon as

the phase angle drops due to wetting, it is very challenging to identify the reason of further phase angle drop. In case of a dry polluted insulator, there are few stages before the contamination flashover happens. The phase drop is significant when the pollution layer gets exposed to the moisture, but during the development of short dry-band arcs and the growth of those arcs to long arcs and even the flashover, the drop is not that significant and therefore it is very hard to assess insulators condition in those stages by just measuring the phase difference. The other difficulty in using this method is differentiating humidity and the pollution as they both increase the conductivity of the surface and result in a phase drop.

3.2.4.5 Time–Frequency Analysis

Wavelet is a time-frequency analysis tool that can be very useful in analyzing the leakage current. The application of wavelet is not limited to the leakage current and it can be used in a wide range of applications to analyze the captured information. In [8], using a discrete wavelet transform (DWT) and multiresolution signal decomposition (MRSD) techniques, the time-frequency characteristic of the leakage current was studied. A standard single disc cap and pin porcelain insulator was put under 11 kV rms, 50 Hz voltage source to assess the contamination level. The insulator was hung vertically inside a 1.5m × 1.5m × 1.5m clean fog chamber. The leakage current is sampled through a resistor in series with the ground wire. The leakage current was then sampled and stored on a computer for further analysis. The leakage current was decomposed into seven levels using wavelet functions. The standard deviations and the mean of each decomposed signal in each level was studied. The distortion ratio is defined as the ratio of standard deviation value of detailed components # 3, 4 and 5 to fundamental component # 6. The distortion

ratio increases considerably when the short arcs appear and it decreases when the arcs start to grow into long arcs. Plots of standard deviation versus decomposition level are presented in this work to explain the behavior of each detailed component at different flashover stages. The fifth detailed component also changes quite significantly during different stages which can be used towards stage identification.

In another recent study [46], a flat glass sheet was used to model an outdoor insulator. This structure was proved to be a very good laboratory model for an outdoor insulator. Two electrodes were mounted on a flat glass sheet to generate electrical stress. The source is a 50 kVA/300 kV RMS, 50 Hz transformer. The surface of the glass was sprayed with a salty solution and different salinities in order to study various contamination levels. Frequency domain tools were applied on the sampled data in order to study the spectrum behavior of recorded data. For analyzing the voltage waveform, however, a continuous wavelet transform and a complex Morlet wavelet transform were used. The behavior of wavelet coefficients in different contamination levels was studied.

3.2.5 Electric Field Measurement

Electric field distribution along the insulators string is one of the important parameters that should be considered during insulators design. High electric field stress on the string can cause audible noise, partial discharge activities, and eventually deterioration of the dielectric material. Studying the electric field distribution around the insulators can avoid the occurrence of flashovers. It has been shown in [14] that when the surface electric field component is sufficiently low, the flashover will not occur. Electric field distribution along the insulators

string can also be used to detect defects on each unit. Instead of solving the complicated structure of insulators string to obtain an analytical solution, computer aided simulation software can be utilized [47]. Many computer aided simulation projects based on different numerical methods such as, finite element method, finite difference method, or boundary element method have been conducted to calculate the electric field distribution and electric potential graphs along the string of insulators [48, 49, 50, 51]. The modelled electric fields have also been compared to the measurement data taken from electric fields along the insulators string in service. Figure 3.2 shows a test setup for measuring the electric field of energized suspension insulators. The DL-1 electric field sensor mounted on the top of a rod has to get close to the energized insulators and capture the fields [52]. The captured data will be transferred to a data logger using a coax cable or a fiber optic link for further analysis. The electric field probe slides along the string and measures the RMS electric field. Some simple methods just use the electric field along the axis on the string to make the decisions of the insulators condition. However more advanced methods take into the account both the radial electric field component(E_r) and the electric field component along the axis of the string (E_z). The electric field method has been reported to have a very good accuracy in detecting conductive defects [52]. The electric field is low near the shells close to the low voltage conductor and starts rising smoothly when it gets closer to the shells near the high voltage conductor. Having a defect in one of the shells, causes a sudden drop in the electric field value close to that defect. Electric field graphs from the string with defects can be compared to the graphs with a string of all healthy insulators to locate the faulty shells. Differences in the graphs are more obvious when the defects are closer to the high voltage conductor. It is harder to identify the defects close to the low

voltage conductor. It should be also noted that when a corona ring is used at the high voltage side, it will be very hard to identify even the defects close to the high voltage conductor [47].

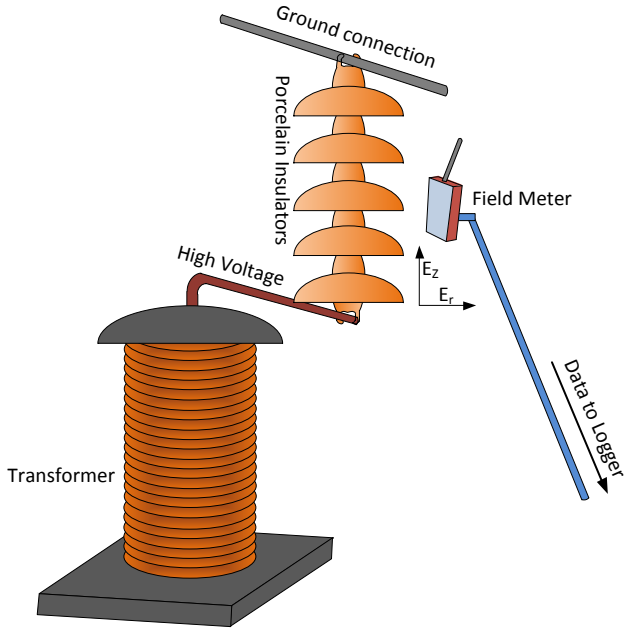

Figure 3.2: Electric field measurement of porcelain insulators.

3.2.6 RF Radiation Detection Method

Partial discharges result from fast movement of electrons. The movement of electrons not only creates the leakage current, but it also creates electromagnetic waves that will radiate. Rapid changes in the current due to the fast movement of electrons extend the spectrum of this waveform to a higher frequency region (around 200 MHz [53]). Using proper antennas designed for the appropriate frequency range, partial discharge radiated pulses can be captured. In one study [54], radiations from a spark gap breakdown were captured using disk-cone antennas. An optimization on

the location of antennas for receiving the best radiation was also performed. The sharp risetime of partial discharge pulses can be easily detected using high frequency sampling and time domain analysis. In another study [55], antenna arrays were mounted on a vehicle to make a mobile RF emission detector. The signals received through the antennas were fed into a 2.5 GS/sec oscilloscope with a bandwidth of 1 GHz. The antenna arrays have a flat frequency response between 100 MHz and 3 GHz. The oscilloscope has a segmented memory feature which allows storing multiple PD pulses without storing the dead time in between them. To analyze the received signals, two diagnosis methods were used; Bearing calculation and RMS time delay error. Bearing calculation method calculates the angle of the incident radiation using wave propagation constant and arrival time delay. When there are just two antennas for receiving the radiations, it is not possible to know if the angle is above the antenna plane or below. This issue can be resolved by using four antennas. RMS time delay method locates the source of radiation more accurately. One of the four antennas was considered to be the reference antenna and the time delay for a signal to travel from the source to each antenna was defined as,

$$T_n = \frac{1}{c}\sqrt{(x_n - x_s)^2 + (y_n - y_s)^2 + (z_n - z_s)^2} \tag{3.1}$$

where (x_s, y_s, z_s) are the coordinates of the source and (x_n, y_n, z_n) with $n \in \{1, 2, 3, 4\}$ are the coordinates of the antennas. Knowing the reference antenna, the delay time differences can be calculated as

$$T_{n1} = T_n - T_1 \tag{3.2}$$

The error function is also defined as,

$$\epsilon_s = \sqrt{\frac{(T_{21} - \tau_{21})^2 - (T_{31} - \tau_{31})^2 - (T_{41} - \tau_{41})^2}{3}} \tag{3.3}$$

where τ_{n1} is the measured time delay between the antenna array n and 1. By sweeping the location of the source and minimizing the error function, the defective unit can be located. As for the field measurement, the researcher took the mobile RF emission detector to a reportedly high RF radiation area near an electrified railway and a 132 kV transmission line. The source of radiations was unknown. The vehicle was parked in two different positions for one hour at each position and gathered 371 samples at each location. Six imaginary sources of radiation were assumed to be at the location of each high voltage string of insulators on the transmission line. The source of radiation was identified by minimizing the error function.

3.3 Classification of Partial Discharge

Modern insulation systems can have different types of insulations such as solid, liquid, or gas insulating materials. Partial discharge in any of type of these insulating materials can degrade the insulation performance and eventually cause system failures. Understanding the partial discharge mechanism helps developing inspection tools to detect and locate the source of partial discharges, one of the essential stages in insulation system monitoring. Signal processing techniques play a big role in this stage by finding unique behaviors in time domain, frequency domain or time-frequency domain parameters of the captured data. A lot of effort has gone into classifying the partial discharges based on the behavior of one or more of these parameters. Studies have shown [56, 57, 58] that because of the randomness of a

partial discharge process, statistical analysis can be a great tool for classification of this random phenomenon. Identifying the source of PD pulses can be summarized into a two stage procedure; extracting the unique information from the captured PD pulses followed by classification and recognition of the source. A survey on partial discharge classification [59] has put to together a wide range of classifiers, feature extraction techniques and pattern recognition methods. Classifiers can be categorized based on the decision function that they use. In the rest of this chapter, classifiers with different decision functions will be briefly discussed.

3.3.1 Distance Function Classifiers

These PD classifiers have a reference library for each class of PD sources. For each unknown measurement, a distance function will be defined and the unknown measurement will be assigned to one of the library reference classes based on the decision made by the distance function [60]. Two examples of these classifiers will be discussed here.

3.3.1.1 Minimum Distance Classifier

This classifier calculates the distance between the vector of unknown PD measurements and the library references [61]. For example, if there are M possible PD sources, then $P_1, P_2, \cdots, P_M$ are predefined vectors corresponding to each class. If x is an unknown PD measurement, the distance of x from the library reference i can be defined as,

$$d_i = \frac{1}{N} \sum_{j=1}^{N} |x_j - m_{ij}| \qquad i = 1, 2, \cdots, M \tag{3.4}$$

where N is the size of vector x. The classifier finds the lowest d_i and assigns x to the i^{th} library.

3.3.1.2 Polynomial Classifier

This classifier converts the measurement vector x to a single score value using a decision function [62]. The decision function is made out of sets of polynomials. The simplest classifier in this group is the linear classifier. The decision function for its i^{th} class is calculated as

$$d_i = w_{i0} + w_{i1}x_1 + w_{i2}x_2 + \cdots + w_{iN}x_N \tag{3.5}$$

where w_{ij} represents the coefficients of the polynomial in the decision function and x is the measurement vector. The matrix representation of this classifier would be

$$D = W \times X \tag{3.6}$$

where W is the weighting matrix with M rows and $N+1$ columns, D is the decision matrix and X is the matrix with all the measurement vectors. If there were L events captured during the tests, then x has $N+1$ rows and L columns. Each column in D represents the output of the decision function for each of the measurement vectors in x. If the decision making function is based on the maximum likelihood function, then in order to assign specific vector x to class i,

$$d_{ij}(x) > d_{kj}(x) \qquad \text{for all } k \neq i \tag{3.7}$$

3.3.2 Statistical Classifiers

These classifiers assess the statistical behavior of the recorded PD measurements and classify the unknown measurement into one of the previously known classes. Generally they can be divided into two groups; Bayes classifiers and recognition rate classifiers [63].

3.3.2.1 Bayes Classifier

The decision function for this classifier is based on minimizing the probability of assigning the unknown measurement vector to the wrong class based on the maximum likelihood criteria [62]. The training sequence will produce the mean vector and the covariance matrix. Having these statistical properties from the training data files, a multivariate density function will be defined to calculate the probability of the unknown measurement vector x belonging to each of reference library classes.

3.3.2.2 Recognition Rate Classifier

In this algorithm, some feature vectors are built from the statistical properties of sampled measurements of already known PD sources [64]. For every known PD source, the mean, standard deviation and the 95% confidence interval are calculated from several samples that have been taken from that source. Depending on the algorithm, other statistical properties can also contribute to the feature vector. Then, for each unknown measurement, each of these statistical properties will be calculated and the algorithm checks if the calculated value lies in the 95% confidence interval of any of the library classes. If it does, one score will be given to that class.

All the parameters get checked with the same technique and at the end, the class with the highest score will be assigned to the unknown measurement vector.

3.3.3 Support Vector Machines (SVM)

In one of the latest studies [65], previously recorded partial discharge measurements from known sources were used to evaluate the capability of the SVM technique to differentiate PD sources. The SVM method is based on statistical learning theory. To understand the fundamental principles of this technique in differentiating different sources, an optimal hyperplane problem is shown in Figure 3.3.

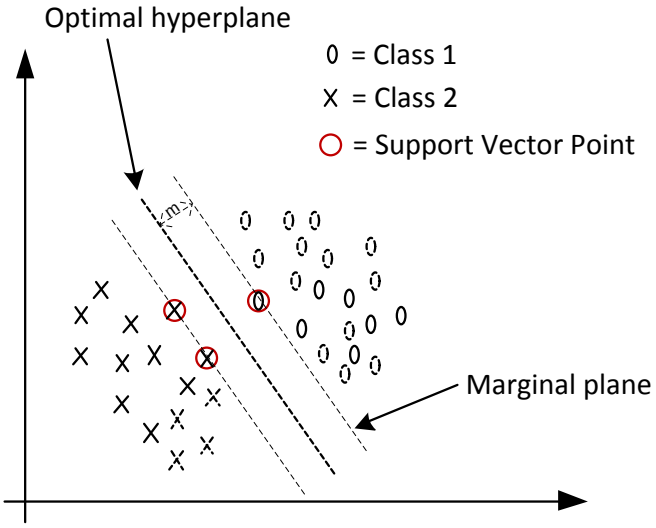

Figure 3.3: Hyperplane problem to illustrate SVM methodology.

A hyperplane is introduced between two sets of separable data classes with margin m. The points on the marginal plane form the support vector and the optimal plane can be driven from support vector points. The optimal hyperplane will be iteratively calculated using training sequences. Support vector points will be stored after each training sequence and the rest of the points will be discarded.

When the training is over, the hyperplane can be applied on unknown data classes to identify each class. Classification of the data classes that are not linearly separable can be quite challenging. Therefore, mapping the input data into a higher dimension space can be a very effective solution to those problems.

For intelligent PD classification algorithms, feature extraction is very critical. Feature extraction involves extracting the most valuable and unique behavior of the parameters from the available information and then mapping them into higher dimensional spaces. Principle component analysis (PCA) is another tool that can be used in conjunction with this method to optimize the mapping. PCA can maximize the linear separation of the data points after mapping. PCA produces a matrix with the same dimension of the input matrix where the first two columns in that matrix contain more than 80% of the total variance of data [66].

3.3.4 Power Spectrum Classifiers

A number of unique features of partial discharge pulses can be found in their power spectrum. No matter where and how the PD samples are taken, power spectrum analysis can reveal distinct properties of the PD source. In one of the latest studies [24], the PD pulses sampled from the leakage current were analyzed using the power spectrum analysis using the amplitude of the Fast Fourier Transform. The goal in this research was to develop a pre-warning stage for monitoring outdoor insulators when the contamination severity is high. Power spectrum estimation of the PD pulses is carried out using parametric auto-regressive (AR) model. Calculation of the estimated AR model is published in [67]. To compare the effect of humidity on the power spectrum, insulators with the same contamination level are placed in the

fog chamber with different humidity levels. To study the power spectrum behavior, plots of the amplitude of the Fast Fourier Transform for each case was developed. Also the harmonic levels in each of those graphs were measured to relate harmonic powers to the contamination severity.

3.3.5 Neural Network and Fuzzy Logic Based Classifiers

The concept of neural networks has been successfully applied to many different PD classification problems. The ability to learn from the previous sets of measurements to improve their performance is a remarkable feature of these classifiers. The performance and methodology of the classifiers in this group could vary based on the way the neural network has been designed. More details on different types of this classifier can be found in [68, 69, 70].

The feature vectors extracted from the measurement data are usually not clear enough to be used for differentiating PD sources. Fuzzy logic classifiers try to map the feature vectors into membership values of fuzzy sets which are defined over the fuzzy domain. The decision making process consists of three steps; fuzzification of the feature vector, inference engine and defuzzification. Although the nature of these classifiers is the same, some classifiers have slightly different classification methodology. For example, in one study [71], the feature vector was first mapped into the membership values and then the probability of that feature vector belonging to each class was calculated. The class with the highest probability will be assigned to that feature vector.

3.3.6 Performance Assessment of Classifiers

One of the first steps after collecting the PD samples from a faulty unit is to decide whether to use the phase information or not. Some researchers believe that classification can be done without using the phase data where others find it easier to do the classification using the phase information. It is almost impossible to compare the performance of all the proposed methods in the published literature. The lab conditions, the source of PD pulses, the assumption made in each case study, the setup configuration and many other parameters are different in each study. However, the rate of successful recognition of unknown PD pulses according to what authors have claimed is the only assessment that we can discuss here. A 70%-80% success rate was reported in [61] using the minimum distance and neural network classifier where gas insulated switch gears were studied. There have also been some successful rate of recognition using statistical classifiers in [64, 72]. In [57], a two parameter Weibull probability density function was fitted to the amplitude of recorded measurements from PD activities with successful results. In another study [73], the feature vector was extracted from the PD measurements using different signal processing methods. Among all the classifiers that were studied during their work, the minimum distance classifier had the highest successful rate of recognition.

3.4 Data Processing Methodology of This Thesis

Based on the publications discussed earlier in this chapter, the classification methods using the phase resolved data are reported to have very successful classification rates. These classifications locate the PD activity on the 360 degree phase domain and build a comprehensive reference library for each defect. Besides the publications available

in the literature on advantages of using phase resolved data, the leading technology in the industry for partial discharge detection during commissioning tests of other high voltage equipment, such as underground cables, is also based on phase resolved analysis [74, 75].

Because of the random nature of partial discharge pulses, statistical analysis of PD pulses reveals valuable information on the source of discharges. During the literature review of this thesis, publications with high successful classification rates either developed statistical classifiers or distance classifiers using extracted statistical features of PD pulses. Another advantage of using statistical features versus time domain pulse characteristics of PD pulses is avoiding misleading and inaccurate classification of PD sources based on one dominant PD pulse. The statistical features derived from analyzing many partial discharge activities can identify the trend of discharges and better categorize the source of discharges.

After performing a preliminary round of measurements and analysis during the initial stages of this research [10], a number of different probability distribution functions were studied to find the best statistical function that can represent the trend of discharges. There has been previous research providing physical justifications for the use of Weibull statistics in the assessment of dielectric breakdown [76]. Keeping in mind the application of Weibull distributions in describing the dielectric breakdown process and the successful preliminary results on using Weibull distributions for data processing of the captured radiations, a Weibull probability distribution function was selected as the main statistical feature to represent the partial discharge behaviors. Weibull probability density functions are known for describing and analysing the trend of partial discharges in other publications as well [57, 58, 77, 78]. However, the weighted phase resolved Weibull

distribution (Section 5.1.3) introduced in this thesis has never been reported for analysing and classifying the PD sources.

It should be noted that there is a broad range of parameters that can be extracted from the recorded measurements to be used by the classification algorithm. During the early stages of developing the data processing algorithm, there were many other features that were calculated and extracted from recorded measurement in order to enhance the classification. However, many of these extracted features, such as higher statistical moments, concurrent discharge behaviors, etc. did not show distinct information about the PD sources of defective insulators and therefore were discarded from the classification algorithm.

A number of publications [79, 80] have reported successful classification of PD pulses using the fractal dimension. Other publications have reported unique features in the spectrum of partial discharge pulses [24, 67, 81]. Combining the two concepts, a frequency domain fractal feature was included in the data processing feature extraction algorithm. This parameter was described based on the transform fractal feature introduced in [82]. More details on calculating the frequency domain fractal feature is presented in Section 5.1.4. This feature along with the statistical features extracted from the PD activities (Section 5.1) are the main outputs of the feature extracting algorithm.

After finalizing the selection of features that will be extracted from the PD pulses, a proper classifier is required to classify the type of insulators based on the extracted features of PD pulses. After extracting the features from all the normal, punctured, and contaminated insulators, it was clear that a linear classifier will not be able to separate the source of defects in any of the feature domains (Section 5.3.1 explains the classification challenges in more detail). The classifier not only should be able

to calculate non-linear decision boundaries in the feature domains, it also should be able to account for mislabelled observations and maximize the margin of the decision boundary (also known as soft margin capability). Amongst the classifiers presented in Section 3.3, the SVM classier was the best solution for this application since it had both of the required capabilities. The SVM classifiers can map the observation points to higher dimension feature domains where the observation points are linearly separable and then return the linear decision boundary in the higher domain into the original feature domain where the linear decision boundary will be translated into a polynomial in the feature domain (also known as kernel trick). The SVM classifiers which are basically non-linear distance classifier with the capability of classifying overlapped data points using the soft margin algorithms, have also been successfully used in other PD classification problems [56]. In many classification problems, such as the PD classification in this thesis (Section 5.2), there are many overlapping feature points in the feature domains where the SVM classifier can find a maximum margin hyperplane and minimize the number of mislabelled data points by taking advantage of the polynomial kernel mapping feature.

3.5 Summary

In this chapter, a summary of available inspection methods for assessment of defective porcelain insulators was presented. The difficulties and advantages involved in using each method was discussed. The data processing involved in classification of defective insulators includes extracting features with distinct information about the source of defect and training a classifier to properly differentiate the type of defects. A selection of classifiers that have been reported

in publications for PD pattern recognition was also presented. Moreover, the data processing techniques and the classifier selected for classification of defective insulators in this thesis were described.

In a one of the recent publications in this field [83], failed insulators in service were taken to the lab where the performance of four different types of inspection tools on detecting the failed units were investigated. The study reports that out of 460 failed units tested by all four inspecting tools, RF tools and Ultrasound tools properly identified 69% and 41 % of the failed unit respectively. However, the infrared and ultraviolet tools did not identify any of the failed units.

Other publications using ultrasound techniques for detecting defects on porcelain insulators have reported separable time and frequency features on captured sound waves [84], however no classification was performed. Similar research on contaminated glass insulators using captured ultrasound emissions concludes the indications in time and frequency domain that can be used for early detection of contaminated insulators, however no classification was reported [85].

4

Experimental Setup

This chapter describes the lab measurement setup and data analysis. The initial measurements were performed in the High Voltage Lab at the University of Manitoba. The test procedure developed in this thesis also involves a number of IEC standards that will be discussed in this chapter. A MATLAB [86] based graphical user interface (GUI) was developed to perform the data analysis, feature extraction, and classification on the recorded measurements. Details on the signal processing analysis performed within the GUI interface will be also presented in this chapter.

4.1 IEC Standards Referenced in this Research

The test procedures performed in our study are mainly adopted from IEC, IEEE, and CIGRE standards. Although IEEE and CIGRE standards have been used as a reference for some of the tests, the main reference library for most of the tests was adopted from IEC standard libraries. The testing procedures in this research are mostly based on three IEC standards that will be discussed in more details here.

4.1.1 IEC 60507: "Artificial pollution tests on high-voltage insulators to be used on a.c. systems"

The IEC 60507 [20] is focused on artificial pollution tests on insulators. It addresses two different ways of making contaminated insulators; salt fog method and solid layer method. The salt fog method requires a salt fog chamber which was not available in High Voltage Lab at the University of Manitoba. However, the solid layer method does not require a salt fog chamber and the procedure only involves depositing the specified suspension on the insulators. The details of these methods have been explained thoroughly in the standard. One of the most important steps during testing the artificially polluted insulators made by the solid layer method is properly wetting the insulators. The standard explains two possible techniques; wetting before and during the energization or wetting just after the energization. The procedure of washing off the contaminants is also described. Reference tables explaining the relationship between the salinity, volume conductivity and density of the solution are also available in the standard. The correction factors for temperature variations as well as all the equations for calculating Equivalent Salt Deposit Density (ESDD) of contaminated insulators are also presented in the standard. The IEC 60507 standard was mainly used in creating contaminated insulators in the lab and calculating their contamination level (Section 4.2.6.1).

4.1.2 IEC 60815: "Selection and dimensioning of high-voltage insulators for polluted conditions"

The IEC 60815 [27] is mainly focused on evaluating the contamination severity at installation sites. The standard also provides guidelines and recommendations on

selecting proper insulators knowing the site contamination profile. For final selection of the insulators, the insulators should be tested for contamination withstand. The insulators with the best results will be selected for the installation. It should be noted that there have been some inconsistencies in the relation between the ESDD and site severity in different standard definitions. Table 4.1 shows different definitions based on IEEE, IEC and CIGRE Standards [27, 87, 88].

Table 4.1: Comparing available standards for site severity definitions based on the ESDD level.

Site Severity	**ESDD (mg/cm^2)**		
	IEC	**IEEE**	**CIGRE**
Very Light	–	0 – 0.03	0.015 – 0.03
Light	0.03 – 0.06	0.03 – 0.06	0.03 – 0.06
Medium	0.1 – 0.2	0.06 – 0.1	0.06 – 0.12
Heavy	0.3 – 0.6	> 0.1	0.12 – 0.24
Very heavy	–	–	0.24 – 0.48

In our study, we followed the IEEE definition for labelling site severity levels [87]. Although labelling the site contamination severity has been reported differently in these standards, the definition of ESDD is the same in all of them. The definition of contamination severity and the standard procedures for measuring it was adopted and used in this thesis (Section 4.2.6.1).

4.1.3 IEC 60383-1: "Insulators for overhead lines with a nominal voltage above 1000 V"

The IEC 60383-1 [89] mainly focuses on performing standard tests on AC high voltage porcelain and glass insulators. The details of different tests such as type tests, sample tests, and routine tests are described and the verification criteria are given. For electrical tests, the standard atmospheric conditions as well as

the correction factors for different atmospheric conditions are provided. Test procedures for lightning impulse testing and the acceptance criteria are described. Details on the puncture withstand test on porcelain insulators are also presented in this standard which is particularly of interest to this research. According to the puncture withstand test, the insulators should be immersed in a tank full of liquid insulation material when the high voltage is rapidly applied across the insulators. The procedure for electromechanical failing load test is also described. The characteristics of the load, the distribution of voltage stress on the string and the acceptance criteria are presented. Few other test procedures such as thermal-mechanical performance test and temperature cycle tests are also available in this standard. The IEC 60383-1 standard was mainly used in creating punctured insulators in the lab based on the puncture withstand test described in the standard (Section 4.2.6.2).

4.2 Lab Test Setup

Figure 4.1 shows the main equipment arrangement for the test setup. The test setup consists of a high voltage source, a divider, an RF receiver, an oscilloscope, and the string of insulators under test. When the HV source is energized, the insulators inside the clean fog chamber will experience high voltage stresses, resulting is partial discharge activities. The divider provides a synchronised waveform of the HV source for phased resolved analysis. The radiation captured by the RF receiver and the leakage current waveform measured by the CT are present at the oscilloscope input terminals for sampling and storing. Copper braided wire was used for grounding the insulators string. It should be noted that all the recorded measurements during

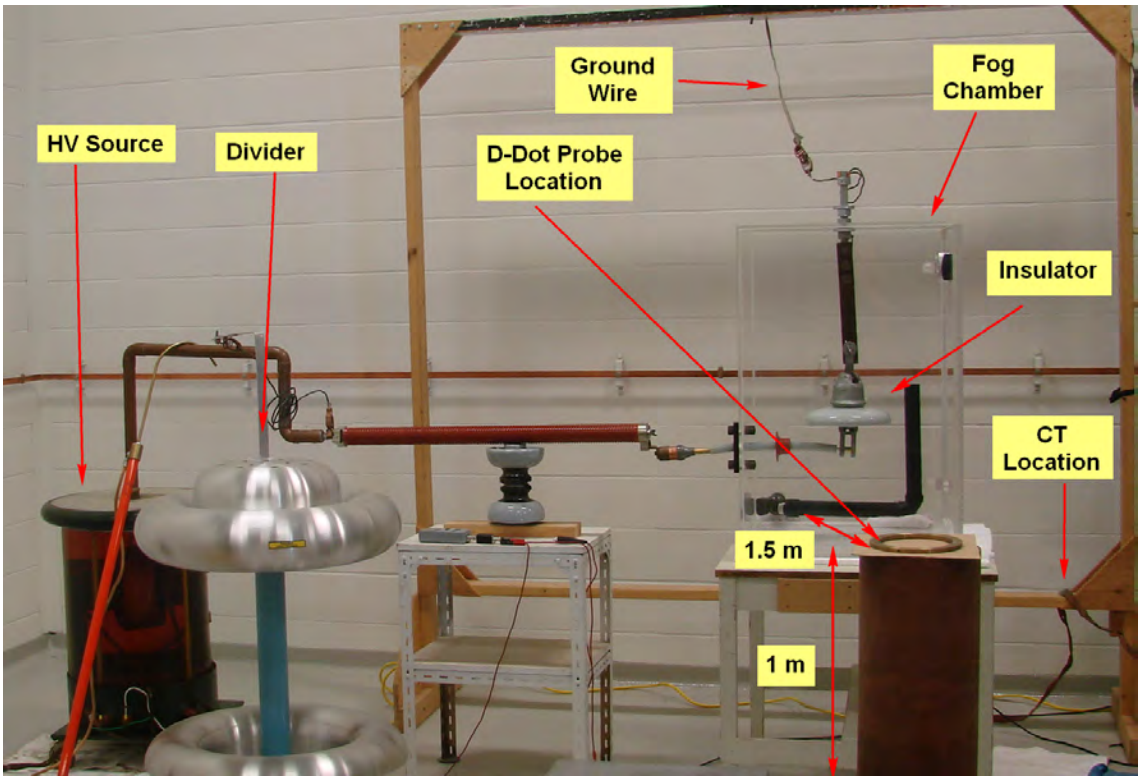

Figure 4.1: Test arrangement in the High Voltage Lab.

this research always included two insulators on the string while the condition of the insulator attached to the high voltage bus was different depending on the test scenario.

4.2.1 High Voltage AC Transformers

Two different high voltage sources were available in the Lab; a 45 kV oil filled transformer and a 230 kV potential transformer.

- **45 kV Oil Filled Transformer:**

The initial measurements were performed using the 45 kV oil filled transformer

that is shown in Figure 4.1. To control the output voltage of this transformer, a variac was placed in the circuit to adjust the output voltage. A calibration was performed under no-load conditions and the reference calibration graphs were developed. A multimeter connected to the primary input of the variac can precisely read the input voltage of the variac. Using the readings on the multimeter and the reference calibration graphs, the output voltage can be found at any time during the test.

► **230 kV Potential Transformer:**

Figure 4.2: 230 kV potential transformer.

The 230 kV potential transformer, as shown is Figure 4.2, was the main power supply for the lab measurements. Potential transformers are classified as instrument transformers. The main application of these transformers is stepping down the voltage for the measuring instruments to get a proper reading off the line voltage. However, they can also be used as power sources to provide the power to the circuit. Due to low power ratings on these units, caution should be taken before energizing the circuit with these transformers. The short circuit characteristics as well as the overvoltage ratings should be considered for each test. Same as the 45 kV transformer, a variac was used to adjust the output voltage. A calibration has also been performed on this unit to develop the primary-secondary reference calibration graphs.

This transformer was also used when a higher voltage was required for performing puncture tests on the insulators. Details on the puncture tests are available in Section 4.2.6.2

4.2.2 Divider

To measure the output voltage of the transformer, a high voltage divider was connected to the high voltage bus of the test set up as shown in Figure 4.1. The capacitive divider used in this project is rated for 225 kV and is manufactured by Ross Engineering [90].The voltage waveform from the divider was used for generating the 60 Hz reference waveform during the phase resolved analysis.

4.2.3 D-dot Electric Field Sensor

The electromagnetic field sensors are passive devices can provide a voltage on their output terminals as a replica of the incident fields. In case of D-dot sensors, the voltage is proportional to the time derivative of the electric displacement field.

Figure 4.3 shows a Prodyn's ACD-S30 passive D-dot sensor which was used in this study which has a bandwidth of 1 GHz [91]. The output voltage of the D-dot sensor is given by,

$$V_0 = R \times A_{eq} \times \frac{\partial}{\partial t} D \times \cos\theta \tag{4.1}$$

Figure 4.3: Prodyn's ACD-S30 Sensor.

where, R is sensor's load characteristic impedance (50 ohms in this case), A_{eq} is the sensor equivalent area provided by the manufacturer, D is the magnitude of electric displacement vector and θ is the angle between the normal vector of sensor ground plane and the incident electric field, E.

To compare the voltage received at the terminal of the D-dot sensor and

the actual discharge current on the insulator, one of the spare channels on the oscilloscope was used to capture the leakage current using a high frequency current transformer (HFCT). As shown in Figure 4.4 the peak location of the waveform detected by the D-dot probe is only 10 ns from the the peak of the waveform detected by the CT. Since the focus of this experiment is on the relative phase location of the discharge peaks, this difference in the peak location is negligible when performing 60 Hz phase resolved analysis (around 2×10^{-4} degrees).

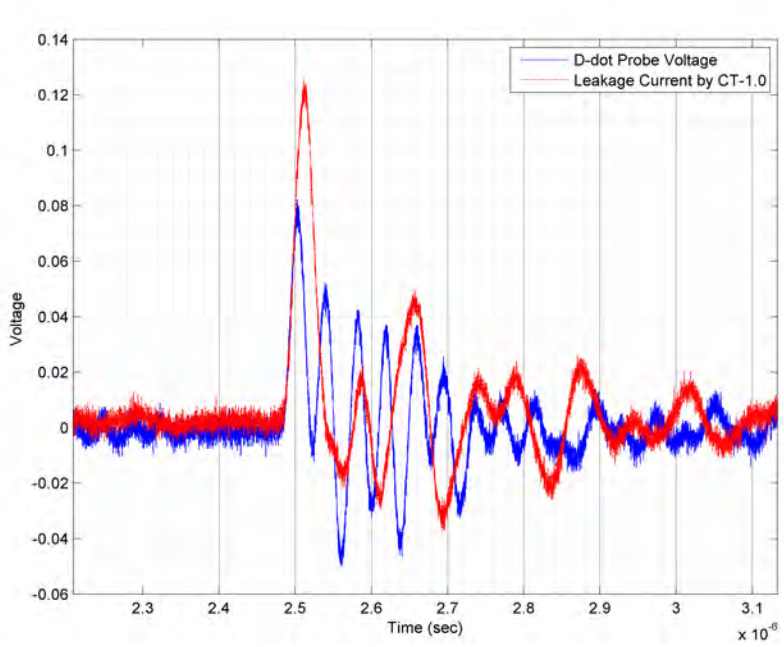

Figure 4.4: Recorded voltage of D-dot probe and the CT during a PD activity.

4.2.4 Current Transformer (CT)

Current transformers (CT) were placed on the ground wire during the initial phases of the project for validation purposes. It should be noted that any other sensor/antenna can be used as a receiver for this purpose as long as its bandwidth

is broad enough and its transfer function is known. The bandwidth of the receiver has to be broad enough to capture all the required high frequency components. PD radiation spectrum is mostly below 200 MHz [92] and therefore receivers with a bandwidth higher than of 200 MHz can be used for this application. The current transformers used in this research were manufactured by Magnelab (previously owned by Bergoz [93]). The CTs were used to compare the radiation signature to the partial discharge activities in the ground wire. Also the CT signals were used to generate the 60 Hz reference signal and compare with the divider phase reference voltage during the phase resolved analysis. The CTs come in different sizes and bandwidth. The CTs used in this research were CT-C1.0 (bandwidth of 500 MHz and a one to one ratio) and CT-C0.5 (bandwidth of 200 MHz and half ratio). A picture of these current transformers is shown in Figure 4.5.

Figure 4.5: Current transformers manufactured by Magnelab/Bergoz [93].

4.2.5 Oscilloscope

All the analog signals captured by the receivers have to be sampled and digitalized before storing on digital memories. There are three key features that should be

considered in choosing the right oscilloscope for any application; the bandwidth, sampling rate, and maximum storage points. For this research, a minimum bandwidth of 1 GHz was required. Sampling rates could vary depending on the number of channels in use and also the length of the time window. At smaller time windows, the oscilloscope can operate at its maximum sampling rate. In case of larger time frames, the sampling rate will be limited by the maximum storage point in the memory. For example, consider an oscilloscope with a sampling rate of 4 GS/sec and an 8 million point memory storage capacity. When the time division is set to 2 *ms/div*, the total screen covers 10×2 *ms/div*=20 *ms* of the recorded data. Now if the oscilloscope samples this waveform at 4 GS/sec, the total points required to save this information would be 80 million points which is larger the oscilloscope's built-in memory. Therefore, in this case, the oscilloscope will sample at 400 MS/sec to be able to store the 8 million sample points in its memory. In case of smaller time frames, although the built-in memory is capable of storing higher sampling rates, we are limited by the maximum sampling rate specified by the manufacturer of the unit. To summarize this discussion, When the time frame is large, we are limited by oscilloscope's memory size and when the time frame is small, we are limited by oscilloscope's maximum sampling rate. In this research, a 7104A Agilent digital oscilloscope [94] is used for digitization and storage of captured electromagnetic radiations. The oscilloscope has a bandwidth of 1 GHz and a maximum sampling rate of 4 GS/sec and a 4 million point memory storage capacity. The oscilloscope is set on the external rising edge trigger mode that stores the waveforms when it detects a partial discharge pulse on the input channel assigned for triggering.

4.2.6 Defective Porcelain Insulators

The transformer energizes the porcelain insulators under test and the radiation captured by the sensors is digitalized and stored on the oscilloscope. The string of insulators is hung off a pi-shaped wooden structure as shown in Figure 4.1. The string is connected to the ground from the top, and to the high voltage bus through the bottom insulator. During all the measurements, the string had two insulators where the insulator near the ground wire was always a normal, healthy, and clean insulator. The other insulator, connected to the HV bus, was altered during the tests to study the punctured, contaminated, and normal radiation signatures. There are also various types of porcelain insulators available in the market. The insulators used in this project were the class B, 15000 lbs NGK units [95] since Manitoba Hydro is using a large number of these units in their system. The scope of this project involved studying the radiation signature of contaminated and punctured insulators. To duplicate these defective insulators, a lab procedure was developed. Details on the procedures of making defective insulators in the lab is presented in the next section.

4.2.6.1 Contaminated Insulators

To make contaminated insulators in the lab, we followed the IEC 60507 standard [20] that was discussed in more details in Section 4.1.1. According to IEC 60507 and Table 4.1, the site contamination level can be categorized in four groups; very light, light, moderate and heavy. Insulators studied in this research were made to a heavy contamination level. In order to make a contaminated insulators with a

desired contamination level, the proper suspension should be made and sprayed on the insulators. The conductivity of the suspension was calculated based on the IEC standard where the relation between the Equivalent Salt Deposit Density (ESDD) level and suspension's conductivity is given [20]. To ensure uniformity and proper dosage, nozzle should be kept 30 cm away and the insulator should be rotated 360 degrees. To make contaminated insulators with other ESDD levels, the conductivity of the suspension should change accordingly.

The type of contaminants that can be deposited on the insulators in the field depends on the area that they are installed. Contaminants can be classified as soluble or non-soluble. Soluble contaminants have a much higher impact on insulators performance. To standardize and classify the contamination level of insulators, the measure of Equivalent Salt Deposit Density (ESDD) is used in this study. It should be noted that in order to precisely classify the contamination level of outdoor insulators, the Non-soluble Deposit Density (NSDD) level, representing the level of non-soluble contaminants, must also be taken into account. However the impact of NSSD is very small [96] and therefore it was not considered in this research.

The IEC procedure [20] was followed to make the proper suspension required to be sprayed on the insulators. First, 40 grams of Kaolin was mixed into 1000 grams of tap water. The conductivity of tap water in the lab was 357 μS/cm, measured by Orion 3-Star Plus, a portable conductivity meter manufactured by Thermo Scientific [97]. Eighty five grams of commercially-available salt was added to the solution to raise the conductivity of the solution to 11.2 S/m. This solution was then sprayed on the insulators in order to produce the desired ESDD level of 0.28 mg/cm^2. Figure 4.6 shows a string of two insulators where the bottom insulator has been sprayed with the contaminated suspension.

Figure 4.6: Contaminated insulator under the test; clean and healthy unit on top and contaminated unit at the bottom.

Depending on how the suspension is sprayed on the insulators and also the condition of the insulator prior to spraying, the ESDD level of the insulator can be different. Therefore, to ensure the ESDD level of the insulators after spraying this suspension is close to the desired value of 0.28 mg/cm^2, different scenarios were investigated. The effect of washing, drying, and cleaning prior to applying the suspension, the angle of spray nozzle, and number of sprays on the final ESDD level was studied. For each scenario, the ESDD level after applying the suspension was calculated based on the method presented in IEC 60507.

Figure 4.7 shows the procedure of measuring the ESDD level of the contaminated insulators. An area on the insulator was completely wiped off using previously cleaned and dried cotton balls. After collecting all the dirt and contaminants, cotton

Figure 4.7: Measuring the ESDD level in the lab.

balls were immersed in distilled water to dissolve any contaminants absorbed by the cotton balls and the conductivity of the solution was then measured. Knowing the area that was cleaned with the cotton balls and also the volume of distilled water that the cotton balls were dissolved in, the ESDD level of the polluted insulator was calculated using [20]:

$$S_a = (5.7 \times \sigma_{20})^{1.03} \tag{4.2}$$

$$SDD = \frac{S_a \times V}{A} \tag{4.3}$$

where SSD is the salt deposit density (mg/cm^2), σ_{20} is the volume conductivity of the suspension, S_a (kg/m^3) is the salinity of the suspension, V is the volume of distilled water, and A is the area that was wiped off by cotton balls. To imitate the real pollution on the insulators, the insulators were wetted before and after the energization according to the wetting procedure given in [20].

After trying different methods for applying the suspension on the insulators and measuring the ESDD level of each sample, a procedure was developed and followed to achieve the same ESDD level knowing the suspension conductivity. Also, throughout the measurement, the ESDD of some samples were randomly checked to ensure the contamination level is within the acceptable range.

4.2.6.2 Punctured Insulators

Internal punctures are one of the most common defects in porcelain insulators. The formation of puncture paths inside the insulators is mostly due to the cement expansion near the cap and pin joint. Low quality cement materials absorb the moisture and expand over time, causing undesired puncture paths. Lightning can also cause punctures in the cap. Punctured insulators are very hard to inspect visually. There two routine tests which are described in IEC standard [89] that were inspiring for making punctured insulators in the lab.

(1) Electromechanical Failing Load Test:

IEC has a standard testing procedure for performing tensile tests on porcelain insulators. The IEC refers to this test as an electromechanical failing load test. During the test, the string of porcelain insulators will be subjected to the AC power source while the tensile load is applied to the string at the same time. According to the IEC Standard 60383-1 [89], the tensile load should rapidly but smoothly increase from 0 to 75% of the rated failing load value and then gradually increase to 100%. One way to make punctured insulators is utilizing a similar procedure. The idea is to put one porcelain insulator under an adjustable tensile load using

the tensile testing machine. A tensile machine is available in one of University of Manitoba Structure Lab and can be controlled by a computer that programs load characteristics. Increasing the tension will eventually develop punctures in the insulator. One way to monitor the condition of the insulator is measuring the resistance across the unit while it is under the tensile load. When the puncture develops between the cap and pin, the resistance of the insulator should drop significantly. Fluke 1507 was the Megger used for the resistance monitoring during the tensile load test and can measure resistance up to 10 GΩ [98].

Insulators were taken to the University of Manitoba Structure lab and were placed and secured inside the Instron 300 DX tensile tester. To fit the unit into the tensile tester, special links were made out of steel plates, considering the maximum mechanical withstand of the insulators. Figure 4.8 shows the test setup for the puncture test using the tensile tester. During multiple tries on different insulators, we noticed that the bottom metallic pin is the first part that fails the tensile test (Figure 4.8, top right). Therefore, we were never able to apply enough force to exceed the nominal mechanical strength of the insulators to introduce the puncture. At this point we decided to make the puncture insulators using high voltage stresses instead of mechanical forces.

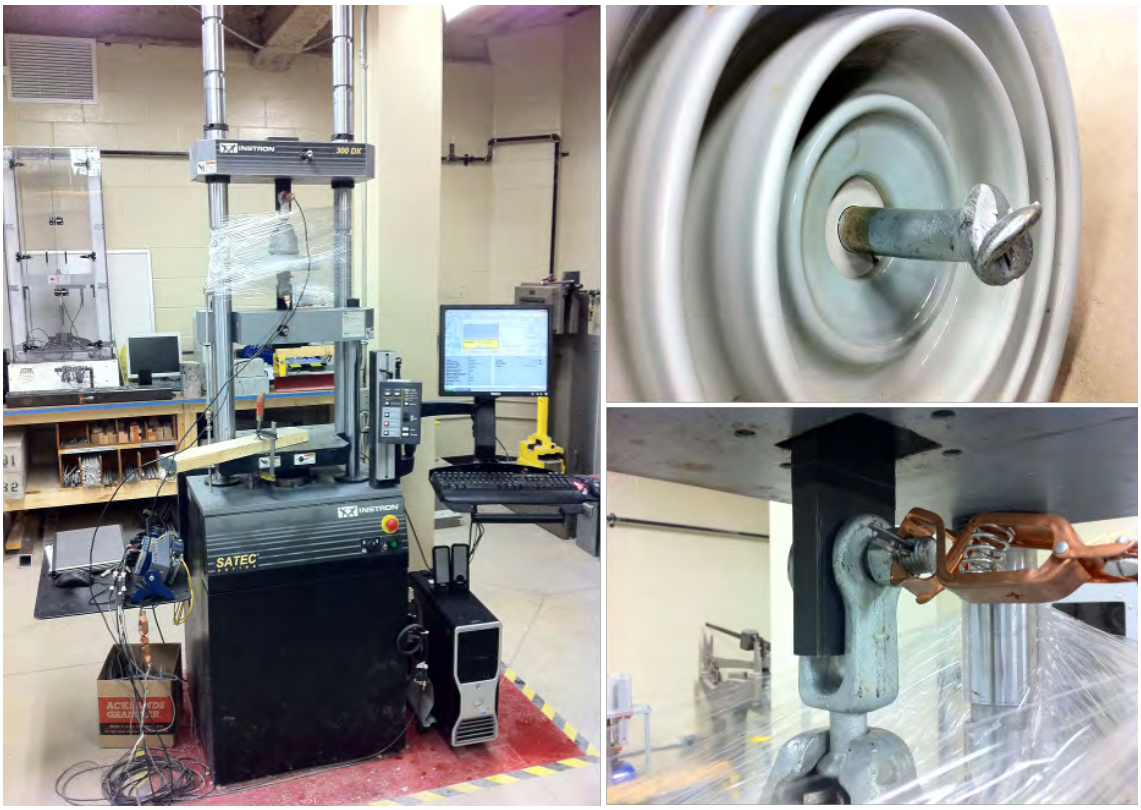

Figure 4.8: Puncture test arrangement using Tensile Machine Instron DX300; test setup on left, failed pin on top right, and custom built link and resistance monitoring on bottom right.

(2) Puncture Withstand Test:

Section 15 of the IEC standard 60383-1 [89] explains the puncture withstand test for testing porcelain insulators. According to the standard, the insulators should be cleaned and dried before the test. Then the insulator should be immersed in a tank filled with liquid insulating materials. The temperature of this liquid insulating material should be at the room temperature. While immersing the insulator in the tank, precautions should be taken to avoid forming air bubbles underneath the shells. The power frequency voltage across the unit should then rapidly raise to the

withstand level specified by the manufacturer. If no puncture occurs while ramping up the voltage to the withstand voltage, the insulator passes the test. If one is interested in recording the puncture voltage, the voltage can be raised above the specified withstand voltage limit until the puncture occurs. We decided to follow this test procedure and apply higher voltage stresses across the insulators until a puncture develops inside the insulation.

Figure 4.9 shows the test arrangement for making punctured insulators. When the puncture path develops inside the insulator, the insulator can not withstand the nominal puncture withstand voltage any more.

Figure 4.9: Puncture test arrangement using IEC 60383-1; test setup on left, insulator immersed in oil and under high voltage stress on top right, development of puncture on middle right, and punctured insulator ready to be tested for radiation signature on bottom right.

4.2.6.3 Insulator Identification

As explained earlier in this Chapter, puncture and contamination are the two types of defects that have been studied in this research. Also, strings of normal healthy and clean insulators were energized and their electromagnetic radiations were captured and analysed. Testing normal healthy and clean insulators provides a baseline signature pattern that can be compared will defective units. Table 4.2 shows the eight insulators studied in this research showing the type of defect each one had.

Table 4.2: Identification table for studied insulators

Type of Defect	**Total Number of Cycles of Captured PD Events**	**Collected Datasets**	**Total Samples**
Clean/Normal	90,000	176	3
Contaminated	145,000	288	3
Punctured	175,000	342	2
Total	**410,000**	**806**	**8**

It should be noted that in case of testing the contaminated insulators, all three sample insulators were first made into the desired ESDD level of 0.28 mg/cm^2, using the procedures explained in the previous sections. When the contaminated insulator was placed inside the fog chamber and one dataset of partial discharge radiation was captured, the contaminated insulator was taken off the string and replaced with another contaminated insulator that has never been tested inside the fog chamber. The contaminated insulators that were taken off the string after being tested in the fog chamber were then properly washed and cleaned. The clean and washed

insulators went under the same contamination procedure to make new contaminated insulators with the same desired ESDD levels. The reason for implementing the cycle of washing, cleaning, and redepositing the contamination layer was to ensure the contamination layer is not getting washed off after being in the fog chamber to a long period of time.

4.3 Summary

In the chapter, the experimental setup and equipment employed in this thesis were described. The test setup for collecting the measurements and the role of each equipment in the test setup was explained. The lab procedures as well as the IEC standards that were followed for making contaminated and punctured insulators were also discussed.

5

Data Processing and Classification

A total of 410,000 cycles (806 datasets) of the recorded measurements were analysed. This chapter presents the processing techniques employed in this thesis and summarizes the results obtained from extracting the statistical features of captured radiations. The classification algorithm for differentiating punctured and contaminated insulators using their radiation signature is also presented.

5.1 Data Processing

The two most common types of defective porcelain insulators made in lab (details were presented in Section 4.2.6), were placed under high voltage stresses (test setup shown in Figure 4.1) to investigate their radiation signature. When the defective insulators are placed under high voltage stresses, partial discharge activities initiate. These discharges are basically the electrons bridging the insulation (internal in case of puncture path and external in case of surface contamination) and can be detected by monitoring the leakage current and radiation signature of the insulators.

The focus of this thesis is to capture and process the radiation signature of these discharges to find the relation between the radiation signature patterns and type of defects. In this section, the signal processing techniques that were applied and studied on the radiated signatures of recorded measurements will be presented. Punctured insulators, contaminated insulators, and normal (healthy and clean) insulators were studied and the radiation signature for each case was recorded and compared with the others. The test setup for this measurement had two insulators on the string connected to a 55 kV power frequency high voltage bus. The source voltage of 55 kV was chosen based on the PD inception voltage when the string had only normal insulators.

The oscilloscope was programmed to trigger when a discharge occurs and to capture one 60 Hz cycle of data. One cycle of data that contains the partial discharge data is referred to one "Segment" in this thesis. After capturing one segment, the oscilloscope will be automatically re-armed and wait for the next partial discharge to trigger and record it in the next segment. The oscilloscope is capable of recording multiple segments. A total of 512 segments is referred to one "Dataset". Due to memory limitation on the oscilloscope, after capturing 512 segments (or one dataset) the data had to be stored on the hard drive.

After collecting the data from the tested insulators, the information should be processed to extract the unique features of radiated pulses. These features will eventually help the classifier to identify the radiation signatures. Identifying and extracting these features can be done in different domains. A wide range of data processing techniques can be used to extract the unique features of radiated pulses. The focus of our data processing techniques was on the phased resolved statistical behaviour of partial discharges. Preliminary analysis performed on the

captured radiation pulses showed distinct features in the pattern of the probability density functions of the PD pulses. The signal possessing on the recorded data was performed in MATLAB [86]. The recorded datasets captured by the oscilloscope were loaded into MATLAB, where a graphical user interface (GUI) was developed to perform the analysis. The GUI allows the user to select different datasets/segments and perform a number of signal processing analysis on them. Figure 5.1 shows a view of the GUI that was developed for this research. One of the first steps prior to performing the data processing was to properly identify and locate the location of partial discharge pulses. Figure 5.2 shows a sample of captured partial discharge pulse in red while the peaks of the waveform are identified and shown with blue points. However, this activity corresponds to only one discharge pulse and the resonance following the initial discharge is due to the system response [99]. Therefore, only one peak location (maximum) will be extracted from this discharge activity for data processing analysis.

In the remainder of this section, details of the signal processing techniques used for extracting the features will be discussed.

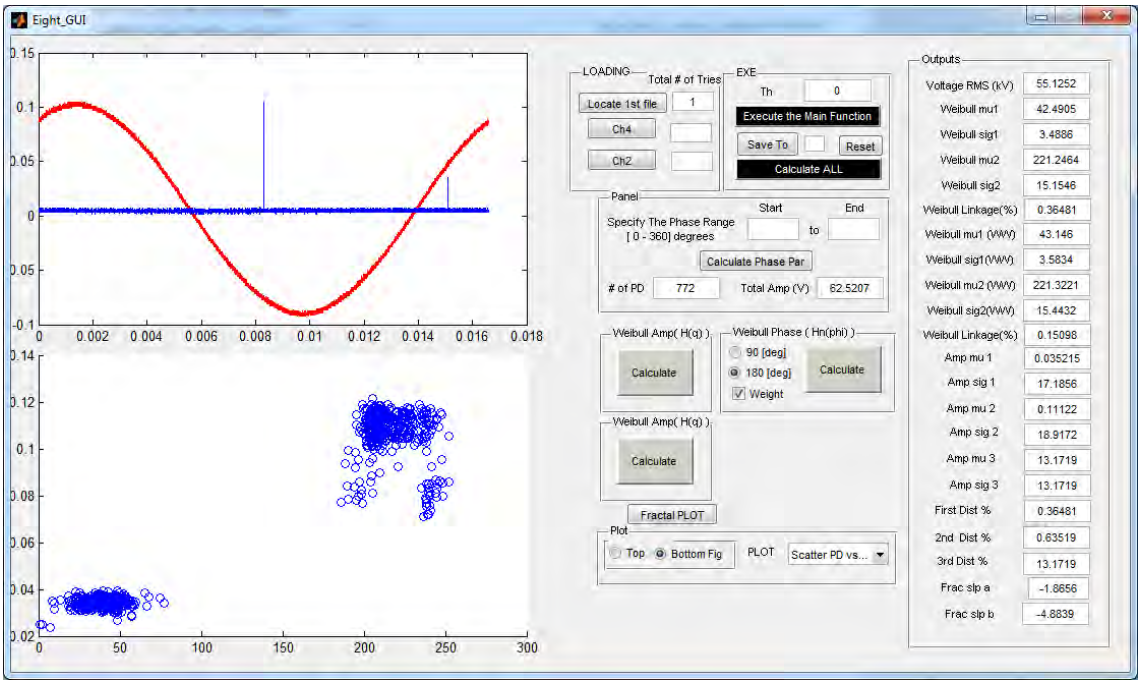

Figure 5.1: View of the Graphical User Interface (GUI) developed in MATLAB for performing signal processing.

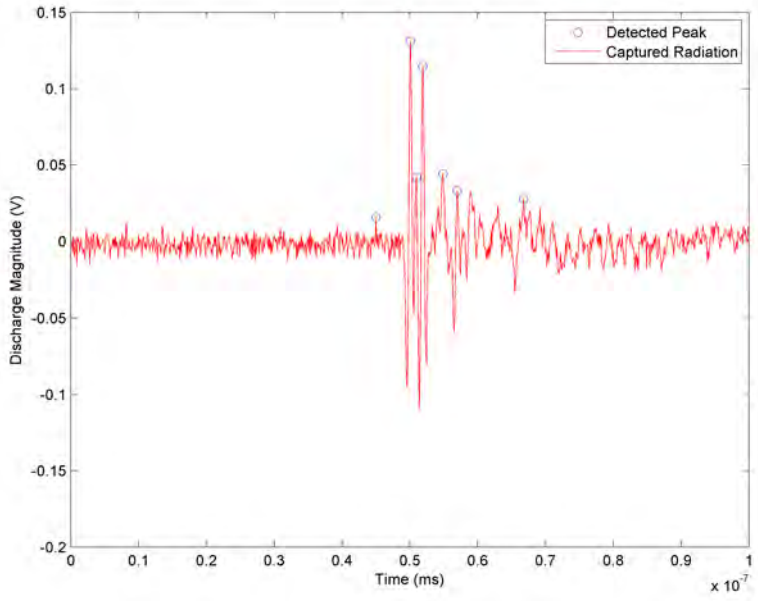

Figure 5.2: Identifying peak locations on the recorded partial discharge pulse.

5.1.1 Weibull PDF Fitting on Phase Location of PD Pulses

One feature of the radiated PD pulses studied in this research is the phase location of where the PD pulses happen. Figure 5.3 shows a sample of a recorded data of one segment captured by the oscilloscope. In the example shown in Figure 5.3, two PD pulses are present in the captured segment (one 60 Hz cycle); the first discharge happens around phase location of 220 degrees and the second discharge happens at the phase location of 20 degrees. The phase location of PD pulses on all segments of each dataset are extracted and a two sided Weibull probability density function (PDF) is fit to the extracted histogram of the phase location of the peak.

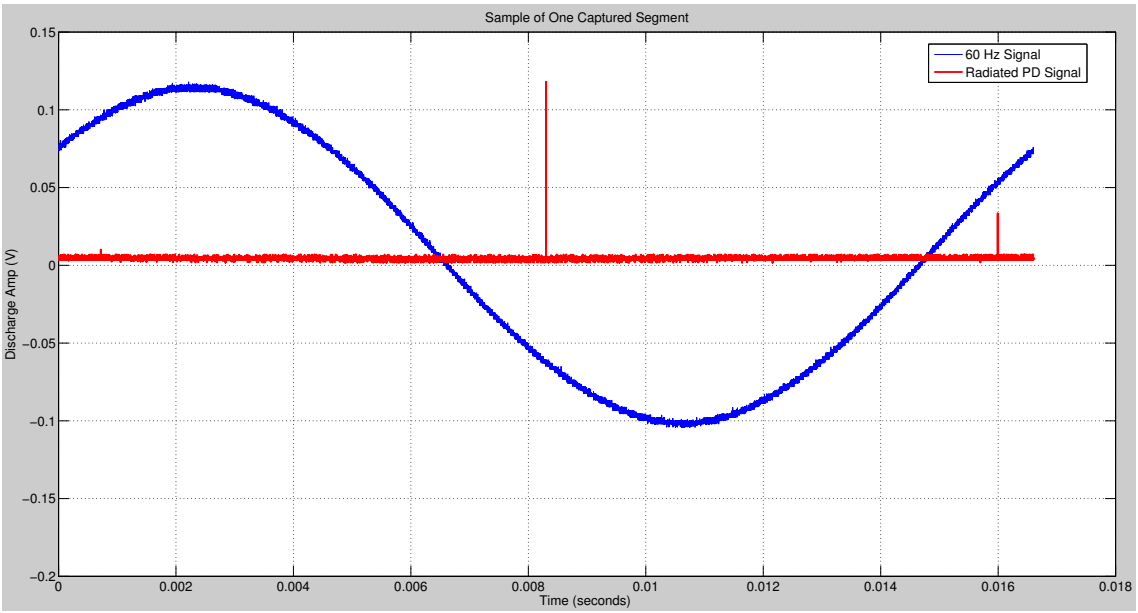

Figure 5.3: Sample of recorded measurements in one cycle.

A Weibull probability density function is given by

$$f(x|\, a, b) = \frac{b}{a}\,(\frac{x}{a})^{b-1} e^{-(\frac{x}{a})^{b}} \tag{5.1}$$

where:

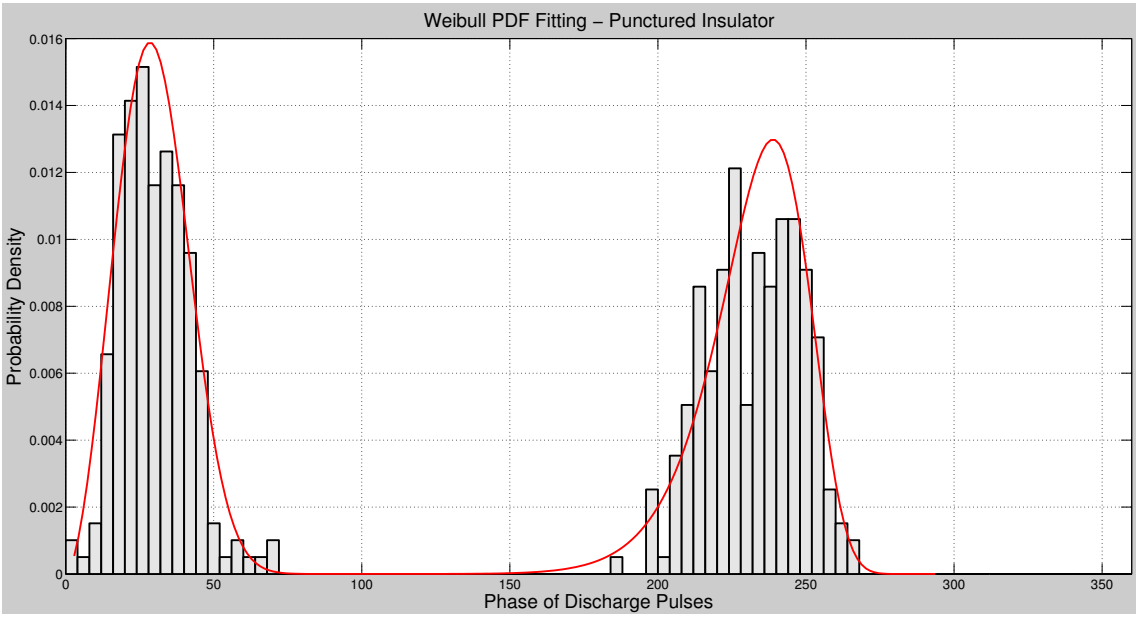

Figure 5.4: Fitting a two sided Weibull distribution to phase of PD pulses of 512 segments.

"a" is the shape parameter

"b" is the scale parameter

Figure 5.4 shows a Weibull fitting on one dataset of captured radiations. After finding the Weibull fit at each dataset, the shape and scale parameters (a and b in Equation 5.1) of the Weibull function at each side,and also the linkage between the sides is calculated and stored. To fit a two sided Weibull distribution, two separate Weibull distributions were fit into each side of the phase resolved graphs, each having their own shape and scale parameters. The linkage is defined as a normalized weighting function combining the two density functions when using the maximum likelihood algorithm. In other words, the two sided distribution function is a mixture PDF distribution where the linkage parameter (defined in this thesis) is the mixture weight associated with each distribution.

The shape (two values, one per side), scale (two values, one per side) and linkage of the two sided Weibull density function for each dataset is then calculated and recorded. The same procedure is repeated for all the recorded datasets.

5.1.2 Weibull PDF Fitting on Amplitude of PD Pulses

Another feature of the captured radiated PD pulses, is the amplitude of the discharge. As shown in Figure 5.3, the amplitude the PD pulse is different in the two events that are captured in the cycle. Therefore, the amplitude of the PD pulses on all segments of each dataset are extracted and a two sided Weibull probability density function (PDF) is fit to the extracted scatter plot, similar to the phase of PD pulses. An example of Weibull amplitude curve fitting is presented in Figure 5.5

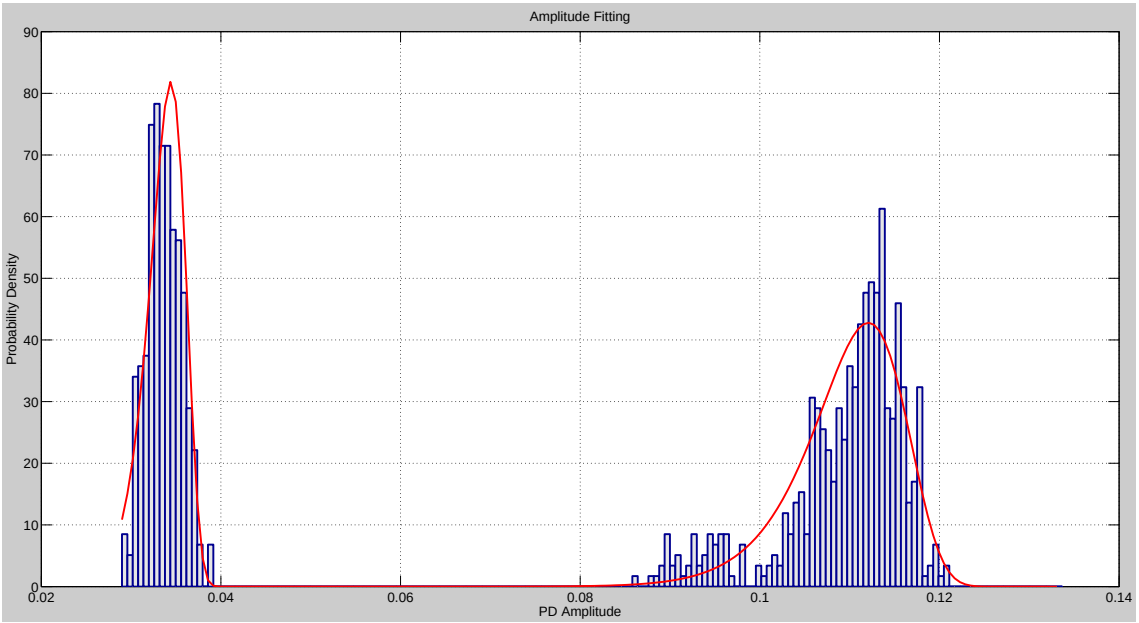

Figure 5.5: Fitting a two sided Weibull distribution to the amplitude of PD pulses.

The shape (two values, one per side), scale (two values, one per side) and linkage

of the two sided Weibull density function for each dataset is then calculated and recorded. The same procedure is repeated for all the recorded datasets.

5.1.3 Weibull PDF Fitting on Weighted Phase of PD Pulses

To simultaneously investigate both the amplitude and phase characteristics of the PD pulses, a weighted phase plot was generated. In this representation, based on the amplitude of the PD pulses, the number of discharges per each phase window is weighted. The idea behind this representation is to study the statistical pattern of the PD pulses in terms of phase location of PD peaks and the amplitude of PD pulses simultaneously. Similar to previous Weibull fittings, a two sided Weibull probability density function is fit to the calculated histograms and the shape (two values, one per side), scale (two values, one per side) and linkage of the two sided Weibull density function for each dataset is calculated and recorded. Figure 5.6 shows an example of the weighted phase fitting.

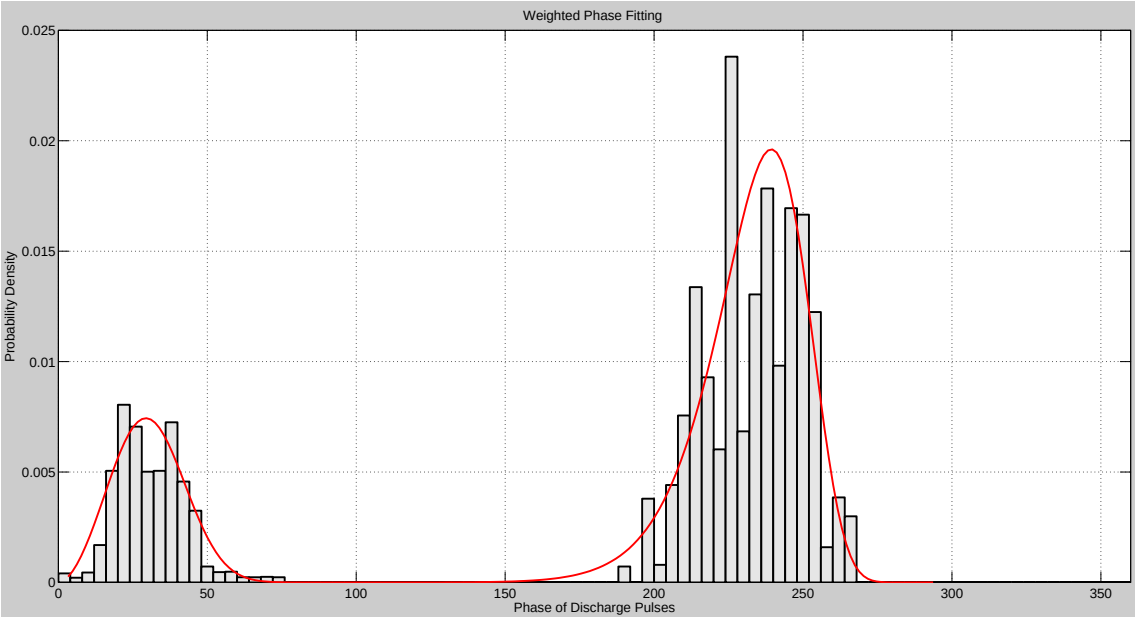

Figure 5.6: Fitting a two sided Weibull distribution to the weighted phase of PD pulses.

5.1.4 Spectral Fractal Analysis

To study the signature of concurrent discharge activities on the radiated fields, the concept of spectral fractal analysis was used. The power density spectrum of the signal provides an estimate of the fluctuations of the signal vs frequency. According to [82], if the underlying process has periodic (or quasi-periodic) behavior, the power spectrum of the signal has equally spaced harmonics with significant power at very low frequencies. During the initial rounds of measurements, in some of the captured cycles, low amplitude concurrent discharges were observed. In order to investigate these discharges within one cycle of captured radiations, the spectral fractal exponent, which is the slope of the linear fit to the log log spectrum of the signal in lower frequencies, was calculated [82].

Therefore, the power spectrum of each of the 512 segments in each dataset was

calculated and a linear line in the range of 100 Hz to 10 kHz was fit to the log-log spectrum. The line parameters of the linear fit for each dataset are stored and averaged at the end of each run. Figure 5.7 shows an example of spectral fractal parameters calculated for one segment of a dataset where the signal spectrum is shown in blue and a linear curve fitting is shown in red.

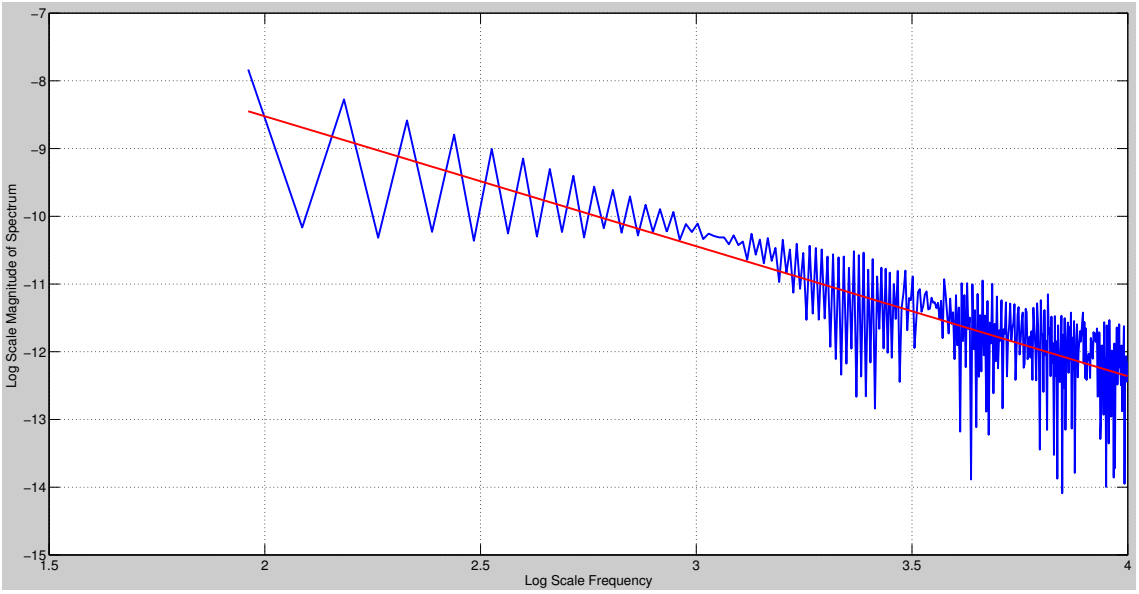

Figure 5.7: Parameters of spectral fractal curve fitting.

5.2 Data Processing Results

The string of insulators containing different combinations of defective and healthy units were placed under high voltage stresses to capture the electromagnetic radiation off PD pulses. This section presents the signature statistical graphs calculated based on the analysis described in Section 5.1 for the three types of insulators that were studied in this research; normal (healthy and clean), punctured, and contaminated insulators. The graphs presented in this section

contain the statistical features of the captured electromagnetic radiation calculated for each dataset of recorded measurements. From the total of 410,000 recorded measurements, 90,000 cycles (176 datasets) of recorded radiations are from normal insulators, 175,000 cycles (342 datasets) from punctured insulators, and 145,000 cycles (288 datasets) from contaminated insulators. This section presents the statistical features resulted from the processing performed on the captured measurements.

5.2.1 Weibull PDF Fitting on Phase Location of PD Pulses

As explained earlier in Section 5.1, a two sided Weibull distribution is fitted to the phase location of discharge activities of each dataset (512 cycles) of captured electromagnetic radiations. The extracted parameters of each Weibull fit include the shape and scale parameter of positive half cycle (blue points), the shape and scale parameter of negative half cycle (red points) and the linkage between the two distributions. Figures 5.8, 5.9, 5.10 present the Weibull phase fit parameters in a 3D representation, where the x axis is the shape parameter of the Weibull fit, the y axis is the scale parameter of the Weibull fit, and the z axis is the linkage between the two distributions for normal, punctured, and contaminated insulators respectively.

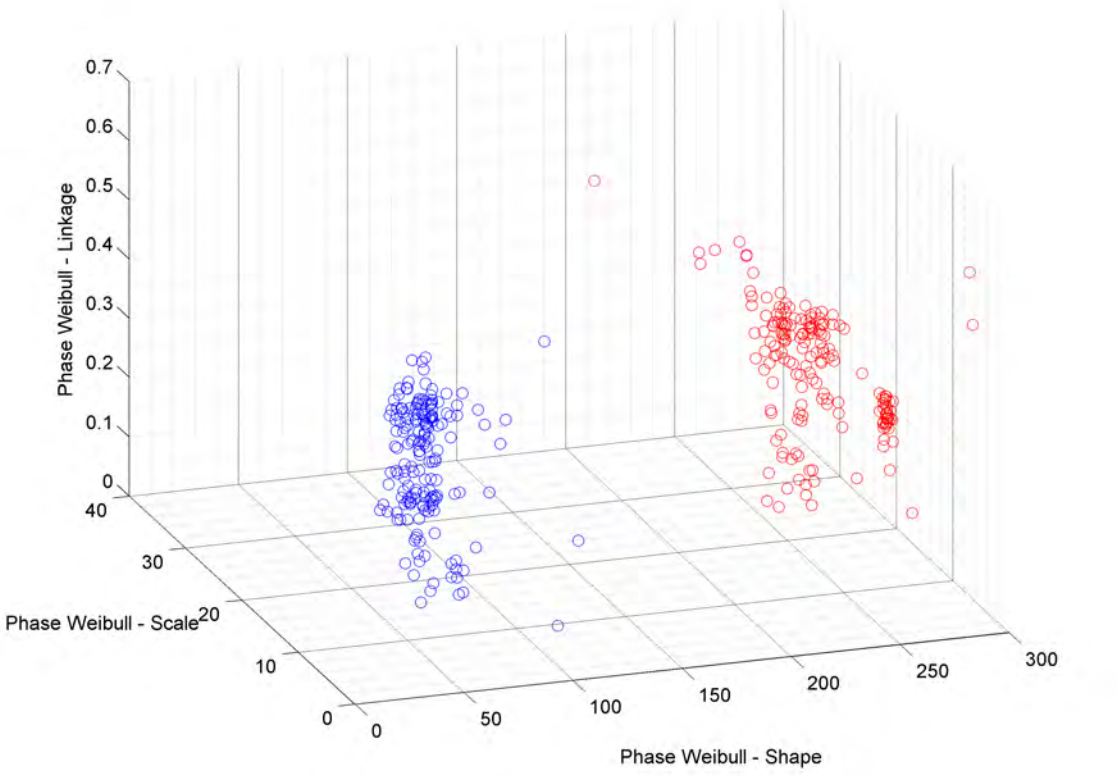

Figure 5.8: Fitted phase Weibull parameters - normal insulator; one blue point (positive half cycle) and one red point (negative half cycle) represent the extracted features from one of the 176 datasets during the phase Weibull fitting.

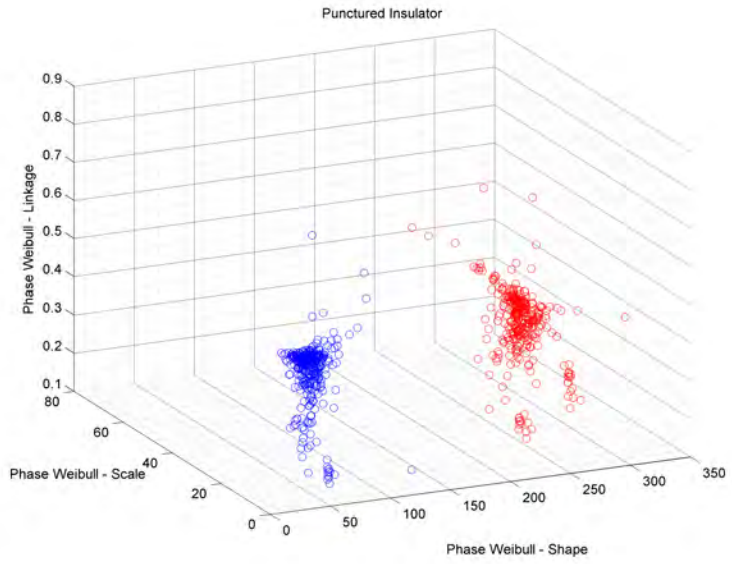

Figure 5.9: Fitted phase Weibull parameters - punctured insulator; one blue point (positive half cycle) and one red point (negative half cycle) represent the extracted features from one of the 342 datasets during the phase Weibull fitting.

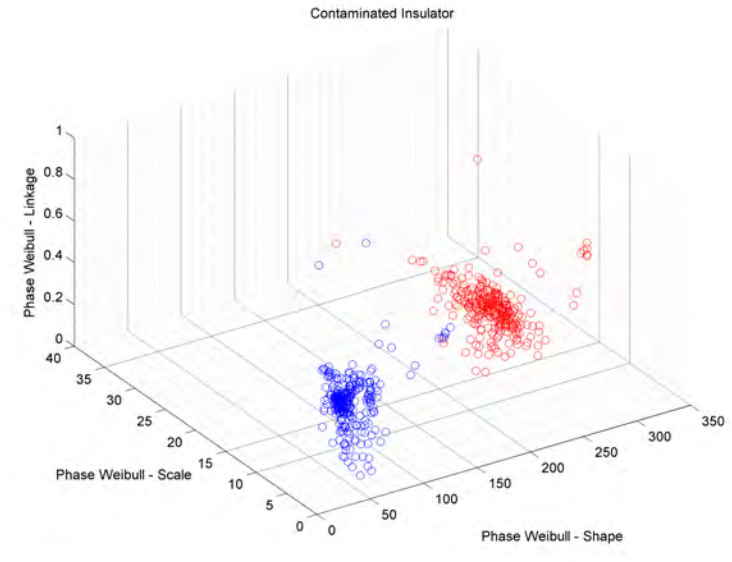

Figure 5.10: Fitted phase Weibull parameters - contaminated insulator; one blue point (positive half cycle) and one red point (negative half cycle) represent the extracted features from one of the 288 datasets during the phase Weibull fitting.

5.2.2 Weibull PDF Fitting on Amplitude of PD Pulses

As explained earlier in Section 5.1, a two sided Weibull distribution is fitted to the amplitude of discharges of each dataset (512 cycles) of captured electromagnetic radiation. The extracted parameters of each Weibull fit include the shape and scale parameter of the lower magnitude discharge (blue points), the shape and scale parameter of the higher magnitude discharge (red points) and the linkage between the two distributions. Figures 5.11, 5.12, 5.13 present the Weibull amplitude fit parameters in a 3D representation, where the x axis is the shape parameter of the Weibull fit, the y axis is the scale parameter of the Weibull fit, and the z axis is the linkage between the two distributions for normal, punctured, and contaminated insulators respectively.

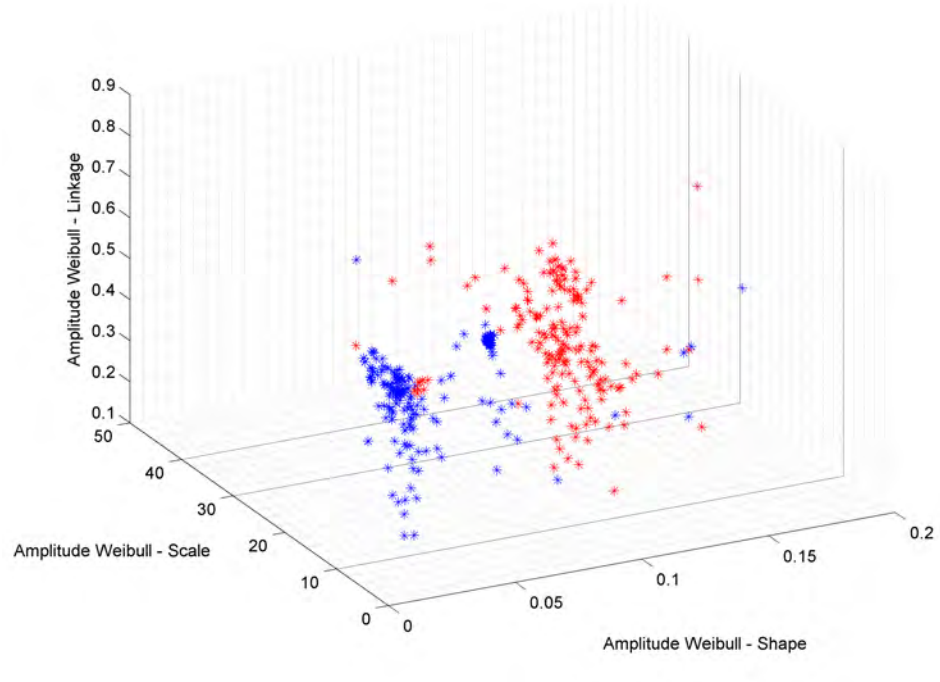

Figure 5.11: Fitted amplitude Weibull parameters - normal insulator; one blue point (lower magnitude discharge) and one red point (higher magnitude discharge) represent the extracted features from one of the 176 datasets during the amplitude Weibull fitting.

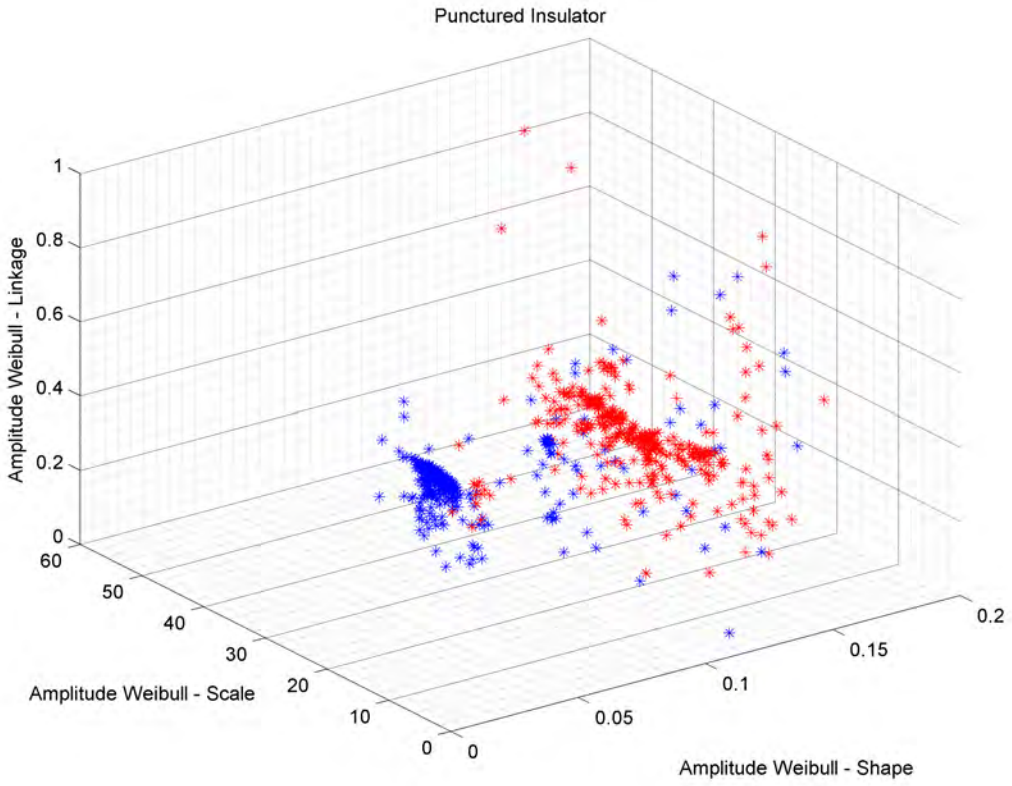

Figure 5.12: Fitted amplitude Weibull parameters - punctured insulator; one blue point (lower magnitude discharge) and one red point (higher magnitude discharge) represent the extracted features from one of the 342 datasets during the amplitude Weibull fitting.

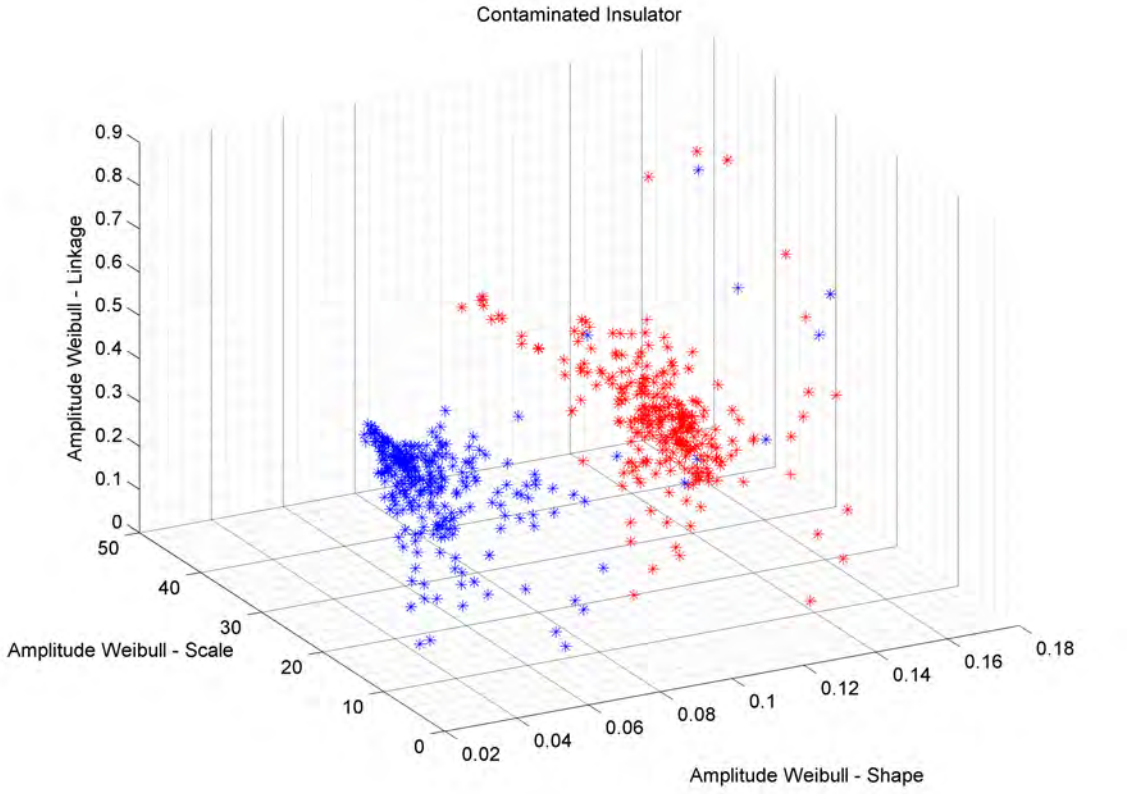

Figure 5.13: Fitted amplitude Weibull parameters - contaminated insulator; one blue point (lower magnitude discharge) and one red point (higher magnitude discharge) represent the extracted features from one of the 288 datasets during the amplitude Weibull fitting.

5.2.3 Weibull PDF Fitting on Weighted Phase of PD Pulses

As explained earlier in Section 5.1, a two sided Weibull distribution is fitted to the weighted phase of discharges of each dataset (512 cycles) of captured electromagnetic radiation. The extracted parameters of each weighted Weibull fit include the shape and scale parameter of positive half cycle (blue points), the shape and scale parameter of negative half cycle (red points) and the linkage between the two distributions. Figures 5.14, 5.15, 5.16 present the weighted Weibull phase fit parameters in a 3D representation, where the x axis is the shape parameter of the weighted Weibull fit, the y axis is the scale parameter of the weighted Weibull fit, and the z axis is the linkage between the two distributions for normal, punctured, and contaminated insulators respectively.

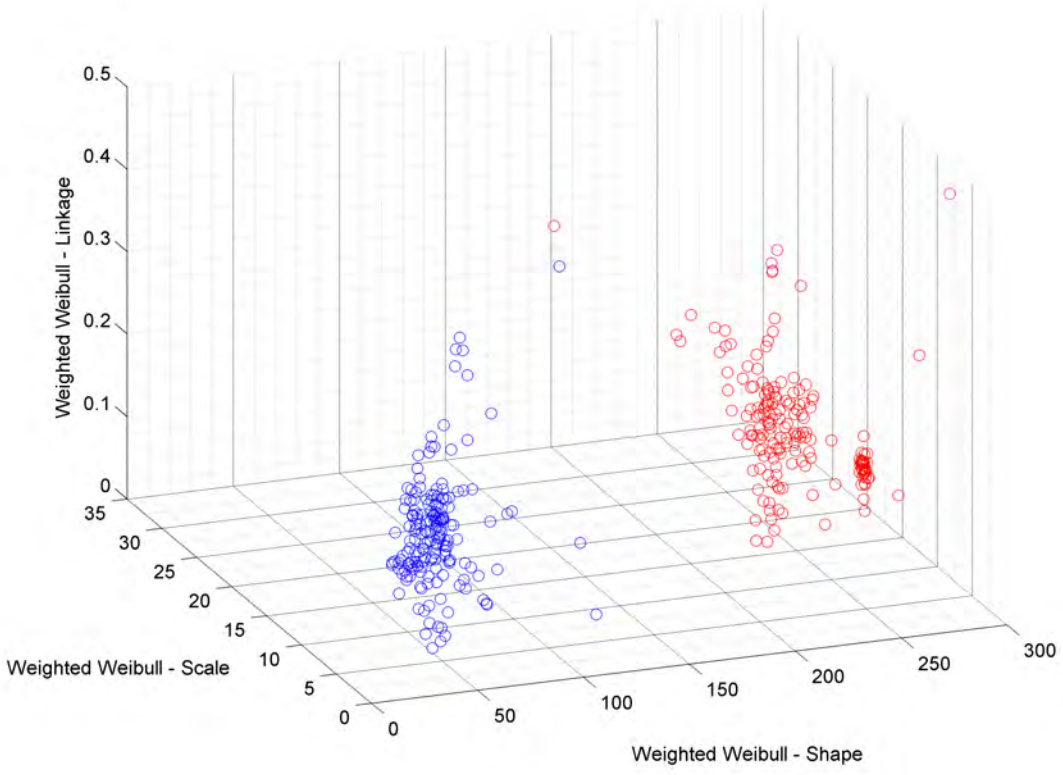

Figure 5.14: Fitted weighted Weibull parameters - normal insulator; one blue point (positive half cycle) and one red point (negative half cycle) represent the extracted features from one of the 176 datasets during the weighted phase Weibull fitting.

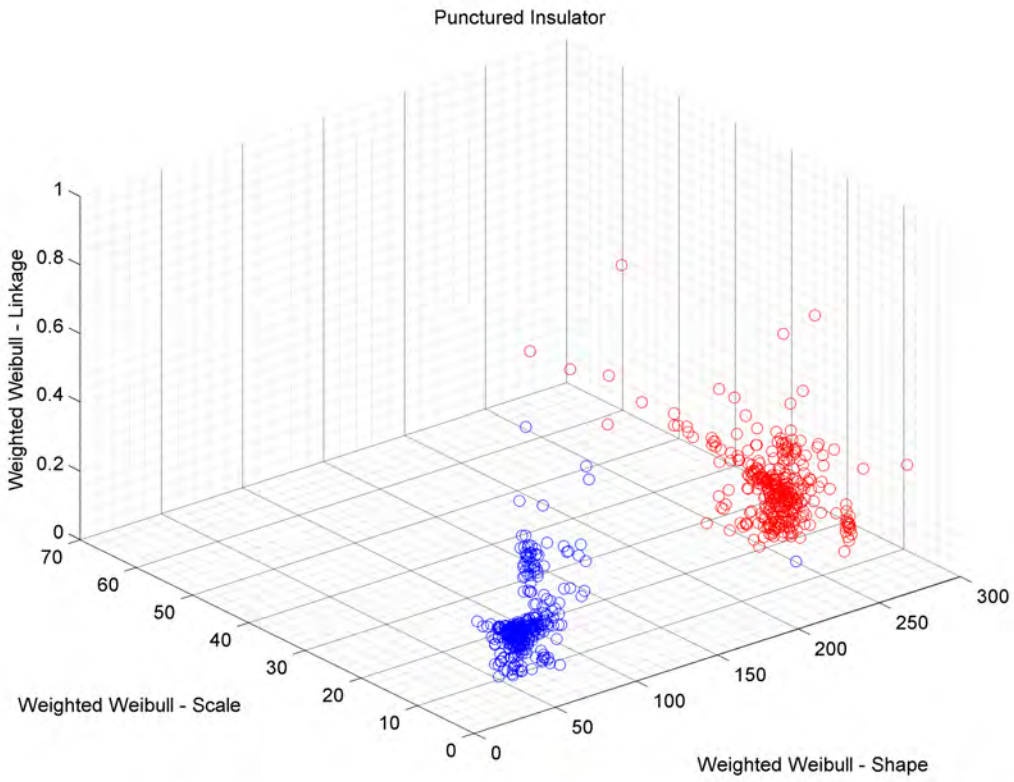

Figure 5.15: Fitted weighted Weibull parameters - punctured insulator; one blue point (positive half cycle) and one red point (negative half cycle) represent the extracted features from one of the 342 datasets during the weighted phase Weibull fitting.

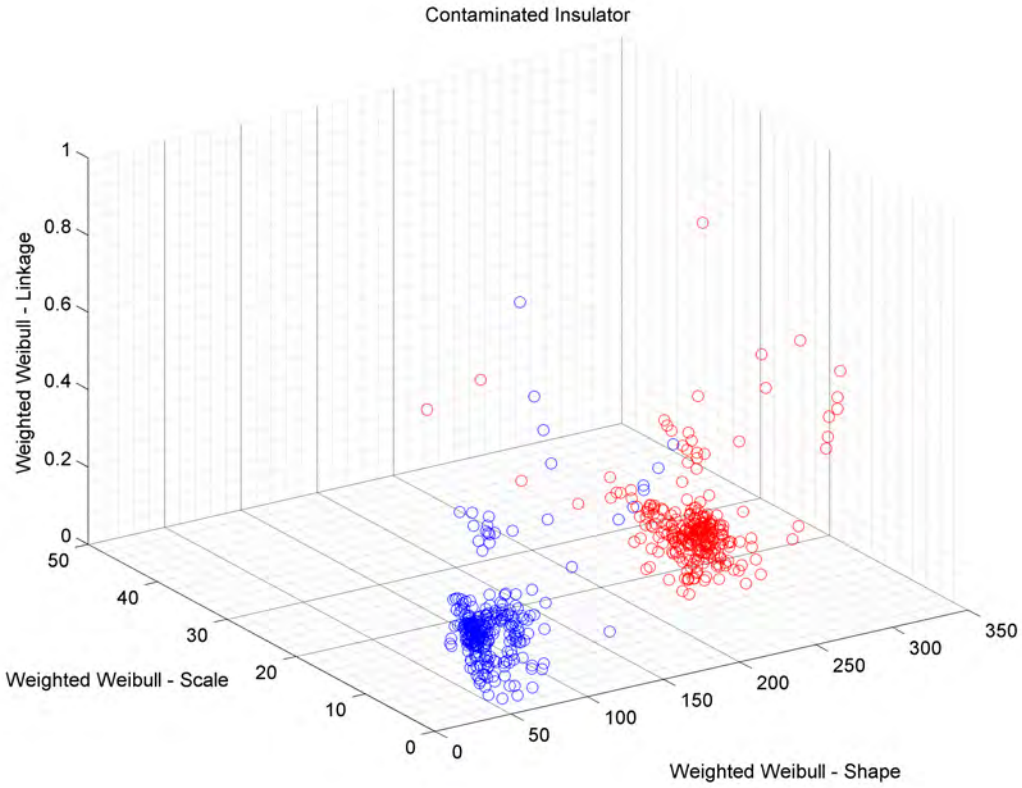

Figure 5.16: Fitted weighted Weibull parameters - contaminated insulator; one blue point (positive half cycle) and one red point (negative half cycle) represent the extracted features from one of the 288 datasets during the weighted phase Weibull fitting.

5.2.4 Spectral Fractal Analysis

As explained earlier in Section 5.1, the spectral fractal parameters for each segment of the dataset is calculated as part of the signal processing on the recorded electromagnetic radiations. The extracted parameters include the line parameters of a linear fit to the log-log spectrum of each electromagnetic radiation waveform in the range of 100 Hz to 10 kHz. The slope and Y-intercept of the fitted line in averaged over the 512 segments in each dataset and ultimately two averaged parameters will be extracted from each dataset. Figures 5.17,5.18,5.19 present the spectral fractal line parameters where the x axis is the slope of the fitted line, the y axis is the y-intercept parameter of the fitted line for normal, punctured, and contaminated insulators respectively.

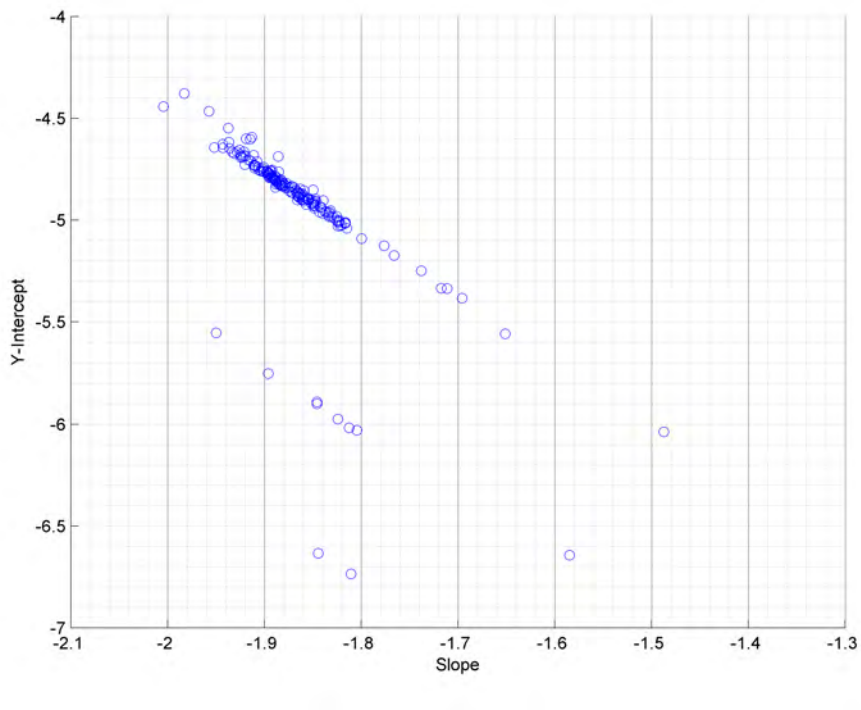

Figure 5.17: Line parameters of the spectral fractal analysis - normal insulator; each point represents the average of the fitted line parameters to 512 segments in each of the 176 datasets.

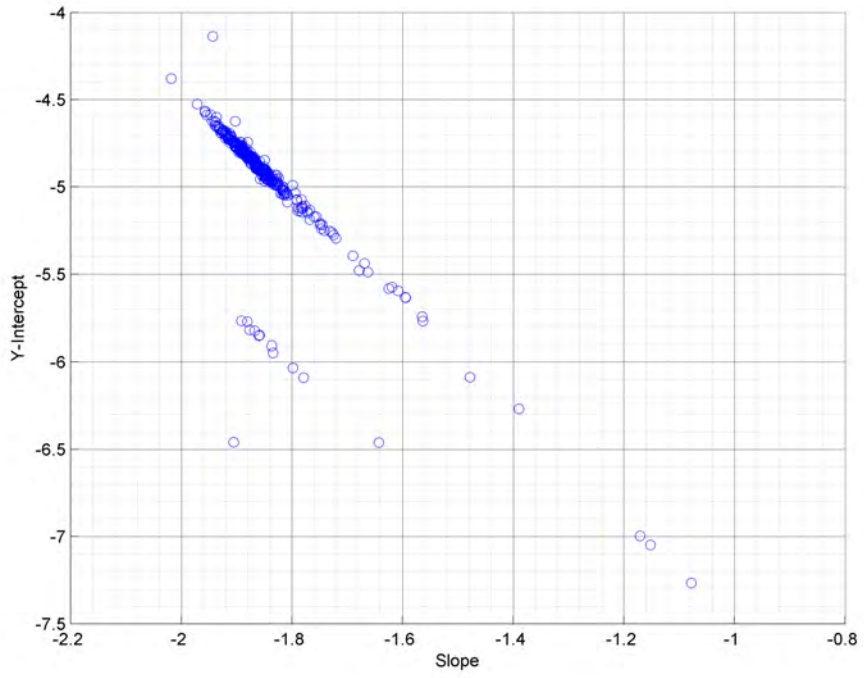

Figure 5.18: Line parameters of the spectral fractal analysis - punctured insulator; each point represents the average of the fitted line parameters to 512 segments in each of the 342 datasets.

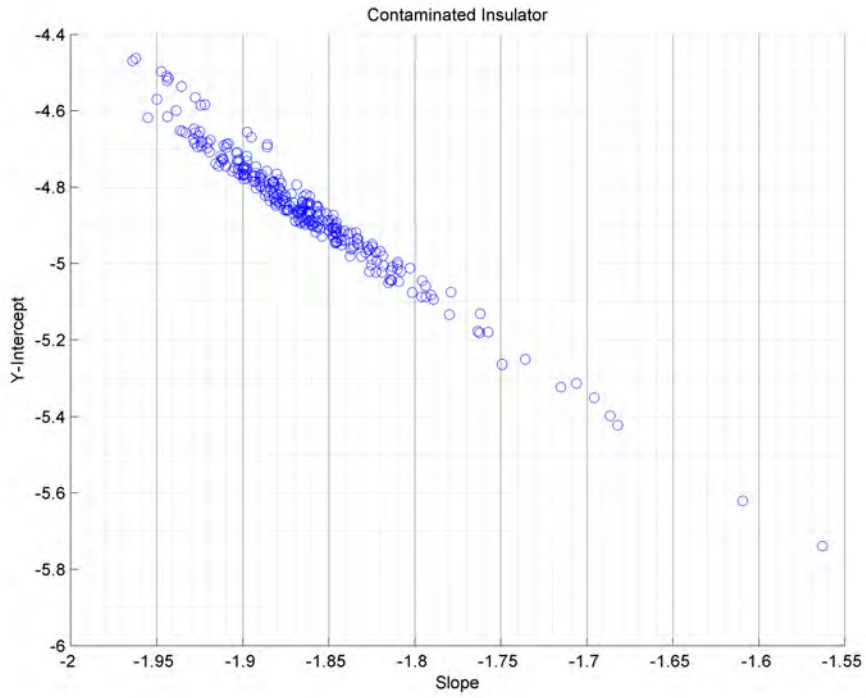

Figure 5.19: Line parameters of the spectral fractal analysis - contaminated insulator; each point represents the average of the fitted line parameters to 512 segments in each of the 288 datasets.

5.3 Classification

As described in Section 5.1, a total of 17 features were extracted from the electromagnetic radiation signature of insulators under test. These 17 features include five parameters from the phase Weibull fit, five parameters from the amplitude Weibull fit, five parameters from the weighted Weibull fit, and two parameters from the spectral fractal analysis. To investigate the signature of defective insulators within the extracted features, a 2D support vector machine (SVM) classifier was developed. The SVM classifier targets to classify the type of

insulators by searching distinct information in all 2D possible combinations of the extracted features. Having 17 features, there are 136 unique possible combinations (${}_2C_{17}$ = 136) for a 2D feature domain that the SVM classifier can look for distinct features. The performance of the classifier is also measured by its ability to correctly classify the recorded radiations. This section explains the algorithm for the SVM classifier and classification performance.

5.3.1 Classification Algorithm

For each type of insulator, a matrix with 17 rows corresponding to the 17 features was created. The number of columns on these matrices depends on the number of observation datasets available for each type of defect. Each column represents the statistical features from 512 cycles of recorded measurements. To identify the features with the maximum variance of information suitable for classification, a 2D support vector machine (SVM) classifier is developed. By supplying known observation sequences to the SVM algorithm, the classifier tries to find the best polynomial which can separate the 2D group of data from each other in the specified domain. The classifier uses support vectors s_i and weights a_i and a bias value b to find the optimized polynomial differentiating the two known categories. After finding the best polynomial (k, the kernel function), any observation x can be passed on to the SVM classifier where it calculates c using:

$$c = \sum_i a_i \, k(s_i, x) + b \tag{5.2}$$

If $c \geqslant 0$, x will be classified in the first category and and if $c \leqslant 0$, it will be classified in the second category.

In the following section, using the extracted features and the classification method explained earlier, every two types of insulators will be compared and analysed to study unique features of each type of insulators.

5.3.2 Fundamental 2D Classification of All Insulators

Having the feature matrix for each type of insulators, the classifier was trained for all possible 136 combinations of the 17 extracted features ($_2C_{17}$) of recorded observation datasets. In order to identify the features with maximum classification information, during each 2D classification, four random samples from the first type and four random samples from the second type of insulator were selected and a MATLAB code was developed to classify these eight samples using 136 different classifiers. At the end of this run, if a certain feature combination was able to correctly classify three or four of the random samples correctly in both categories, that combination was stored. This process is repeated for 10,000 times to evaluate the information in various combination of the extracted features.

5.3.2.1 Puncture vs Contamination

Figure 5.20 shows the results of 10,000 classifications performed on measurement datasets of punctured and contaminated insulators. The four most successful combinations in differentiating the punctured and contaminated insulators are shown in Table 5.1.

As shown in Table 5.1, the shape of fitted weighted Weibull in the negative cycle appears in all the combinations. To better illustrate the classification process, a classification using the combination ID 92 (see Table 5.1) is shown in Figure 5.21. The highlighted area in Figure 5.21 is zoomed in and presented in Figure 5.22

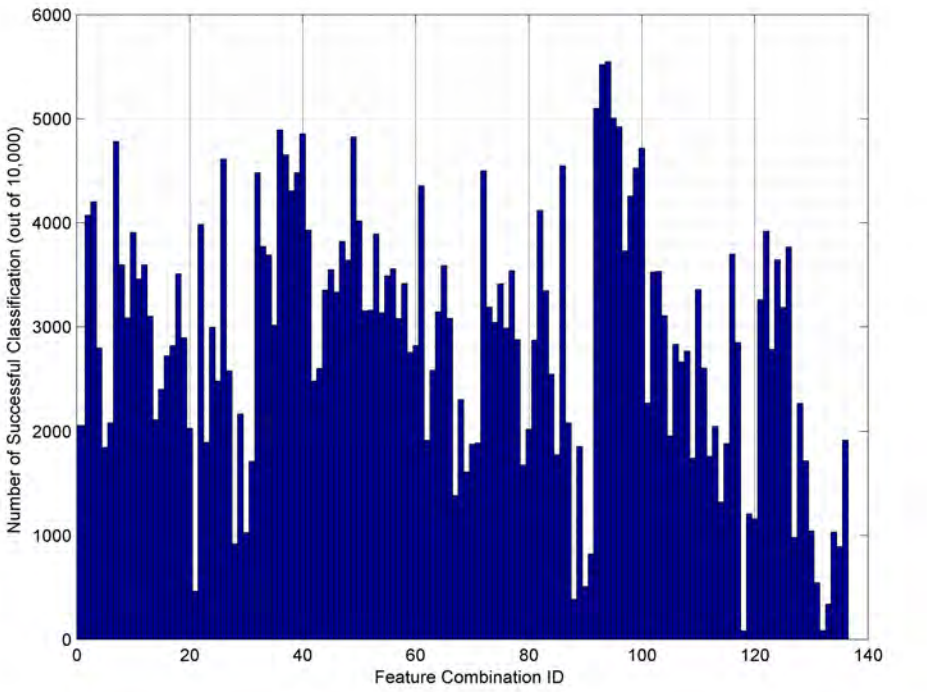

Figure 5.20: Successful classification rate of contaminated and punctured insulators using various combinations of extracted features.

to illustrate the performance of the classifier in differentiating contaminated and punctured insulators. Needless to say, many sets of features from both defects overlap in the Figure 5.22 and it is not possible to distinguish between the two. This proves that there are many common discharge activities that occur on both punctured and contaminated insulators.

The red line in Figure 5.21 and Figure 5.22 is the polynomial representing the decision function, separating the extracted features of punctured and contaminated insulators in Domain ID 92.

Table 5.1: Features with highest successful classification in Figure 5.20.

Combination ID	Successful Classification	Feature 1	Feature 2
92	5100	Weighted Weibull : Shape - Negative cycle	Weighted Weibull: Scale - Negative cycle
93	5520	Weighted Weibull : Shape - Negative cycle	Weighted Weibull: Linkage
94	5549	Weighted Weibull : Shape - Negative cycle	Amplitude Weibull: Shape - Positive Cycle
95	5006	Weighted Weibull: Shape - Negative cycle	Amplitude Weibull: Scale - Positive Cycle

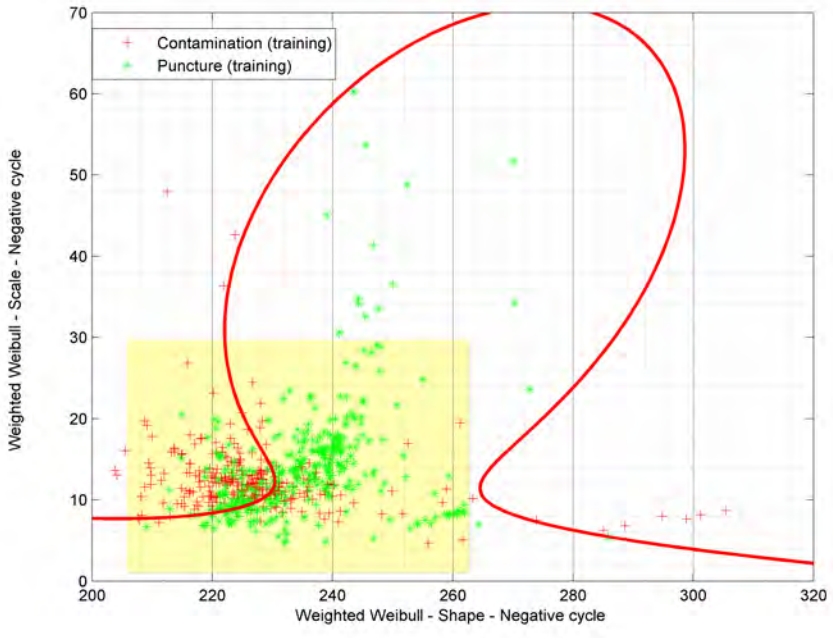

Figure 5.21: Sample of 2D classification of contaminated and punctured insulators using Combination ID 92.

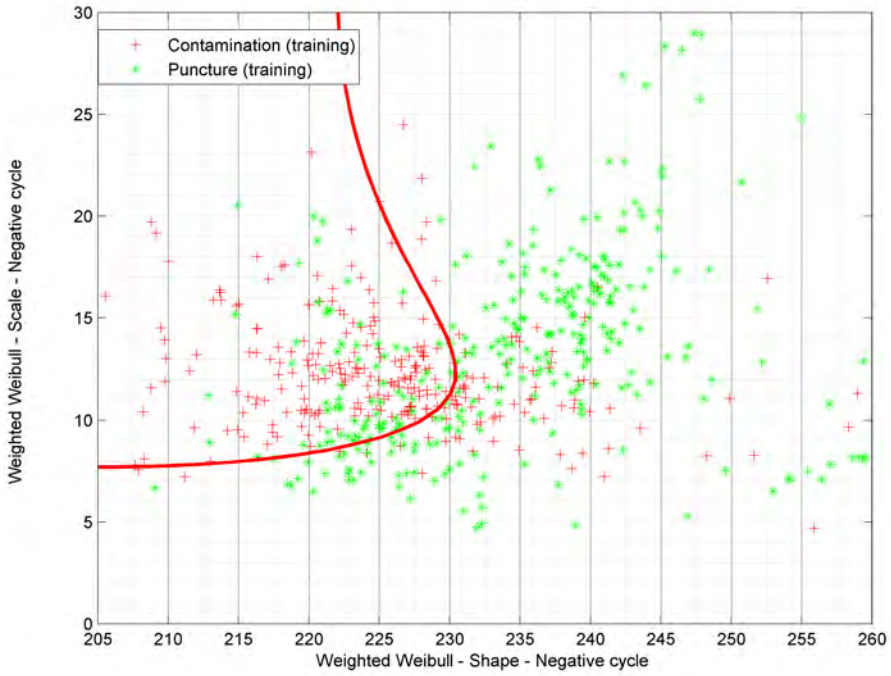

Figure 5.22: Zoomed highlighted area of Figure 5.21.

5.3.2.2 Puncture vs Normal

Figure 5.23 shows the results of 10,000 classifications performed on measurement datasets of punctured and normal insulators. The four most successful combinations in differentiating the punctured and normal insulators are shown in Table 5.2. No unique feature stands out in this classification for having a high successful classification rate. To better illustrate an example of classification in this category, classification of combination ID 66 is presented in Figure 5.24. The highlighted area in Figure 5.24 is zoomed in and presented in Figure 5.25 to show the performance of the classifier in differentiating between punctured and normal insulators. As it can be concluded from the relatively lower successful classification rate in this category (Figure 5.23), the features in these two categories overlap in various combinations (Figure 5.25). Therefore, it is very difficult to find a polynomial that can completely separate the features related to each type.

Table 5.2: Features with highest successful classification in Figure 5.23.

Combination ID	Successful Classification	Feature 1	Feature 2
64	3293	Phase Weibull: Linkage	Amplitude Weibull : Shape- Positive Cycle
66	3355	Phase Weibull: Linkage	Amplitude Weibull : Shape - Negative Cycle
110	3260	Weighted Weibull : Linkage	Amplitude Weibull : Scale - Positive Cycle
124	3190	Amplitude Weibull: Scale - Positive Cycle	Amplitude Weibull - Linkage

The red line in Figure 5.24 and Figure 5.25 is the polynomial representing the decision function, separating the extracted features of normal and punctured insulators in Domain ID 66. The red circles in Figure 5.24 show four random

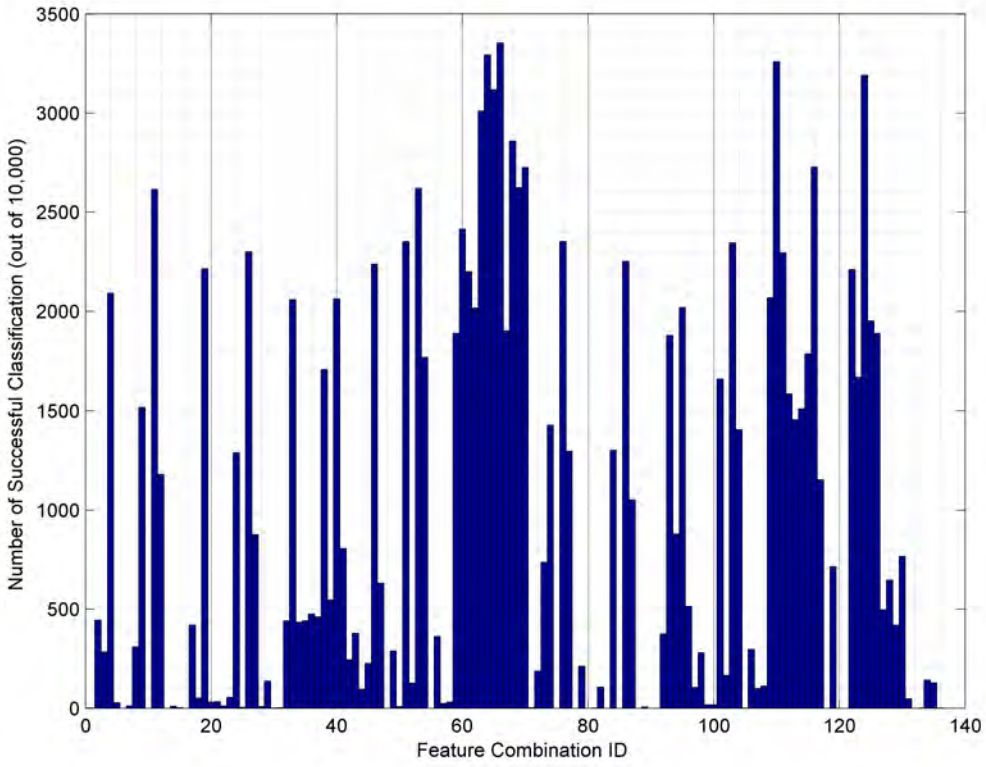

Figure 5.23: Successful classification rate of punctured and normal insulators using various combinations of extracted features.

puncture samples that were classified using the polynomial (in red) in this feature domain. Three out of four random samples have been classified correctly while one sample is classified incorrectly as normal. Similarly, the green circles in Figure 5.24 show four random normal samples that were classified using the polynomial (in red) in this feature domain. Three out of four random samples have been classified correctly while one sample is classified incorrectly as punctured.

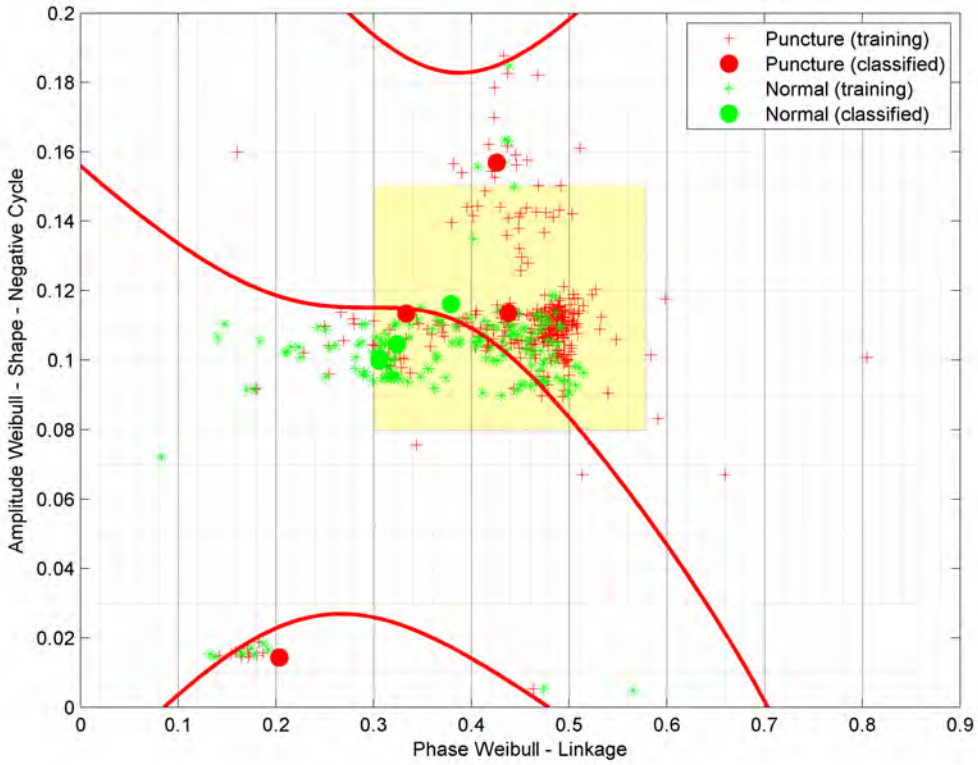

Figure 5.24: Sample of 2D classification of punctured and normal insulators using Combination ID 66.

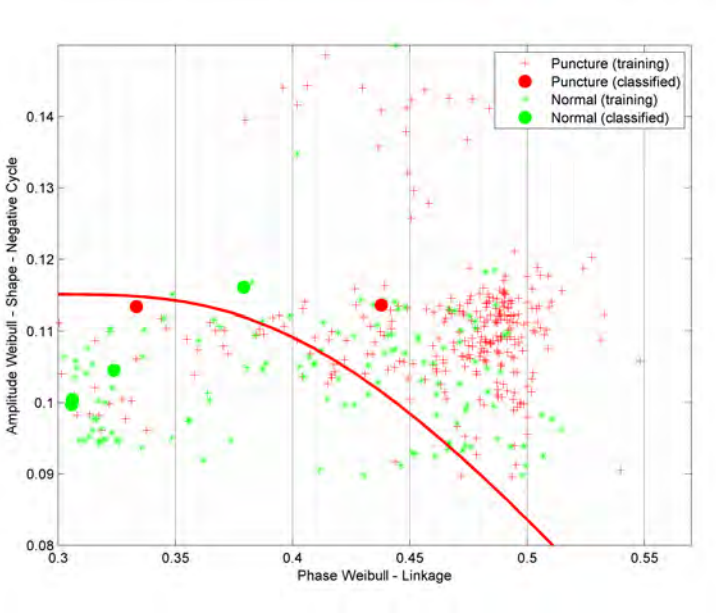

Figure 5.25: Zoomed highlighted area of Figure 5.24.

5.3.2.3 Contamination vs Normal

Figure 5.26 shows the results of 10,000 classifications performed on measurement datasets of contaminated and normal insulators. The four most successful combinations in differentiating the contaminated and normal insulators are shown in Table 5.3. Similar to classification of punctured and normal insulators, no unique feature stands out in this classification for having a high successful classification rate. To better illustrate an example of classification in this category, classification of combination ID 47 is presented in Figure 5.27. The highlighted area in Figure 5.27 is zoomed in and presented in Figure 5.28 to show the performance of the classifier in differentiating between contaminated and normal insulators. As it can be concluded from the relatively lower successful classification rate in this category (Figure 5.26), the features in these two categories overlap in various combinations (Figure 5.28). Therefore, it is very difficult to find a polynomial that can completely separate the features related to each type.

Table 5.3: Features with highest successful classification in Figure 5.26.

Combination ID	Successful Classification	Feature 1	Feature 2
12	2785	Phase Weibull: Shape - Positive Cycle	Amplitude Weibull: Shape - Negative Cycle
47	3438	Phase Weibull : Scale - Negative cycle	Weighted Weibull: Shape - Positive cycle
75	2440	Weighted Weibull : Shape - Positive cycle	Amplitude Weibull: Shape - Positive Cycle
77	2571	Weighted Weibull : Shape - Positive cycle	Amplitude Weibull : Shape - Negative Cycle

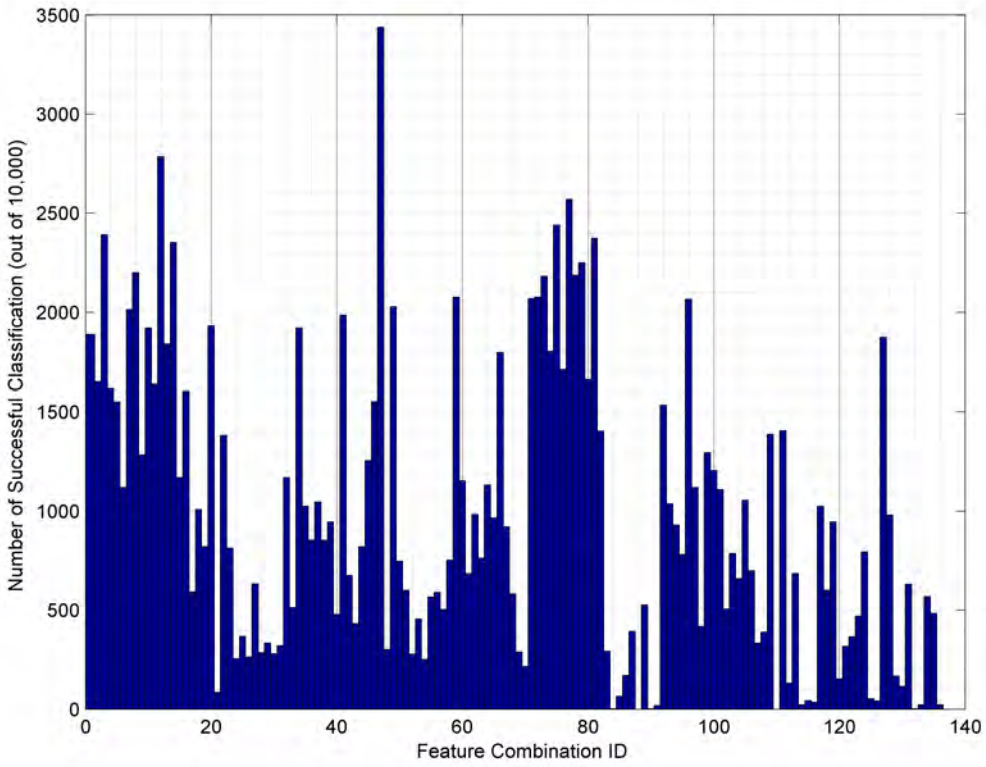

Figure 5.26: Successful classification rate of contaminated and normal insulators using various combinations of extracted features.

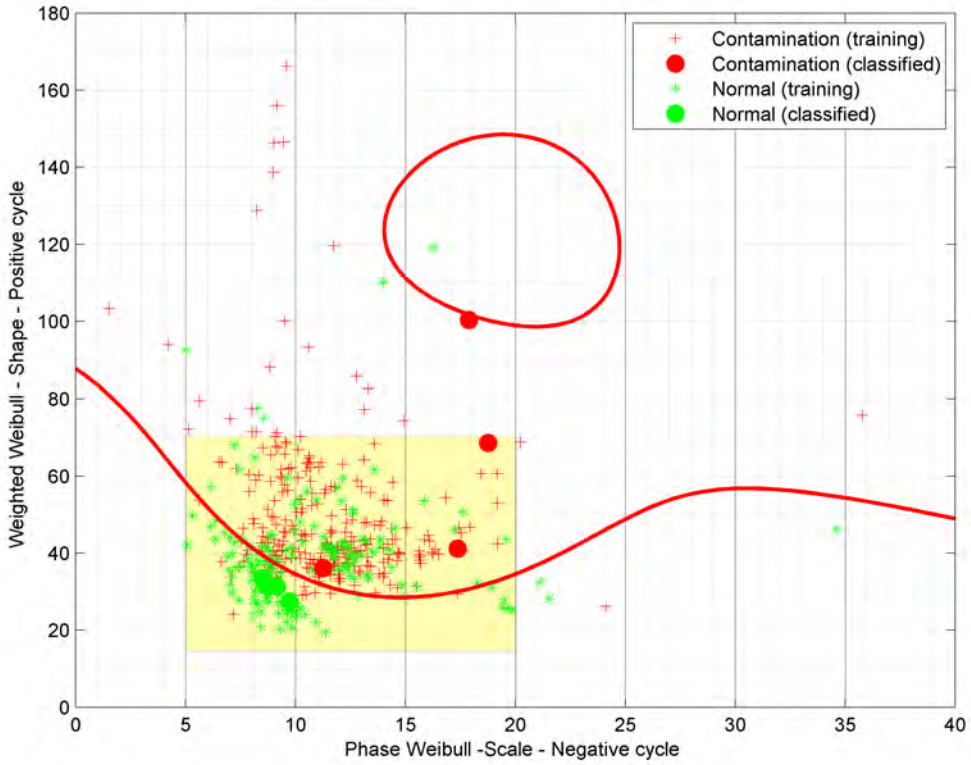

Figure 5.27: Sample of 2D classification of contaminated and normal insulators using Combination ID 47.

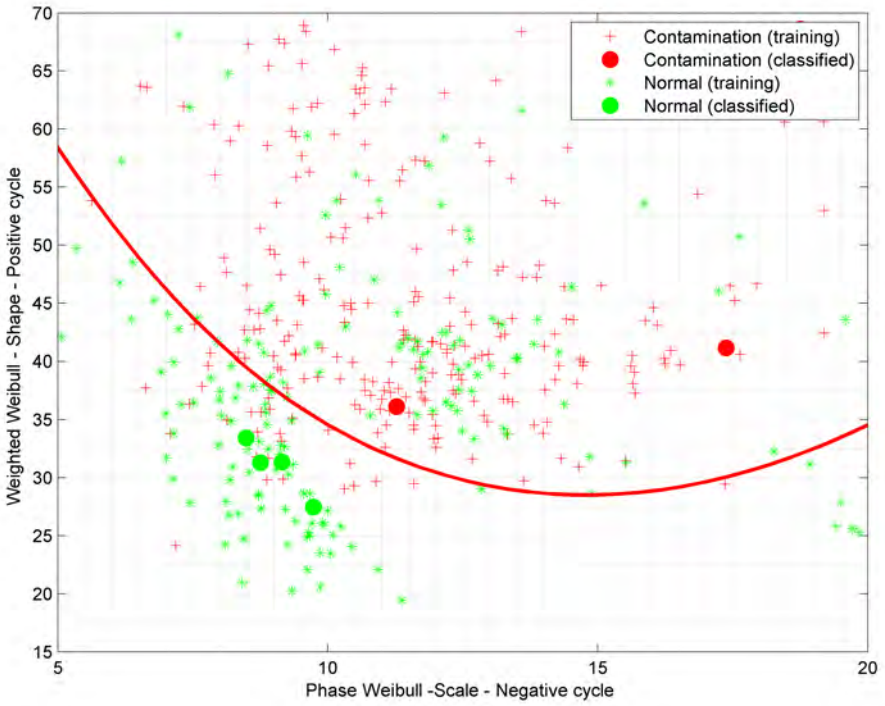

Figure 5.28: Zoomed highlighted area of Figure 5.27.

5.3.2.4 Discussion on the Results of 2D Classifications

As presented in the previous section, many sets of features from all three types of insulators overlap in many domains and it is not possible to find a decision boundary that can successfully split the sets of features related to each defect even when considering the concept of soft margin statistical classifiers [100].

The main reason for having so many overlapping datasets is in the nature of the measurements. Partial discharge pulses are not solely originated from the defects on the insulators. There are many other sources of partial discharges that are common is all three different settings such as the PD sources within the transformer, corona, and discharges due to high voltage stress around metal fittings of the insulators. Since the HV source has a nominal rating of 230 kV, it is very unlikely that it can be the source of PD around 55 kV, however there is no guarantee that the source is PD free.

The classification results indicated that common discharge activities on all three different test setups must be present, regardless of the type of defect on the insulators. To investigate this common discharge activity, pictures with a corona camera were taken from energized insulators in all three setups. Figure 5.29 shows a normal discharge activity on a punctured insulator under high voltage stress. There are many discharges around the metal fitting of the insulator. These discharge activities are present even in the case of normal healthy insulators, contaminated insulators and punctured insulators. These discharges are invisible to the naked eye but can be seen using a corona camera. Figure 5.30 shows a discharge bridging the puncture path in a punctured insulator differentiating the common discharge activities from a puncture discharge.

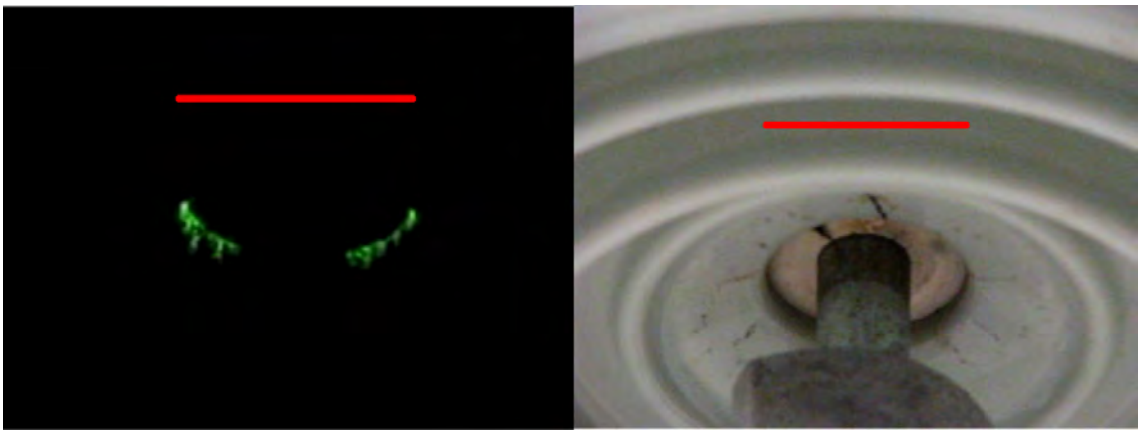

Figure 5.29: Normal discharge activities near the metal fitting on a punctured insulator; corona camera on left and normal camera on right.

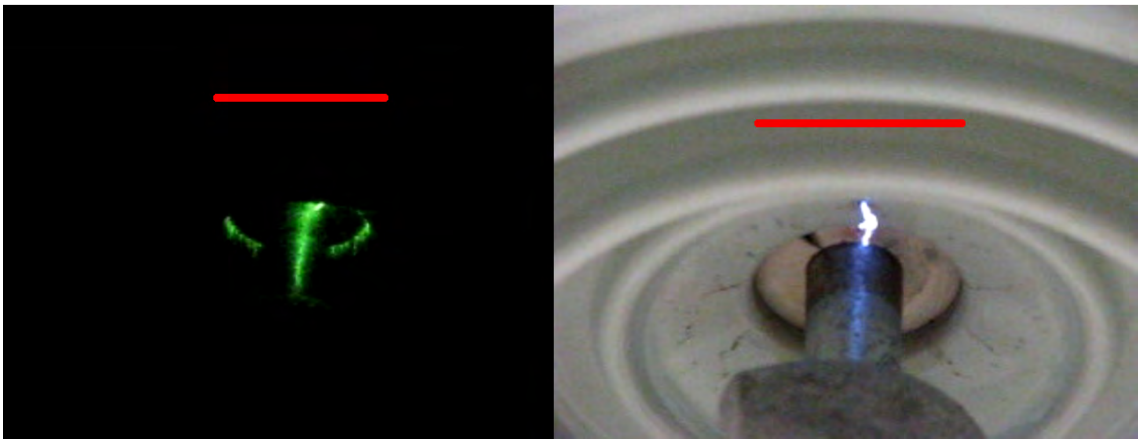

Figure 5.30: Discharge through the puncture path of a punctured insulator; corona camera on left and normal camera on right.

According to the pictures taken by a corona camera and also the results presented in the past sections, it was clear that a significant signature of normal discharge activities will be present in the captured radiation of all insulators. Therefore, a gating based algorithm was developed ([101],[102]) to filter out the common features present in the discharge activities of normal insulators. The concept is to eliminate the PD signatures that are present in the measurements recorded when only normal insulators were on the tested string. The following section elaborates more on the

gating algorithm and the results obtained after applying the gating algorithm.

5.3.3 Gating Algorithm

The measurement results show that normal discharge activities are quite dominant in all types of studied insulators. Therefore, a gating algorithm was developed to eliminate the signature of normal discharge activities from the captured electromagnetic radiation of contaminated and punctured insulators. Examining the successful rate of 2D classification of punctured and contaminated insulators shown in Figure 5.20, the 2D Domain 92 (Domain parameters shown in Table 5.1) was chosen to be the focus of the gating algorithm.

The gating algorithm discards any feature observation pair from the contaminated or punctured insulator when they are in the vicinity of any feature observation of normal insulators.The algorithm was implemented in the Domain 92 only and a new feature matrix was generated that excluded the overlaps of normal insulators with contaminated and punctured insulators.

In other words, the normal discharge activities are treated like noise in the classification algorithm. IEC 60270 [101] explains the use of gating algorithm for noise cancellation applications as well as PD locating algorithms. OMICRON [75] (one of the lead companies in building commercial PD detection systems) has also implemented statistical gating algorithms in their PD acquisition system [103].

As shown in Figure 5.31, the successful classification rate has raised almost 50% from 5100 successful classification in Table 5.1 to 7575 successful classification as shown in Figure 5.31. The new classification shows unique information regarding the type of defect in Domain 92.

Figure 5.32 shows the 2D classification of between the punctured and contaminated insulators when the overlapped normal discharge activities were removed from the captured radiations of contaminated and punctured insulators.

Figure 5.33 shows the overlapped data in Domain 92 from normal, contaminated and punctured insulators that were taken out by the gating algorithm.

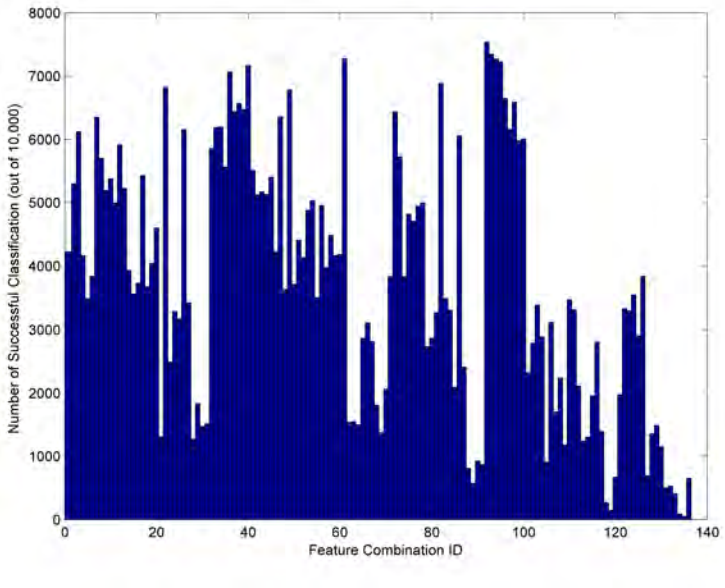

Figure 5.31: Successful classification rate of punctured and contaminated insulators excluding the overlapped normal discharge activities using various combinations of extracted features.

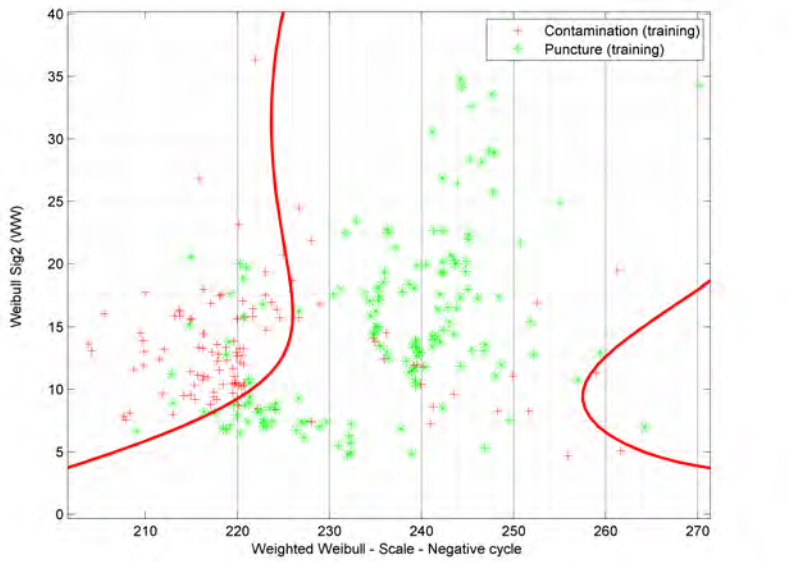

Figure 5.32: 2D Classification of punctured and contaminated insulators using Combination ID 92.

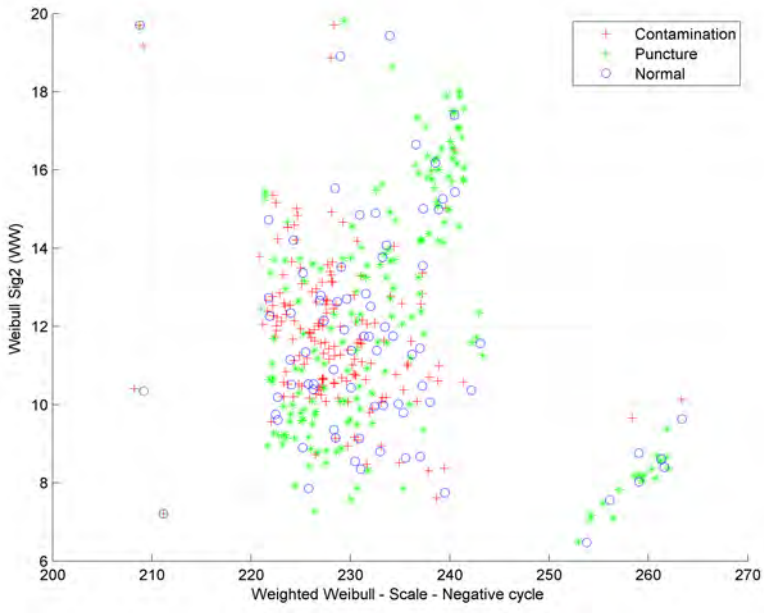

Figure 5.33: Eliminated sets of features during the gating algorithm.

5.3.4 Analysis of Gated Classification Results

Statistical processing on the captured electromagnetic radiation due to partial discharge activities from normal, contaminated, and punctured insulators shows that there are unique features that can separate the radiation signature of defective units. The main challenge in separating the features of defective units is the common normal partial discharge activities that are present on all three types of insulators. As shown in Figure 5.29, the high voltage stress near the bottom metallic fitting of porcelain insulators constantly causes discharge activities. Similar discharge activities on normal and clean porcelain insulators have been also reported in other publications [104]. The gating algorithm explained in the previous section eliminates the observations that are suspected to be related to normal partial discharge activities. After applying the gating algorithm, the 2D classification of punctured and contaminated insulators had a significantly higher successful classification rate, highlighting unique statistical features of each defect.

As shown in Figure 5.32, the signatures of punctured and contaminated insulators in Domain 92 have separable features. To explain the mapping and features of Domain 92, four sample Weibull distributions are presented in Figure 5.34. The four Weibull distributions plots shown in Figure 5.34 represent the four highlighted area shown in Figure 5.35.

Regions 1, 2, and 3 in Figure 5.35 correspond to puncture feature signatures, representing discharge activities that have higher negative cycle phase occurrences compared to Region 4 which relates to the signature of contaminated insulators. The higher phase angles (closer to 270 degrees) on radiated signature of punctured insulators indicate that the discharge requires higher electric stress to bridge the

insulation. On the other hand, the discharge activities on the contaminated insulators occur in lower phase angles, corresponding to lower required voltage.

When the recorded puncture observations shown in Figure 5.35 were traced back to the measurement logbook, it was observed that the Region 1 points mostly relate to punctured insulators that were tested right after they were made in the lab. Similarly, the features in Region 3 mostly relate to the measurements that were recorded in the last month of the lab work. By inspecting the sample distribution plots shown in Figure 5.34, it can be concluded that the puncture path characteristics change when the puncture channel has been under continuous electric stress. The partial discharge activities on the early stages of puncture path (Region 1) are mainly concentrated in higher negative cycle phase angles. As the puncture path experiences continuous discharge activities, a wider phase range of discharges will occur and the centre phase shifts to lower phase angles. This behaviour should be related to the chemical reactions within the puncture track while the unit is kept under electric stress which eventually changes the characteristic of the puncture channel.

In conclusion, the statistical analysis performed on the radiation signature of punctured and contaminated insulators indicate separable features in the distribution of partial discharge activities. These features relate to the partial discharge activities in the negative half cycle of the voltage.

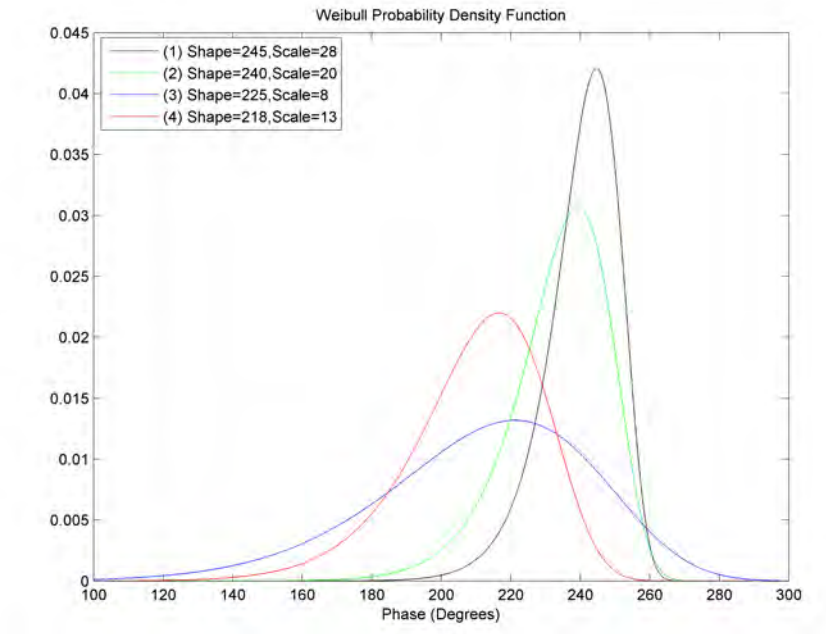

Figure 5.34: Four sample Weibull distribution functions.

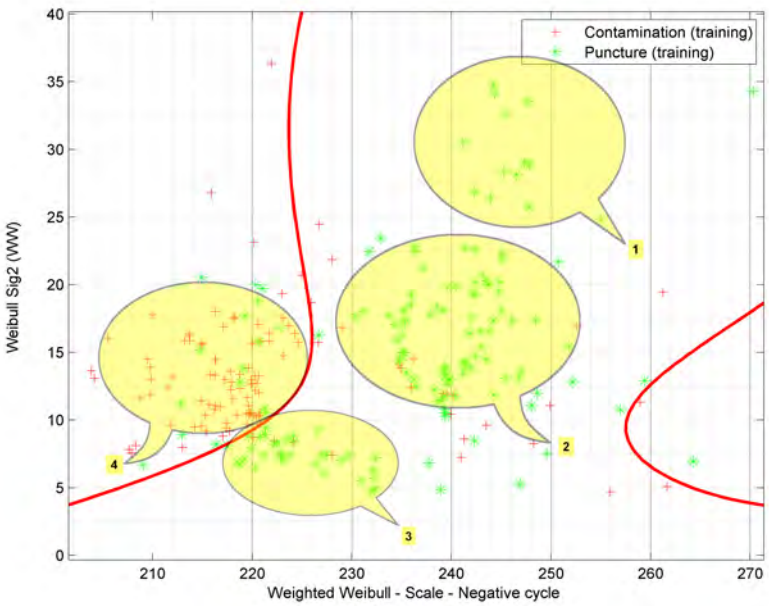

Figure 5.35: Four clusters in 2D classification using Domain ID 92.

5.4 Summary

The signal processing algorithms for extracting the features from the captured electromagnetic radiations were explained in this chapter. Also scatter plots showing the results of feature extracting algorithm on all three types of insulators under test were presented. After extracting 17 features from each type of insulator, the SVM classifier was programmed to find the best feature domain to separate the radiation signatures. Difficulties in classifying the radiation signatures were improved by introducing a gating algorithm, using the common discharge activities as a baseline to unmask the unique features of each defect.

Prior to implementing the gating algorithm, the classifier's successful classification rate in differentiating contaminated and punctured insulators was about 51 %. After implementing the gating algorithm, the successful classification rate increased to about 75 %.

6

Conclusions and Future Work

6.1 Conclusions

Physical defects such as punctures and contamination can degrade the insulators performance and result in power outages, potentiating costs to utilities. Therefore, condition assessment of line insulators has always been one of the most important aspects of maintenance programs in power networks. A novel approach for inspecting the condition of porcelain insulators based on statistical analysis of electromagnetic radiations of live insulators was proposed in this thesis. The methodology presented in this thesis is based on recording the electromagnetic radiations from porcelain insulators using a wideband electric field sensor (the D-dot sensor) and performing statistical analysis and classification.

During the preliminary discussions with the Manitoba Hydro Field Testing Group, contamination and punctures were identified as the two most common types of defects on porcelain insulators. Punctured insulators were created in the lab by applying high voltage stresses on the insulators submerged in oil, following the

puncture withstand test specified in the IEC standard [89]. Contaminated insulators were developed in the lab following the IEC standards [20] using the concept of Equivalent Salt Deposit Density (ESDD). The contaminated insulators studied in this research with the ESDD level of 0.28 mg/cm^2, can be categorized as heavily contaminated insulators according to the contamination level definitions provided in the IEEE standard 1313.2 [87]. To duplicate realistic environmental conditions, a fog chamber was built and included in the measurement setup. The fog chamber helped to control the level of humidity when the insulators were tested.

During the experimental part of this thesis, a multitude of tests were conducted and resulted in a large amount of lab measurements. A total of 410,000 cycles of discharge activities were measured and recorded. From the total of 410,000 recorded measurements, 90,000 cycles (176 datasets) of recorded radiations originated from normal insulators, 175,000 cycles (342 datasets) from punctured insulators, and 145,000 cycles (288 datasets) from contaminated insulators. To analyse the raw measurement data obtained throughout testing, a MATLAB graphical user interface (GUI) capable of performing various data processing techniques was developed. Due to the random nature of partial discharges, the data processing was focused on statistical features of the recorded measurements.

A total of 17 features were identified that were mainly focused on the phased resolved pattern of discharges and were extracted from each dataset of recorded measurements. Weibull distribution functions were fit to the histogram of the raw data to extract the trends of discharge patterns of each type of insulators. Even normal and healthy insulators under high voltage stresses experience partial discharge activities, mainly near the bottom metallic fitting (see the corona camera image shown in Figure 5.29). The signature of these partial discharge activities

are not only present in the leakage current (ground wire current) but also in the radiated electromagnetic fields (see Figure 4.4). To overcome this issue, a gating algorithm was developed to eliminate the signature of normal, over-stressed partial discharge activities. Also, a SVM classifier was developed to differentiate the radiated signature of punctured and contaminated insulators from healthy functioning insulators. The classification has shown promising detection rates, confirming the classification ability of the novel remote assessment tool proposed in this thesis. The statistical analysis of radiated signature of defective insulators shows the partial discharge activities on the punctured insulators have higher negative cycle phase occurrences compared to the contaminated insulators. The higher phase angles (closer to 270 degrees) indicate that the discharges require more electric stress to bridge the insulation in the case of punctured insulators. On the other hand, the discharge activities on the contaminated insulators occur in lower phase angles, indicating lower required voltages for discharges to occur. In conclusion, the shape parameter of Weibull distribution fit to the weighted phase location of partial discharges has unique information in the negative half cycle, which can be used for the classification of punctured and contaminated insulators.

6.2 Main Contributions

The achievements and main contributions of this thesis are summarized as follows.

- Introduction of a new porcelain insulator inspection technique that can remotely identify normal, punctured, and contaminated porcelain insulators using their electromagnetic radiation signature in a laboratory environment,
- Demonstration of the ability and performance of the novel idea of utilizing an electric field sensor to capture partial discharge radiations from defective insulators. The use of D-Dot sensors in PD detection on line insulators has not been reported in literature or industry,
- Development of unique statistical feature extraction that can reveal distinguishable information within each of the defective insulators studied in the thesis,
- Capturing and recording a total of 410,000 cycles of discharge activities during the lab measurements that resulted in developing a meaningful population of data to support the statistical feature extraction algorithm,
- Development a 2D Support Vector Machine (SVM) classifier to differentiate the signature of defects in various 2D feature domains and identifying the feature domains with the maximum distinct information,
- Overcoming the problem of overlapped sections of extracted features in the 2D feature domains which led to identifying the source of a common signature; normal discharge activities near the bottom pin of the insulators. Knowing the source of common signature, a novel gating algorithm was developed based

on the extracted features of normal insulators. The performance of the SVM classifier improved significantly after implementing the gating algorithm.

6.3 Future Work

The work described in this thesis is based on measurements recorded in a controlled lab environment. The next steps for continuing this work involve data acquisition from a string of insulators in service. To ensure the existence of a defective insulator on the string, close contact methods (such as DC resistance meter or buzz method) can be used. When the defective unit is identified on the string, a similar setup can be used to record the electromagnetic radiations. Measurements from normal and healthy insulators should also be taken to identify the baseline discharge activities of normal insulators.

Field implementation of inspection techniques similar to the one presented in this research can be quite challenging. The measurements results reported in this research were obtained in a controlled lab environment with very low levels of environmental noise. As part of furthering this research, noise cancellation algorithms can be developed to improve the signal to noise ratio on the captured radiations.

Furthermore, during the span of 6 months of lab measurements, the discharge patterns of punctured insulators exhibited correlations with the age of puncture tracks. The results indicate that the properties of the puncture track change when it is exposed to continuous discharge activities. Studying the puncture track ageing behaviour and investigating the effect of discharge activities on the overall insulation properties of the porcelain insulator can be helpful in understanding the effect of puncture track properties on the discharge signature, another development initiated by this research.

Appendix A

Partial Discharges under AC Voltage

A.1 Definitions

By definition, partial discharge is an electrical discharge that occurs over a portion of the dielectric between two high voltage electrodes and does not bridge the whole gap [105]. Partial discharges may occur in cavities within solid insulation, on the surface of insulating material or around the sharp edges of high voltage electrodes. The term corona is often used for the partial discharge around the sharp points which manifests in gaseous media around conductors and remote from solid or liquid insulation. "Corona (in air) is a luminous discharge due to ionization of the air surrounding a conductor caused by a voltage gradient exceeding a certain critical value" [88]. The term "Flashover" is used when a surface discharge bridges the insulation. However, these terms are used interchangeably in high voltage articles and textbooks. Other than the terms that were mentioned, terms such as "local

breakdown", "sparking", "streamer", "partial breakdown" and " swarming PD" have been used in many papers to describe different types of partial discharge phenomena concerning the discharge ionization mechanism or discharge location [92]. In this report, the term "partial discharge" is defined based on IEC standards. According to the IEC 60270[101], "partial discharge is a localized electrical discharge that only partially bridges the insulation between conductors which can or cannot occur adjacent to a conductor. Partial discharges are in general a consequence of local electrical stress concentrations in the insulation or on the surface of the insulation. Generally, such discharges appear as pulses having a duration of much less than 1 picosecond. More continuous forms can, however, occur, such as the so-called pulseless discharges in gaseous dielectrics. Partial discharges are often accompanied by emission of sound, light, heat, and chemical reactions."

A.2 Partial discharge process in voids under AC conditions

One of the most common reasons for an insulator's failure is the presence of voids inside the insulation material. Depending on the type of insulation material and also the manufacturing process, different shaped voids can develop inside insulation systems. Having a void inside the insulation does not necessarily mean that the insulation will fail over time; it highly depends on the level of partial discharge activities inside that void under the normal voltage stress. In this section, the partial discharge process inside voids will be discussed briefly. Voids inside the insulating material are always under higher electrical stress compared to the surrounding

insulation. Consider a flat void as shown in figure A.1.(a):

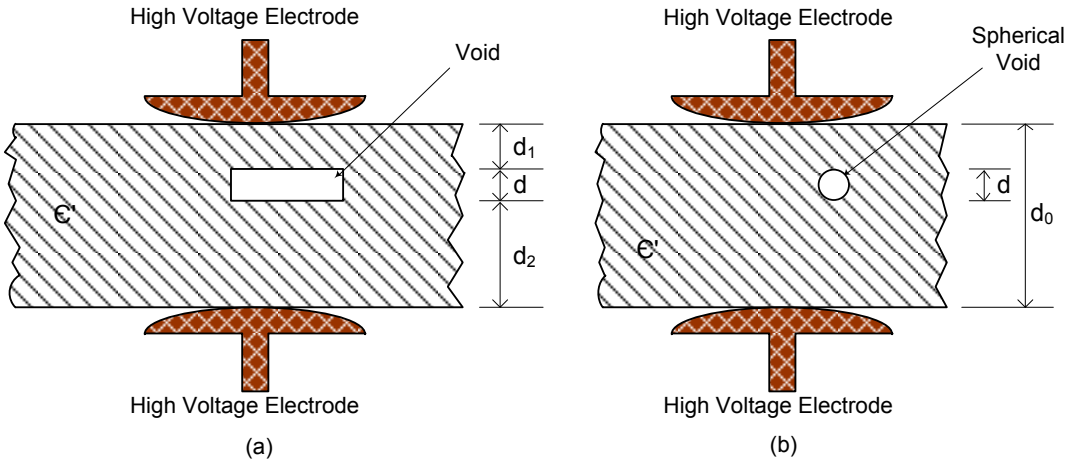

Figure A.1: Voids inside insulation system.
(a) Rectangular void
(b) Spherical void

If E is the average electric field inside the insulation and E_b is the breakdown voltage of the void, the electric field required to cause the breakdown inside the void is given by [16]:

$$E = E_b + E_d = E_b(1 + \frac{d_1 + d_2}{d\epsilon'}) \tag{A.1}$$

Where E_d is the voltage drop across the dielectric layers surrounding the void. In other words, in order for breakdown to occue, the void needs at least E_b across its walls. Now to have E_b across the void, the electric field E has to be across the whole gap. The electric field inside the void is a function of the void geometry. As shown in Figure A.1.(b), most of the actual voids in the insulation systems have approximately spherical shapes. The equation A.1 should be slightly modified in order to properly formulate the required electric field for the gap breakdown of spherical voids. Equation A.2 which is given by [106] can be used for the case of

spherical voids.

$$E = \frac{E_b}{d}\left[d + \frac{d_0(1+2\epsilon')}{3\epsilon'}\right] \tag{A.2}$$

Where d_0 is the total thickness of the dielectric and d is the diameter of the void. There has been substantial work on calculating E_b for different geometries of voids. It has been shown that E_b is a function of the product of pressure and gap separation (pd) and also involves Paschen's law. Measurements were done for different geometries and the graphs are available to relate the required E_b for specific pd in each case [107]. The breakdown voltage also depends on the dielectric constant of the material inside the void, but in the most of practical cases voids are filled by air. The breakdown mechanism of metallic surfaced gaps under uniform electric field stresses can be interpreted by the Townsend discharge process. The breakdown mechanism can be explained using Townsend coefficients and the concept of electron avalanche [17]. However, this mechanism cannot be easily extended to the breakdown inside the voids as they have dielectric walls compared to the gap. For example, Townsend's second coefficient which measures the electron regeneration probability highly depends on the cathode and anode materials. Moreover, the electric field inside the void is more distorted compared to metallic surfaced gaps. Some studies have tried explaining the breakdown mechanism using streamer discharge theory [18, 108]. According to this theory, the high electric field stress will accelerate the electrons and these fast electrons will give rise to other electrons on their way. Ions move at much slower speeds compared to electrons, which is how the streamer forms inside the gap. When there are enough high speed free electrons on the streamer, they bridge the gap and the breakdown happens. When the streamer completely bridges the gap, a conductive plasma

channel is developed inside the gap and the spark can be observed. In summary, the two types of discharge that can occur in metallic surfaced gaps are the Townsend's discharge and streamer discharge. The detected discharge resulting from Townsend's discharge is faster with lower amplitude compared to streamer's discharge. On a metallic surface gap, by increasing the voltage across the gap, Townsend's discharge will be observed first and as the voltage increases and the channel becomes ionized, the streamer discharge can be observed. Now to extend these theories to discharge mechanisms inside voids, we have to consider some differences:

- The electric field distribution inside the void is not only dependent on the voltage across the electrodes, but also on the surface charge distribution on the dielectric boundaries.

- When a discharge occurs on metallic surfaced gaps, the total charge will be discharged into the metallic electrodes. However, due to the relatively high resistance of the electrodes, in the dielectric surfaced gaps, there could be more than one discharge happening at the same time to discharge all the electrons.

- When a discharge happens on a specific point of the surface of a dielectric surfaced gap, the charge distribution on other parts of the surface remains unchanged. This is mainly due to the immobility of surface charges.

To investigate the discharge mechanism in voids inside dielectrics, some experiments were done on a test setup that involved one metallic electrode and one dielectric electrode [109]. In case of DC voltage supply, different discharge patterns were recorded depending on the polarity of the dielectric electrode [110]. When the AC voltage was applied, a combination of different patterns were observed and collected

by changing the polarity of the DC voltage in the DC test setup. One certain conclusion that was determined by these experiments was the fact that more than one discharge is needed to entirely discharge the capacitance of the physical voids inside the insulation. This means that the discharge amplitude in dielectric surfaced gaps is lower compared to the metallic surfaced gaps.

A.3 Equivalent electric circuit for voids inside insulating material

Knowing the electrical equivalent circuit of voids can be very helpful in understanding the discharge parameters such as discharge waveform, rise time, amplitude, etc. One of the first experiments that has been reported on this topic consists of a very simple test setup with a capacitor in series with a metallic gap while the oscilloscope is connected across the gap [111]. Four discharges were recorded per cycle when the applied voltage across the gap was larger than the discharge onset voltage. Based on this experiment, a very simple circuit model was proposed which is shown in Figure A.2.

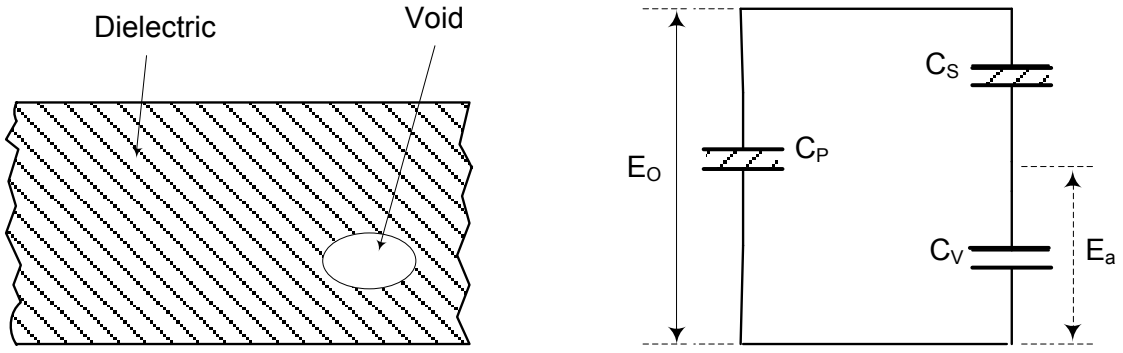

Figure A.2: Circuit model for a void inside the insulation system

In this circuit, C_V represents the capacitance of void, C_S represents the total capacitance in series with the void and C_P represents the remaining capacitance which is in parallel with C_V and C_S in series. Although the circuit is very simplified and totally neglects the surface leakage effect on the dielectric walls, it still can be used to explain the basic discharge mechanism in voids. If E_b is the breakdown voltage of the void, when there is enough voltage across the dielectric gap that provides E_b across the void, the breakdown happens. When the breakdown occurs, the voltage across the void drops significantly to a new voltage that is called E_r. The difference between these two voltages is $\Delta E(\Delta E = E_b - E_r)$. In order to charge up the void capacitance again to the voltage E_b, charge ΔQ is needed to be drawn from C_P

$$\Delta Q = \frac{\Delta E C_V C_S}{C_V + C_S} \tag{A.3}$$

In most structure, $C_S \ll C_V \ll C_P$, so the above equation can be simplified to A.4:

$$\Delta Q = \Delta E \times C_S \tag{A.4}$$

So ΔQ is a good measure for discharge magnitude as it directly relates to ΔE. Now we can calculate ΔW ,the average power dissipated in each discharge, using the approximation given by [112]:

$$\Delta W = C_V \Delta E \left(E_b - \frac{1}{2} \Delta E \right) \tag{A.5}$$

When the void is completely discharged ($E_r = 0$), the discharge power will be

simplified into:

$$\Delta W = \frac{1}{2} C_V \left[\Delta E\right]^2 \tag{A.6}$$

Discharge power is a very important parameter as it directly relates to the rate of degradation in insulation systems. However in practical applications, C_V and ΔE can't be found easily.

A.4 Discharge waveform of metallic surfaced gap under AC supply

When a void is under AC voltage stress that is higher than its breakdown voltage, the discharge will occur anytime that the voltage exceeds the breakdown voltage. Because the AC signal repeats its pattern every cycle and the fact that discharge happens at a very fast time frame compared to the applied voltage, studying just one cycle would be sufficient. For simplicity let's assume that there is a metallic gap with breakdown voltage of E_b and the residual voltage is zero ($E_r = 0$). The "apparent voltage" is defined as the voltage that would appear across the void assuming the breakdown voltage of the void to be infinity. Using this definition, the peak of apparent voltage across the void using the circuit model in Figure A.2 would be:

$$E_a = \frac{E_o C_S}{C_S + C_V} \tag{A.7}$$

Now considering that the breakdown voltage is equal in both polarities of the applied voltage and the time that discharge happens is negligible compared to the 60 Hz cycle, we are going to investigate the case where the applied voltage is 1.5

times the breakdown voltage. The gap we are studying here is an ideal gap with metallic electrodes which means that the applied voltage is the apparent voltage that appears on the gap. As it is shown in Figure A.3, when the voltage across the gap reaches the breakdown voltage, the discharge happens and the voltage inside the gap drops to E_r which in this case is zero. The sudden drop of voltage across C_V will cause a sudden jump of the voltage across the C_S. After the discharge extinguishes, the voltage inside the gap starts increasing again but this time it will not reach the E_b at the positive half cycle. During the negative half cycle however, the voltage reaches t[illegible] the second breakdown happens.

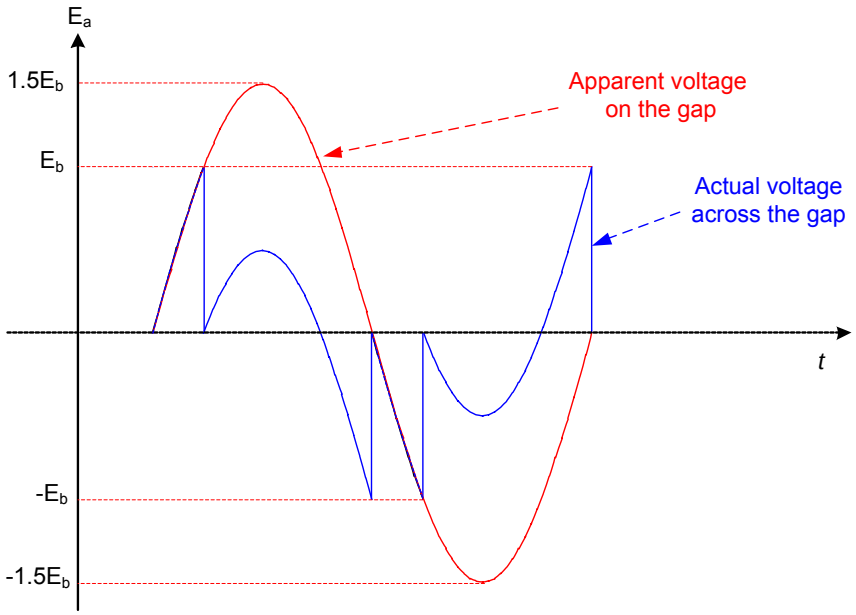

Figure A.3: Voltage waveform across an ideal cavity with $E_r = 0$ and $E_a = 1.5\,E_b$

It should be noted that the discharge time duration in the Figures was assumed to be zero as it is very small compared to the 60 Hz cycle. Figure A.3 also tells us that when apparent voltage is 1.5 times bigger than the breakdown voltage, four

discharges will ha ıt voltage is increased
by an integer nun · of discharges will be
multiplied by tha ıs when the apparent
voltage is three ti scharges will occur.

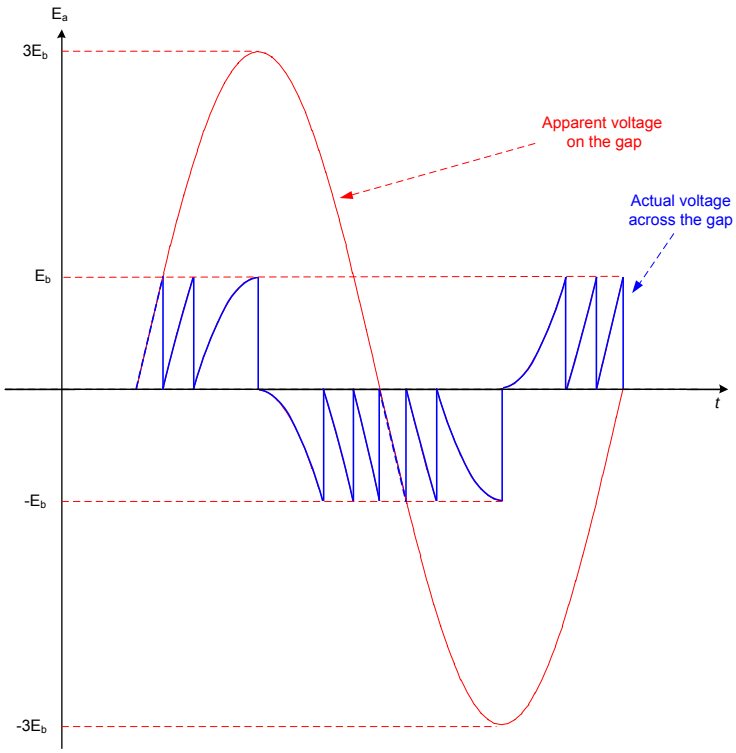

Figure A.4: Voltage waveform across an ideal cavity with $E_r = 0$ and $E_a = 3\,E_b$

Although we assumed that breakdown voltage is equal in both polarities, in actual experiments, it was shown that they are not equal and that is why the discharge pattern is different for each half cycle. The residual voltage may also vary in each polarity depending on the ionization inside the void. In order to model the discharge pattern more appropriately, unequal residual voltage and breakdown voltage in different polarities and even in the same polarity should be taken into account.

A.5 Discharge waveform of dielectric surfaced gap under AC supply

Studying the discharge mechanism of dielectric surfaced gaps is more complicated than metallic electrode gaps that was discussed in the previous section. The applied voltage on the whole gap is the voltage that is across the gaseous gap in series with the dielectric (C_S and C_V in series) therefore, the exact voltage on the gaseous gap and the dielectric layer is not available. To study the discharge waveform for this case, an experimental setup given by [113] was used which is shown in Figure A.5.

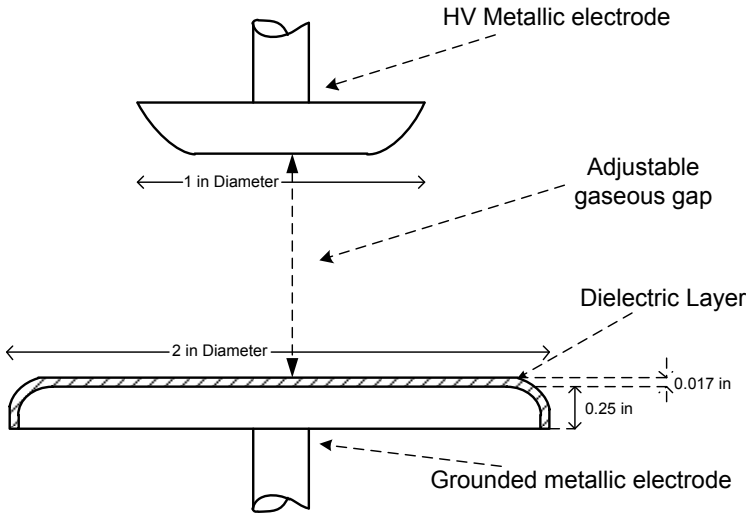

Figure A.5: Experimental test setup for studying the voltage waveform of dielectric-metallic electrode

The setup has two metallic electrodes where a dielectric layer is molded on the ground electrode. The details of this process is available in [114] as they followed specific procedure to avoid the development of voids and flaws between this layer and the metallic electrode. The other metallic electrode can be adjusted to have the desired gaseous gap size between the electrodes. In order to compare the results with

the case where both electrodes were metallic, in some experiments, a Tin film layer was used on top of the dielectric layer and the gap size was adjusted considering the thickness of this layer. To measure the voltage in this setup, they put the whole structure in series with a discharge free capacitor and then the whole combination was placed in parallel with another discharge free capacitor. The equivalent circuit for this new test setup is given in [113] and is shown in Figure A.6:

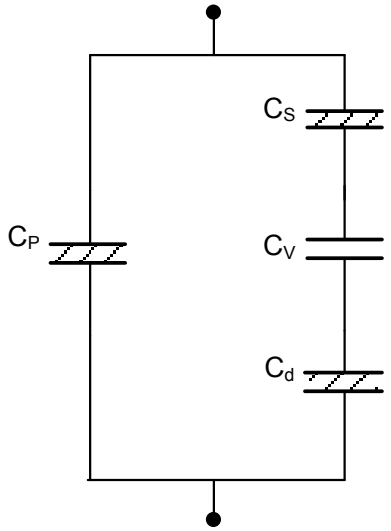

Figure A.6: Circuit model for the experimental test shown in Figure A.5

Where C_V represents the gaseous gap between the dielectric layer and the metallic electrode and was filled by Helium in this experiment. C_d represents the capacitance of the dielectric layer molded on the ground electrode and C_s and C_P are the discharge free capacitors in series and parallel with the structure for measurement purposes. Figure A.7 explains the shape of waveforms considering the discharges. In this test setup the apparent voltage across the gaseous gap was assumed to be $3E_b$. The actual voltage across the dielectric layer can be found by superposition of two voltages. The first portion can be found by a voltage division between the gap and the dielectric layer from the total voltage across the electrodes. The second

portion is a result of the current due to discharges in the gaseous gap. As the gap is in series with the dielectric layer, the ΔQ caused by the gap discharge is equal to:

$$\Delta Q = C_V \times \Delta V_1 = C_d \times \Delta V_2 \tag{A.8}$$

But because C_V and C_d are unknown, the ratio $(\Delta V_1/\Delta V_2)$ is unknown as well. ΔV_2 is the voltage that will appear across the dielectric layer due to discharges happening inside the gap. For illustrative purposes ΔV_2 was set to $\frac{1}{3}E_b$. Following this assumption, the first portion of the voltage across the dielectric layer would be equal to one third of the voltage across the gaseous gap. This means that the apparent voltage across the dielectric layer is equal to E_b. Figure A.7(a) shows the breakdown in the gaseous gap which is similar to Figure A.4 that was discussed earlier. Discharges happening in the gaseous gap will result in a discharge current that will change the actual voltage across the dielectric layer. This voltage was named ΔV_2 and Figure A.7(b) shows how the voltage across the dielectric layer changes due to the discharge current. The total voltage across the electrodes can be found by adding the breakdown voltage across the gaseous gap and the voltage across the dielectric layer which is shown in Figure A.7(c). Although Figure A.7(c) shows the waveform across the electrodes for a very ideal case, it has shown a good analogy with some practical experiments [92]. It should be mentioned that in all the waveforms shown in Figure A.7, the residual voltage was considered to be zero. Also it was assumed that there is only one discharge happening at the time. In real experiments however, there could be more than one discharge site at a time that changes the timing between two consecutive discharges. To compare the dielectric electrode with the metallic electrode, the Tin film layer was used on the dielectric

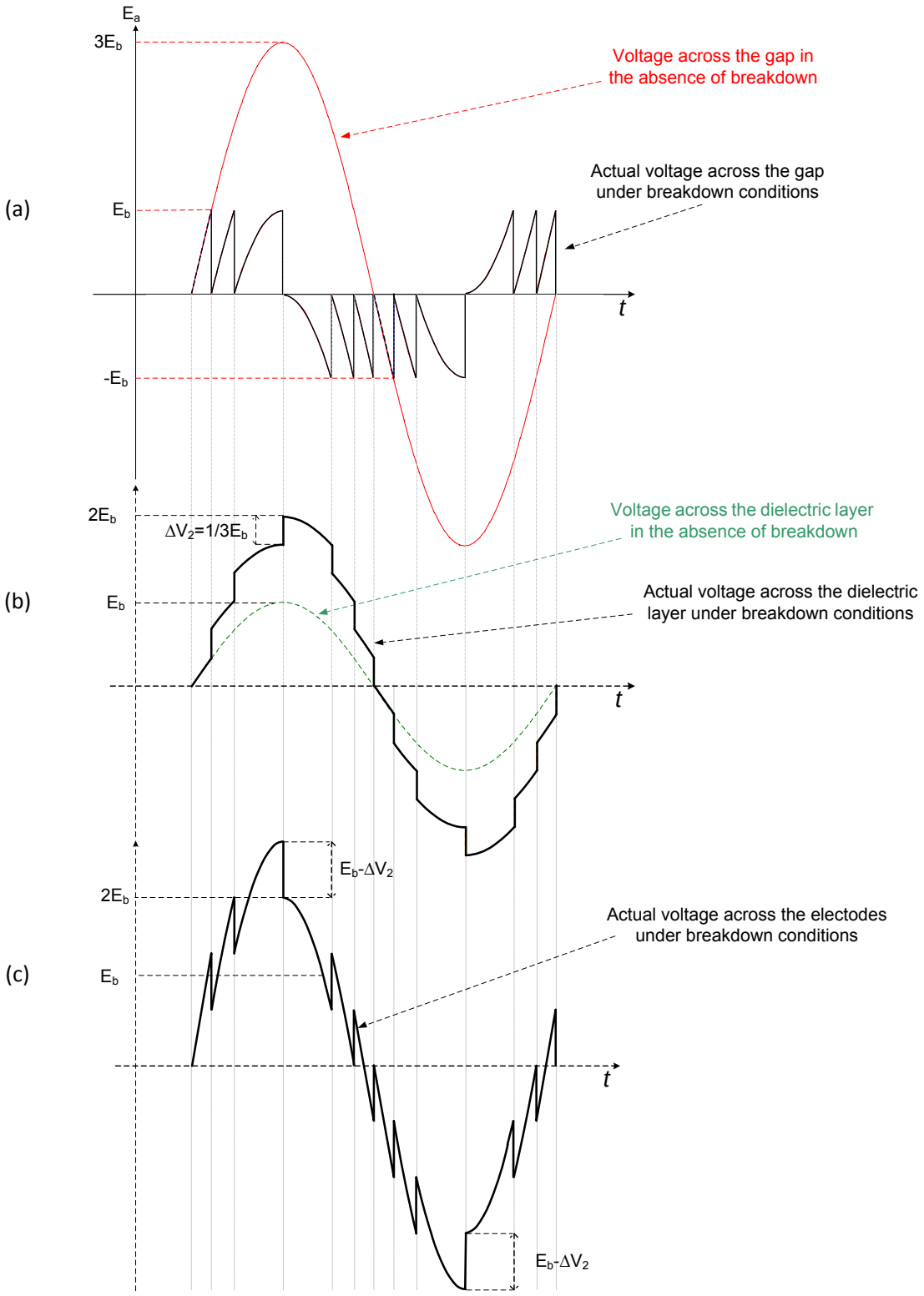

Figure A.7: Experimental test setup for studying the voltage waveform of dielectric-metallic electrode

layer and the results are reported in [114]. There has also been some research on the effect of different gases inside the gap on the discharge behavior and also pseudoglow and glow discharge mechanism in the voids under certain conditions [115].

References

[1] E. Cherney, A. Baker, J. Kuffel, Z. Lodi, and D. S. G. Phillips, A.and Powell, "Evaluation of and replacement strategies for aged high voltage porcelain suspension-type insulators," *IEEE Transactions on Power Delivery*, 2014. 1

[2] M. Farzaneh and W. Chisholm, *Insulators for Icing and Polluted Environments*, ser. IEEE Press Series on Power Engineering. Wiley, 2009. 3

[3] E. Report, "Stress performance of porcelain and glass transmission line insulators: Mechanical and electrical (m&e) and flashover testing results," Tech. Rep., 2014. 3

[4] E. Azordegan, "Group meeting communication with manitoba hydro field testig group," 2011. 3, 20

[5] A. Banik, S. Dalai, and B. Chatterjee, "Condition monitoring of overhead line insulator by measuring surface leakage current," in *2014 Annual IEEE India Conference (INDICON)*, Dec 2014, pp. 1–5. 4, 12, 25

[6] Z. Jia, C. Chen, X. Wang, H. Lu, C. Yang, and T. Li, "Leakage current analysis on rtv coated porcelain insulators during long term fog experiments,"

IEEE Transactions on Dielectrics and Electrical Insulation, vol. 21, no. 4, pp. 1547–1553, August 2014. 4, 25

[7] J. Li, W. Sima, C. Sun, and S. Sebo, "Use of leakage currents of insulators to determine the stage characteristics of the flashover process and contamination level prediction," *IEEE Transactions on Dielectrics and Electrical Insulation*, vol. 17, no. 2, pp. 490–501, 2010. 4, 26

[8] S. Chandrasekar, C. Kalaivanan, A. Cavallini, and G. Montanari, "Investigations on leakage current and phase angle characteristics of porcelain and polymeric insulator under contaminated conditions," *IEEE Transactions on Dielectrics and Electrical Insulation*, vol. 16, no. 2, pp. 574–583, 2009. 4, 12, 27, 28

[9] E. Azordegan, B. Kordi, and D. Swatek, "Radiated electromagnetic field signature of faulty and polluted porcelain insulators," in *2010 International Conference on High Voltage Engineering and Application (ICHVE)*, Oct 2010, pp. 449–452. 5

[10] E. Azordegan, D. R. Swatek, and B. Kordi, "Radiated electromagnetic field signature of cracked and polluted porcelain insulators," *Gaodianya Jishu Journal of High Voltage Engineering*, vol. 37, no. 11, pp. 2649 – 2654, 2011. 5, 41

[11] "Ngk-locke catalog." [Online]. Available: http://www.ngk.co.jp/english/products/power/porcelain/suspension/catalogs.html 7

[12] R. Gorur, E. Cherney, and J. Burnham, *Outdoor insulators*. Ravi S. Gorur, 1999. 7, 9, 19, 20

[13] T. Zhao and R. Bernstorf, "Ageing tests of polymeric housing materials for non-ceramic insulators," *IEEE Electrical Insulation Magazine*, vol. 14, no. 2, pp. 26 –33, march-april 1998. 7

[14] J. Looms, *Insulators for high voltages*. Peter Peregrinus Ltd, 1988, vol. 7. 8, 15, 29

[15] E. Cherney, "Cement growth failure of porcelain suspension insulators," *IEEE Transactions on Power Apparatus and Systems*, no. 8, pp. 2765–2774, 1983. 8

[16] T. Dakin and D. Berg, "Progress in dielectrics," *Theory of Gas Breakdowns*, vol. 4, pp. 167–168, 1962. 10, 122

[17] A. Von Hippel, *Dielectrics and waves*, 1966. 10, 123

[18] J. Devins, "The mechanism of the formation of discharges limited by series dielectrics," in *1961 Annual Report Conference on Electrical Insulation*, 1961, p. 97. 10, 123

[19] *Insulators for overhead lines with a nominal voltage above 1000 V*, Std. IEC 60 383-1, 1993. 11

[20] *Artificial pollution tests on high-voltage insulators to be used on a.c. systems*, Std. IEC 60 507, 1991. 11, 13, 46, 56, 57, 59, 115

[21] E. Cherney and R. Hooton, "Cement growth failure mechanism in porcelain suspension insulators," *Power Delivery, IEEE Transactions on*, vol. 2, no. 1, pp. 249–255, Jan 1987. 12

[22] A. Mishra, R. Gorur, and S. Venkataraman, "Evaluation of porcelain and toughened glass suspension insulators removed from service," *Dielectrics and*

Electrical Insulation, IEEE Transactions on, vol. 15, no. 2, pp. 467–475, April 2008. 12

[23] K. Morita, T. Imakoma, and K. Arakawa, "Long-term performance of ceramic insulators," NGK Publication, Tech. Rep. 12

[24] J. Li, C. Sun, and S. Sebo, "Humidity and contamination severity impact on the leakage currents of porcelain insulators," *IET Generation, Transmission & Distribution*, vol. 5, no. 1, pp. 19–28, 2011. 12, 25, 27, 38, 42

[25] L. Grigsby, *The electric power engineering handbook*. CRC Pr I Llc, 2001. 13

[26] K. Naito, Y. Mizuno, and W. Naganawa, "A study on probabilistic assessment of contamination flashover of high voltage insulator," *Power Delivery, IEEE Transactions on*, vol. 10, no. 3, pp. 1378–1384, Jul 1995. 13

[27] *Selection and dimensioning of high-voltage insulators for polluted conditions*, Std. IEC 60 815, 2002. 14, 46, 47

[28] D. Williams, A. Haddad, A. Rowlands, H. Young, and R. Waters, "Formation and characterization of dry bands in clean fog on polluted insulators," *IEEE Transactions on Dielectrics and Electrical Insulation*, vol. 6, no. 5, pp. 724–731, 1999. 14, 16

[29] B. Hampton, "Flashover mechanism of polluted insulation," *Electronics and Power*, vol. 10, no. 4, p. 113, 1964. 15

[30] "Industrial energy use in canada - emerging trends - energy briefing note," 2008. [Online]. Available: https://www.neb-one.gc.ca/nrg/ntgrtd/mrkt/archive/2010ndstrlnrgscnd/ndstrlnrgscnd-eng.html 18

[31] L. Lawton, M. Sullivan, K. V. Liere, and A. Katz, "A framework and review of customer outage costs: Integration and analysis of electric utility outage cost surveys," Ernest Orlando Lawrence Berkeley National Laboratory, Tech. Rep., November 2003. 18

[32] G. H. Vaillancourt, M. St-Jean, J. P. Bellerive, and C. Jean, "New live line tester for porcelain suspension insulators on high-voltage power lines," *IEEE Transactions on Power Delivery*, vol. 9, pp. 208–219, 1994. 20

[33] Y. Cheng, C. Li, and X. Huang, "Study of corona discharge pattern on high voltage transmission lines for inspecting faulty porcelain insulators," *IEEE Transactions on Power Delivery*, vol. 23, no. 2, pp. 945 –952, april 2008. 20

[34] M. Farzaneh, "Outdoor insulators: overview of in-service experience, inspection practice and future challenges," in *IEEE Electrical Insulation Conference, EIC 2009*, May 2009, pp. 542–550. 21

[35] B. Qi, C. Li, Z. Hao, B. Geng, D. Xu, S. Liu, and C. Deng, "Partial discharge detection for gis: A comparison between uhf and acoustic methods," in *Conference Record of the 2010 IEEE International Symposium on Electrical Insulation (ISEI)*. IEEE, 2010, pp. 1–5. 22

[36] M. Yaacob, M. Alsaedi, J. Rashed, A. Dakhil, and S. Atyah, "Review on partial discharge detection techniques related to high voltage power equipment using different sensors," *Photonic Sensors*, vol. 4, no. 4, pp. 325–337, 2014. 22

[37] K. Wu, C. Pan, Y. Meng, C. Sun, M. Gao, K. Qin, and H. Long, "Study on the characteristics of partial discharges in voids under square voltage by detecting

light emission intensity," *IEEE Transactions on Dielectrics and Electrical Insulation*, vol. 18, no. 5, pp. 1651–1657, 2011. 22

[38] F. Bologna, N. Mahatho, and D. Hoch, "Infra-red and ultra-violet imaging techniques applied to the inspection of outdoor transmission voltage insulators," in *IEEE AFRICON. 6th Africon Conference in Africa*, vol. 2. IEEE, 2002, pp. 593–598. 23

[39] H. Ha, S. Han, and J. Lee, "Fault detection on transmission lines using a microphone array and an infrared thermal imaging camera," *IEEE Transactions on Instrumentation and Measurement*, no. 99, pp. 1–9, 2012. 23

[40] I. Ramirez-Vazquez and J. Fierro-Chavez, "Criteria for the diagnostic of polluted ceramic insulators based on the leakage current monitoring technique," *IEEE Conference on Electrical Insulation and Dielectric Phenomena*, pp. 715–718, 1999. 24

[41] G. Amaldo and F. Geraldo, "Leakage current monitoring of insulators exposed to marine and industrial pollution," *IEEE International Symposium on Electrical Insulation*, pp. 271–274, 1996. 24

[42] T. Suda and S. Member, "Frequency characteristics of leakage current waveforms of a string of suspension insulators," *IEEE Transactions on Power Delivery*, vol. 20, no. 1, pp. 481–488, 2005. 24

[43] J. Li, W. Sima, C. Sun, Z. Li, C. Yang, and J. Deng, "Frequency domain spectrum of leakage currents during discharge detection for contamination insulators [j]," *High Voltage Engineering*, vol. 3, 2008. 26

[44] S. Kumagai and N. Yoshimura, "Leakage current characterization for estimating the conditions of ceramic and polymeric insulating surfaces," *IEEE Transactions on Dielectrics and Electrical Insulation*, vol. 11, no. 4, pp. 681–690, 2004. 27

[45] H. Okubo and N. Hayakawa, "A novel technique for partial discharge and breakdown investigation based on current pulse waveform analysis," *IEEE Transactions on Dielectrics and Electrical Insulation*, vol. 12, no. 4, pp. 736–744, 2005. 27

[46] M. Douar, A. Mekhaldi, and M. Bouzidi, "Investigations on leakage current and voltage waveforms for pollution level monitoring under wetted and contaminated conditions," *IET Science, Measurement & Technology*, vol. 5, no. 2, pp. 67–75, 2011. 29

[47] V. Kontargyri, I. Gonos, I. Stathopulos, and A. Michaelides, "Measurement and verification of the voltage distribution on high voltage insulators," *Proceedings of the 12th Biennial IEEE Conference on Electromagnetic Field Computation*, pp. –, 2006. 30, 31

[48] J. Rasolonjanahary, L. Krahenbuhl, and A. Nicolas, "Computation of electric fields and potential on polluted insulators using a boundary element method," *IEEE Transactions on Magnetics*, vol. 28, no. 2, pp. 1473–1476, 1992. 30

[49] T. Zhao and M. Comber, "Calculation of electric field and potential distribution along nonceramic insulators considering the effects of conductors and transmission towers," *IEEE Transactions on Power Delivery*, vol. 15, no. 1, pp. 313–318, 2000. 30

[50] V. Kontargyri, I. Gonos, I. Stathopulos, and A. Michaelides, "Calculation of the electric field on an insulator string using the finite elements method," in *Proceedings of the 38th International Universities Power Engineering Conference (UPEC 2003)*, 2003, pp. 65–68. 30

[51] J. Du, Z. Peng, J. Li, S. Zhang, N. Li, and C. Fan, "Electric field calculation and grading ring optimization for 1000 kv ac post porcelain insulator," in *2013 IEEE International Conference on Solid Dielectrics (ICSD)*, June 2013, pp. 198–201. 30

[52] Y. Cheng and C. Li, "Online detecting composite insulators by two dimensions electric field distribution," in *Conference Record of the 2006 IEEE International Symposium on Electrical Insulation*, june 2006, pp. 132 –135. 30

[53] X. Liu, D. Kasten, S. Sebo, R. Caldecott, D. Grosjean, and D. Schweickart, "Partial discharge measurements-frequency related considerations," in *2005 Annual Report Conference on Electrical Insulation and Dielectric Phenomena, CEIDP '05*, oct. 2005, pp. 405 – 409. 31

[54] S. Xiao, P. Moore, M. Judd, and I. Portugues, "An investigation into electromagnetic radiation due to partial discharges in high voltage equipment," in *IEEE Power Engineering Society General Meeting.* IEEE, 2007, pp. 1–7. 31

[55] P. Moore, I. Portugues, and I. Glover, "Remote diagnosis of overhead line insulation defects," in *IEEE Power Engineering Society General Meeting.* IEEE, 2004, pp. 1831–1835. 32

[56] R. Sharkawy, R. Mangoubi, T. Abdel-Galil, M. Salama, and R. Bartnikas, "SVM classification of contaminating particles in liquid dielectrics using higher order statistics of electrical and acoustic pd measurements," *IEEE Transactions on Dielectrics and Electrical Insulation*, vol. 14, no. 3, pp. 669–678, June 2007. 33, 43

[57] M. Cacciari, A. Contin, and G. Montanari, "Use of a mixed-weibull distribution for the identification of pd phenomena [corrected version]," *IEEE Transactions on Dielectrics and Electrical Insulation*, vol. 2, no. 6, pp. 1166–1179, 1995. 33, 40, 41

[58] A. Contin, G. Montanari, and C. Ferraro, "Pd source recognition by weibull processing of pulse height distributions," *IEEE Transactions on Dielectrics and Electrical Insulation*, vol. 7, no. 1, pp. 48–58, Feb 2000. 33, 41

[59] N. Sahoo, M. Salama, and R. Bartnikas, "Trends in partial discharge pattern classification: a survey," *IEEE Transactions on Dielectrics and Electrical Insulation*, vol. 12, no. 2, pp. 248–264, 2005. 34

[60] R. González and J. Tou, *Pattern recognition principles*, 1974. 34

[61] H. Kranz, "Diagnosis of partial discharge signals using neural networks and minimum distance classification," *IEEE Transactions on Electrical Insulation*, vol. 28, no. 6, pp. 1016–1024, 1993. 34, 40

[62] W. Ziomek, M. Reformat, and E. Kuffel, "Application of genetic algorithms to pattern recognition of defects in gis," *IEEE Transactions on ielectrics and Electrical Insulation*, vol. 7, no. 2, pp. 161–168, 2000. 35, 36

[63] T. Anderson, *An introduction to multivariate statistical analysis*, ser. Wiley series in probability and mathematical statistics: Probability and mathematical statistics. Wiley, 1984. 36

[64] E. Gulski and A. Krivda, "Neural networks as a tool for recognition of partial discharges," *IEEE Transactions on Electrical Insulation*, vol. 28, no. 6, pp. 984–1001, 1993. 36, 40

[65] J. Hunter, L. Hao, P. Lewin, D. Evagorou, A. Kyprianou, and G. Georghiou, "Comparison of two partial discharge classification methods," in *Conference Record of the 2010 IEEE International Symposium on Electrical Insulation (ISEI)*. IEEE, 2010, pp. 1–5. 37

[66] M. Rahman, R. Arora, and S. Srivastava, "Partial discharge classification using principal component transformation," in *IEE Proceedings-Science, Measurement and Technology*, vol. 147, no. 1. IET, 2000, pp. 7–13. 38

[67] J. Li, C. Sun, W. Sima, and Q. Yang, "Stage pre-warning based on leakage current characteristics before contamination flashover of porcelain and glass insulators," *IET Generation, Transmission & Distribution*, vol. 3, no. 7, pp. 605–615, 2009. 38, 42

[68] M. Salama and R. Bartnikas, "Determination of neural-network topology for partial discharge pulse pattern recognition," *IEEE Transactions on Neural Networks*, vol. 13, no. 2, pp. 446–456, 2002. 39

[69] D. Evagorou, A. Kyprianou, P. Lewin, A. Stavrou, V. Efthymiou, A. Metaxas, and G. Georghiou, "Feature extraction of partial discharge signals using

the wavelet packet transform and classification with a probabilistic neural network," *IET Science, Measurement & Technology*, vol. 4, no. 3, pp. 177–192, 2010. 39

[70] D. Evagorou, A. Kyprianou, P. Lewin, A. Stavrou, V. Efthymiou, and G. Georghiou, "Classification of partial discharge signals using probabilistic neural network," in *IEEE International Conference on Solid Dielectrics, ICSD'07*. IEEE, 2007, pp. 609–615. 39

[71] A. Contin, A. Cavallini, G. Montanari, G. Pasini, and F. Puletti, "Digital detection and fuzzy classification of partial discharge signals," *IEEE Transactions on Dielectrics and Electrical Insulation*, vol. 9, no. 3, pp. 335–348, 2002. 39

[72] R. James and B. Phung, "Development of computer-based measurements and their application to pd pattern analysis," *IEEE Transactions on Dielectrics and Electrical Insulation*, vol. 2, no. 5, pp. 838–856, 1995. 40

[73] T. Hucker and H. Krantz, "Requirements of automated pd diagnosis systems for fault identification in noisy conditions," *IEEE Transactions on Dielectrics and Electrical Insulation*, vol. 2, no. 4, pp. 544–556, 1995. 40

[74] M. Fenger, M. Credland, and H. Sedding, "Recent experiences with ac hipot & pd commissioning testing of xlpe cable systems rated 69kv and above," *CIGRE*, 2012. 41

[75] OMICRON, HIGHVOLT, and Kinectrics, "On-site testing of high-voltage cable systems." [Online]. Available: https:

//www.omicron.at/fileadmin/user_upload/pdf/magazine/MPD_600_On-site_Testing_of_High-voltage_Cable_Systems_2011_issue1.pdf 41, 107

[76] L. Dissado, J. Fothergill, S. Wolfe, and R. Hill, "Weibull statistics in dielectric breakdown; theoretical basis, applications and implications," *Electrical Insulation, IEEE Transactions on*, no. 3, pp. 227–233, 1984. 41

[77] T. Sipahutar, A. Kemma, N. Pattanadech, F. Pratomosiwi, Suwarno, and M. Muhr, "Effect of test method and needle plane configuration on partial discharge inception voltage measurement of mineral oil based on weibull analysis," *Procedia Technology*, vol. 11, no. 0, pp. 411 – 418, 2013, 4th International Conference on Electrical Engineering and Informatics, {ICEEI} 2013. 41

[78] Z. Tang, W. Zhou, J. Yu, and C. Zhou, "Comparison of weibull distribution and crow-amsaa model used in cable failure analysis," in *2012 Spring Congress on Engineering and Technology (S-CET)*, May 2012, pp. 1–4. 41

[79] F.-C. Gu, H.-C. Chang, F.-H. Chen, and C.-C. Kuo, "Partial discharge pattern recognition of power cable joints using extension method with fractal feature enhancement," *Expert Systems with Applications*, vol. 39, no. 3, pp. 2804 – 2812, 2012. 42

[80] H. Li, J. Li, W. Li, X. Zhao, G. Wang, and M. Alim, "Fractal analysis of side channels for breakdown structures in xlpe cable insulation," *Journal of Materials Science: Materials in Electronics*, vol. 24(5), pp. 1640–1643, 2013. 42

[81] V. Jeyabalan and S. Usa, "Frequency domain correlation technique for pd location in transformer winding," *IEEE Transactions on Dielectrics and Electrical Insulation*, vol. 16, no. 4, pp. 1160–1167, August 2009. 42

[82] W. Kinsner, "A unified approach to fractal dimensions," in *Fourth IEEE Conference on Cognitive Informatics (ICCI)*, Aug 2005, pp. 58–72. 42, 75

[83] R. Salustiano, R. Capelini, S. de Abreu, M. Martinez, I. Tavares, G. Ferraz, and M. Romano, "Development of new methodology for insulators inspections on aerial distribution lines based on partial discharge detection tools," in *High Voltage Engineering and Application (ICHVE), 2014 International Conference on*, Sept 2014, pp. 1–4. 44

[84] C. Nyamupangedengu, L. Luhlanga, and T. Letlape, "Acoustic and hf detection of defects on porcelain pin insulators," in *Power Engineering Society Conference and Exposition in Africa, 2007. PowerAfrica '07. IEEE*, July 2007, pp. 1–5. 44

[85] N. Algeelani and M. Piah, "Identification of acoustic signals of surface discharges on glass insulator under different contamination levels," in *Electrical, Control and Computer Engineering (INECCE), 2011 International Conference on*, June 2011, pp. 511–514. 44

[86] MATLAB, *version 7.10.0 (R2010a).* Natick, Massachusetts: The MathWorks Inc., 2010. 45, 69

[87] *IEEE Guide for the Application of Insulation Coordination*, Std. 1313.2, 1999. 47, 115

[88] *Standard Test Method for Detection and Measurement of Partial Discharge (Corona) Pulses in Evaluation of Insulation Systems*, Std. ASTM D1868, 2007. 47, 120

[89] *Insulators for overhead lines with a nominal voltage above 1000 V, Part 1:ceramic or glass insulator units for AC. systems Definitions, test methods and acceptance criteria*, IEC International standard Std. IEC 60 383-1, 1993. 47, 60, 62, 115

[90] "http://www.rossengineeringcorp.com/products/measurement/hv-voltage-dividers.html." 51

[91] P. T. Inc., "Electric field sensors," February 2012. [Online]. Available: http://prodyntech.com/home/page/d_dot_sensor 52

[92] R. Bartnikas and E. McMahon, *Engineering Dielectrics: Corona Measurement and Interpretation.* Astm Intl, 1979. 54, 121, 132

[93] C. Magnelab Current Transformers. [Online]. Available: http://www.gmw.com/electric_current/Magnelab/ct_Specs.html 54

[94] K. InfiniiVision, "Agilent 7104a," November 2014. [Online]. Available: http://www.keysight.com/en/pd-1293645-pn-DSO7104A/oscilloscope-1-ghz-4-analog-channels?&cc=CA&lc=eng 55

[95] "Ngk-locke, inc." January 2015. [Online]. Available: http://www.ngk-locke.com/ 56

[96] G. Montoya, I. Ramirez, and J. Montoya, "Correlation among esdd, nsdd

and leakage current in distribution insulators," *IEE Proceedings-Generation, Transmission and Distribution*, vol. 151, no. 3, pp. 334 – 40, 2004/05/15. 57

[97] T. F. S. Inc., "Orion 3-star plus portable conductivity meter kit," February 2012. [Online]. Available: http://www.thermoscientific.com/ecomm/servlet/productsdetail_11152_L10920_80575_11958237_-1 57

[98] F. Corporation, "Fluke 1507/1503 insulation resistance testers," February 2012. [Online]. Available: http://www.fluke.com/fluke/caen/Digital-Multimeters/Fluke-1507-1503.htm?PID=56007 61

[99] T. Czaszejko and S. Chen, "Ultra wide band response of partial discharge test circuit," in *2010 International Conference on High Voltage Engineering and Application (ICHVE)*, Oct 2010, pp. 61–64. 69

[100] L. Wang, *Support Vector Machines: Theory and Applications*, ser. Studies in Fuzziness and Soft Computing. Springer, 2005. 105

[101] *High-voltage test techniques - Partial discharge measurements*, Std. IEC 60 270, 2000. 106, 107, 121

[102] A. Kraetge, S. Hoek, M. Koch, and W. Koltunowicz, "Robust measurement, monitoring and analysis of partial discharges in transformers and other hv apparatus," *IEEE Transactions on Dielectrics and Electrical Insulation*, vol. 20, no. 6, pp. 2043–2051, December 2013. 106

[103] K. Rethmeier, W. Pichler, M. Krüger, R. Plath, C. Steineke, and O. Ried, "Multi-channel pd measurements on transformers–a new approach for real-

time data evaluation," in *OMICRON Seminar on Diagnostic Measurement on Power Transformers*, 2008. 107

[104] A. Cavallini, S. Chandrasekar, G. C. Montanari, and F. Puletti, "Inferring ceramic insulator pollution by an innovative approach resorting to pd detection," *IEEE Transactions on Dielectrics and Electrical Insulation*, vol. 14, no. 1, pp. 23–29, Feb 2007. 110

[105] M. G. Danikas, "The definitions used for partial discharge phenomena," *IEEE Transactions on Electrical Insulation*, vol. 28, no. 6, pp. 1075–1081, 1993. 120

[106] J. Mason, "Discharge detection and measurements," *Proc. IEE*, vol. 112, no. 7, pp. 1407–1423, 1965. 122

[107] H. Hall and R. Russek, "Discharge inception and extinction in dielectric voids," *Proceedings of the IEE-Part II: Power Engineering*, vol. 101, no. 79, pp. 47–55, 1954. 123

[108] J. Meek and J. Craggs, *Electrical Breakdown of Gases. Clarendon.* Oxford, 1953. 123

[109] J. Birks and J. Schulman, *Progress in dielectrics.* Wiley, 1959, vol. 1. 124

[110] J. Mason, "Breakdown of insulation by discharges," *Proceedings of the IEE-Part IIA: Insulating Materials*, vol. 100, no. 3, pp. 149–158, 1953. 124

[111] A. Gemant and W. Von Philipoff, "Die funkenstrecke mit vorkondensator [spark gaps with front capacitors]," *Z. f. techn. Physik*, vol. 13, no. 9, pp. 425–430, 1932. 125

[112] S. Whitehead, *Dielectric Breakdown of solids.* Oxford, 1953. 126

[113] R. Bartnikas and J. H. E. Levi, "Improved pulsed discharge rate measuring apparatus for ionization discharge studies at low frequencies," *Review of Scientific Instruments*, vol. 37, no. 9, pp. 1245 –1251, sep 1966. 130, 131

[114] R. Bartnikas, "Some observations on the character of corona discharges in short gap spaces," *IEEE Transactions on Electrical Insulation*, vol. EI-6, no. 2, pp. 63 –75, june 1971. 130, 134

[115] ——, "Note on discharges in helium under ac conditions," *Journal of Physics D: Applied Physics*, vol. 1, no. 5, p. 659, 1968. 134